Development of Bio-environmentally Compatible Implant Materials by the Function of Precursors of Apatite

Hasnat Zamin

Development of Bio-environmentally Compatible Implant Materials by the Function of Precursors of Apatite

Contents

Chapter 1

General Introduction

Increased life expectancy has caused an immense aging population increase worldwide, specifically in Japan. To tackle the general health problems of older adults, great emphasis is being given to developing new materials for biomedical application especially implants for bone grafting and prosthodontist application [1-3].

A variety of materials are under investigation as candidates for bone substitutes under the field of bone tissue engineering. These materials can be classified as natural polymers, synthetic polymers, ceramics, metals, and composite materials. Prerequisites for a material to be considered as a bone substitute are biocompatibility, bioactivity, adequate surface behavior for cellular interaction [4-7].

1.1 **Bioceramics**

A biomaterial is defined as '*a material intended to interface with biological systems to evaluate, treat, augment or replace any tissue, organ or function of the body'* [8].

Bioceramics are a subclass of biomaterials, which designates ceramic materials used for repairment or to reconstruct the diseased or defective parts of the musculo-skeletal system [9].

1.2 **History of bioceramics**

Ceramics have a long history as a biomaterial. Porcelain was first used bioceramic material in the 18th century for the treatment of the crown. Similarly, the plaster of Paris was used in the 19th century for the treatment of dental disorders [10]. However, the application of bioceramics increased in the 20th century in the medical field as an alternative to metals which are reactive, that can lead to corrosion and eventual failure is caused by the aggressive nature of body fluids [11]. The primary reasons for the bioceramics application are biocompatibility and high mechanical strength. Additionally, properties like low heat conductance, high melting temperatures, chemical, and shear resistance make bioceramics a body-friendly substitute [12,13].

1.3 **Classification of bioceramics on the basis of bioactivity**

Bioceramics can be broadly classified into three categories bioactive, bioresorptive, and bioinert based on their biological interaction. A bioactive material is defined as “one which has been designed to induce specific biological activity” [8]. In the case of bioactive bioceramics, the ability to induce a positive reaction which results in bonding between the bone and its surface [9].

Table 1 show Hench’s classification of bioceramic based on tissue attachment (reproduced from [26]).

Furthermore, Hench also introduced an index to estimate the degree of bioactivity measured in terms of the rate of development of the bond between the surrounding tissue and the implant.

Table 1 Types of bioceramics - Tissue attachment and bioceramic classification (reproduced from [26]).

Type of bioceramic	Type of attachment	Example
1	Dense, nonporous, nearly inert ceramics attach by bone growth into surface irregularities by cementing the device into the tissues, or by press fitting into a defect (termed morphological fixation).	Al_2O_3 (single crystal and polycrystalline)
2	For porous inert implants bone ingrowth occurs, which mechanically attaches the bone to the material (termed biological fixation)	Al_2O_3 (porous polycrystalline) Hydroxyapatite-coated porous metals
3	Dense, nonporous, surface reactive ceramics, glasses, and glass-ceramics attach directly by chemical bonding with the bone (termed bioactive fixation).	Bioactive glasses, Bioactive glass-ceramics, Hydroxyapatite
4	Dense, nonporous (or porous) resorbable ceramics are designed to be slowly replaced by bone.	Calcium sulfate (plaster of Paris), Tricalcium phosphate, Calcium phosphate salts

This index is represented as

Bioactivity Index, $IB=100/t_{0.5bb}$

Here ($t_{0.5bb}$) depicts the bonding time taken for more than 50% of implants interface to the bone. Based on this index, materials can be classified into Class A and Class B types. Class A materials have an IB greater than 8. These materials are regarded to have both osteogenic and osteoconductive properties, which can bond to both hard and soft tissues such as bioactive glass 45S5 [13-16]. While Class B materials have IB greater than 0 and less than 8. These materials only show osteoconductive properties, which only bond to hard tissue such as synthetic hydroxyapatite and tri-calcium phosphate [17].

1.3.1 *Bioactive ceramics*

Bioactive ceramics have positive interaction with the living tissue and induce response helping regeneration, repair, and reconstruction of body tissues. Upon introduction in the human body, the surface reactive ceramic produces a specific biological response that starts to form a bond between the interface and the tissue [9,18]. Bioactive glass and hydroxyapatite are a few of the well-known examples of bioactive ceramics.

1.3.1.1 *Bioactive glass*

Bioactive glass was first designed and termed by Larry Hench in 1969. Bioactive glasses are amorphous silica-based materials and CaO and P_2O_5 are its main constituent. The initial bioglass (45S5) consisted of 45% silica (SiO_2), 24.5% calcium oxide (CaO), 24.5%sodium oxide (Na_2O), and 6% phosphorous pentoxide (P_2O_5) in weight percentage [19-21]. When exposed to

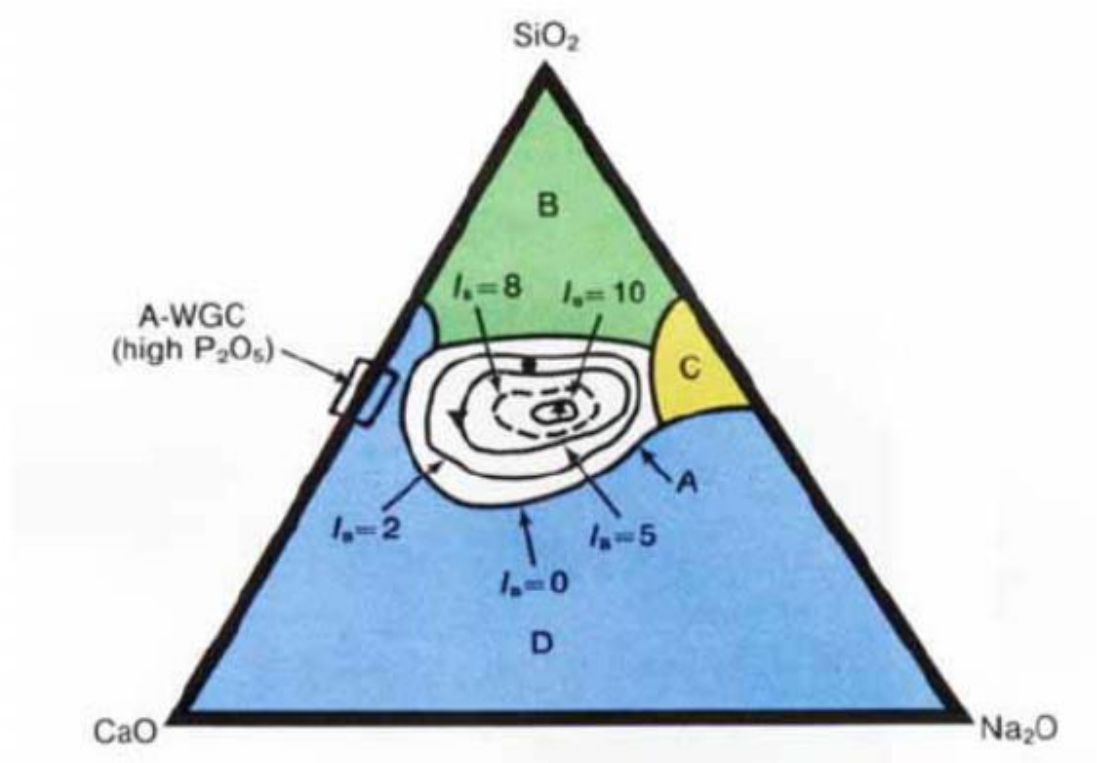

Figure 1 Compositional dependence (in weight percentage) of bioactive glasses and glass ceramics on bonding to bone and soft-tissue (reproduced from [26]).

physiological fluid bioactive glass forms hydroxycarbonate apatite (HCA) at the interface. This HCA has structure and composition similar to bone minerals and helps to form a bond with the bone [9,26]. Bioglasses are biodegradable materials, and their bioactivity depends on the reaction rate and HCA formation. The rate of degradation is strongly related to the composition and surface morphology [22,23]. The compositional dependence of bone and soft tissue bonding and bioglass is depicted in Figure 1 (reproduced from [26]). Based on the composition, bioglass can be classified as bioinert, bioactive, and bioresorbable. Region A is bioactive and can bond with the bone. Region B is bioinert, and region C is bioresorbable, which dissolves in body in 10-30 days. Region D is non-glass forming compositions [24-27].

1.3.1.2 *Hydroxyapatite*

Hydroxyapatite (HAp) is the most widely used synthetic form of calcium phosphate as a bioceramic and has a similar mineral composition as bone. Its stoichiometric formula is $Ca_{10}(PO_4)_6(OH)_2$ with Ca/P ratio around 1.66 [28, 29]. HAp has hexagonal symmetry (space group P63/m) in a slightly non-stoichiometric form and the lattice parameters are a = 0.95 nm and c = 0.68 nm. While stoichiometric HAp has a monoclinic form with P21/b space group [30-33]. Hydroxyapatite has a high biological affinity to living bone and cells and is an excellent carrier of growth factors and osteogenic cells [34].

Porous HAp is osteoconductive, biocompatible, and resorbs with time but the degradation rate is slow, while dense HAp is considered to be non-biodegradable as it has a very low degradation rate in body fluids, which causes less effect on bone tissue formation [35,36].

The bioactive properties of HAp can be enhanced by ionic substitutions, which are similar to ions present in natural bone apatites such as metal cations (Mg^{2+}, Mn^{2+}, Zn^{2+}, Na^{+}, Sr^{2+}) or anions (HPO_4^{2-} or CO_3^{2-}). HAp is capable of accommodating substitute ions within its lattice. The apatites with substituted ions can affect crystal structure parameters, crystallinity, dissolution kinetics dramatically, thereby influencing the biological response in the final applications [37-39].

However, one of the drawbacks of HAp is that its mechanical properties are very low as compared to the natural bone; it is brittle in nature with lower strength and fatigue resistance [40].

1.4 **Bioactive treatment of bioinert materials**

When an artificial material is implanted inside the body, it is surrounded by the fibrous tissue, which is a normal phenomenon of an immune reaction of the body against a foreign substance [41-43]. As mentioned in section 1.3, these nontoxic, bioinert implants attaches to the bone by morphological fixation. However, there is relative movement at the interface and development of nonadherent fibrous capsule of variable thickness as the implant is not chemically or biologically bonded. This movement either causes deterioration of the implant or tissue or both at the implant tissue interface. Hench's bioglass can mitigate this immune reaction of the body and can bond with the living bone through the formation of HCA [9,26]. Hydroxyapatite and sintered β tricalcium phosphate are among the few of calcium phosphate based bioactive ceramics to also show this behavior [34,36,44,45]. Some other well-known glass and apatite based bioactive ceramics are Ceravital® [46], Bioverit® [47], which additionally contains phlogopite, Cerabone A W® [48-

51], and Ilmaplant® [52] both of which additionally contains wollastonite. Most of the bioactive ceramics can bond with a living bone by forming the hydroxyapatite layer at the interface through the proliferation and differentiation of osteoblastic cells on the surface of this layer [53-59]. This results in the formation of living bone on the layer, which ultimately bonds with the surrounding bone tissue.

However, the greatest constrains of utilizing bioactive glasses and glass-based ceramics are their poor mechanical compatibility with bone, especially at mechanically zones such as femoral and tibial bones. They possess lower fracture toughness and higher elastic modulus compared to the human cortical bone [60]. One of the solutions to solve this problem is to coat or integrate these bioactive ceramics with bioinert metals, ceramics, and polymer with desired mechanical properties such as stainless steels, cobalt-chromium alloys, titanium alloys, zirconia, and polyethylene [61-65].

Various kinds of methods have been employed to develop bioactive coatings on bioinert materials such as plasma spraying, sputtering, electrodeposition, and biomimetic coatings [66,67]. Hydroxyapatite based coatings are most prevailing among all types of bioactive ceramics [68].

Biomimetic methods such as simulated body fluid or modified simulated body fluid treatment to induce bioactivity to bioinert materials is highly attractive since it requires low processing temperature and can deposit apatite with similar properties to human bone [69,70].

1.5 **Simulated body fluid**

Kokubo et al. proposed that when a foreign material is implanted inside a living body, it can bond to the living bone through the formation of a bonelike apatite layer on the surface, and this in vivo apatite formation can be mimicked in a biomimetic fluid. This fluid has a similar concentration of inorganic ions present in the human blood plasma and was named as simulated body fluid (SBF) [71-74]. This implied that in vivo bioactivity of a material can be predicted by the SBF test, and Kokubo et al. further analyzed the bioactivity of various materials by hydroxyapatite formation in SBF [75-80]. Since then, the SBF is widely used to test the in vitro apatite forming ability of various materials.

1.6 **Precursors of apatite or apatite nuclei**

By altering the physical parameters of SBF, fine particles are precipitated in the SBF. Yao et al. discovered that when pH, temperature, or concentration of the SBF varied and controlled, fine particles of calcium phosphates are precipitated in the SBF, which were found to be highly active in inducting hydroxyapatite formation in SBF as well as human blood plasma. These precipitates were named as apatite nuclei or precursors of apatite [81,82]. Furthermore, utilizing this attractive property of apatite nuclei, various kinds of materials were fabricated, which had the apatite forming ability in the conventional SBF [83-85]. Considering the above idea, the author studied the preparation of apatite nuclei using two different approaches and fabricated various kinds of bioenvironment compatible implant materials by the application of apatite nuclei.

1.7 **Purpose of the thesis**

The present thesis describes the studies on the development of bioactive materials by the function of precursors of apatite or apatite nuclei (AN).

Four different types of biocompatible materials were selected, and three different procedure were utilized to deposit AN or integrate these materials in the form of composites with AN mentioned in above section 1.6. Finally, after successful AN treatment, the SBF test was carried out to check the in vitro bioactivity of these materials. The four materials are zirconia, tetragonal zirconia polycrystal (3Y-TZP), Polyvinylidene fluoride (PVDF), and polycaprolactone (PCL).

Zirconia is biologically inert and biocompatible ceramic showing no adverse reaction with tissues or cytotoxicity, which is then widely used as ball head of total hip replacements (THR) [86,87]. When stabilized by the addition of ~3% of yttria into the tetragonal phase and known as tetragonal zirconia polycrystal, it shows high fracture toughness and flexural strength. This enhanced mechanical property is due to the phase transformation toughening, from tetragonal to monoclinic in the structure that increases crack propagation resistance [88,89]. Another noteworthy characteristic of 3Y-TZP being white in color is its aesthetic value, which is in contrast to metals that can cause discoloration [90,91].

Zirconia is a highly attractive candidate as a bioceramic; however, it lacks bioactivity or bone bonding-ability. Previous work by Uchida et al. reported the apatite formation in the SBF on zirconia/alumina composites by various surface chemical treatments. It was found that the apatite formation was related to the formation of the Zr-OH group on the surface and the shortest

period of the apatite formation in 3 days SBF immersion for 5M H_3PO_4 chemical treatment [92]. Another work by Dehastani et al. reports apatite formation on 3Y-TZP in 3 weeks SBF immersion by an aqueous solution treatment, which included magnesium ions [93]. In this work, the author aimed to induce apatite formation in a very short time period of 1-day SBF immersion to zirconia and 3Y-TZP. For this, two different kinds of approaches were followed for the zirconia and 3Y-TZP by varying the concentration of inorganic ions and temperature for AN treatments.

PVDF and PCL are biocompatible semi crystalline polymers. PVDF is a non-biodegradable fluoropolymer known for its electroactive properties [94]. Piezoelectric materials are employed for different tissue repair applications, especially in bone repair, where bone formation can be enhanced by mechanical stress induced charges in the materials [95]. The effect of implanted piezoelectric PVDF films on bone regeneration ability was shown by Ficat et al. [96]. PVDF can serve as a suitable biomedical material for bone implants, vascular grafts, neural regeneration, biosensing applications, etc. [97,98] as PVDF possesses piezoelectricity, high elasticity, and good processability. Whereas, PCL is a biodegradable aliphatic polyester also possessing processability because of its low glass transition (~ -60 °C) and melting temperature (~ 60 °C). PCL has a low biosorption rate suitable enough for bone tissue regeneration, which makes it a good candidate for bone tissue engineering [99]. The author used the solvent casting technique to fabricate bioactive PVDF and PCL composites to integrate the polymers with AN.

In chapter 2, the fabrication of bioactive zirconia is presented. In this chapter, the author used a double sandblasting technique to roughen the zirconia surface to allow the deposition of amorphous AN in the surface pores

from a solution that had double the concentration of inorganic ions compared to the conventional SBF. The solution was named as 2.0SBF to distinguish it from the conventional SBF. Finally, bioactivity assessment of the AN deposited zirconia samples was done by the conventional SBF immersion test.

In chapter 3, the author discusses AN treatment of 3Y-TZP to induce hydroxyapatite formation. A different approach is presented in this chapter for the deposition of AN, as mentioned in chapter 2. Two different kinds of calcium-phosphate (Ca-P) aqueous solutions were employed with a similar concentration of calcium and phosphate ions as the conventional SBF. The only difference was that one Ca-P solution additionally contained magnesium (Mg) ions also at a similar concentration as the conventional SBF, while the other Ca-P solution did not contain Mg ions. The rest of the ions were removed to distinguish the effect of Mg ions on the formed hydroxyapatite in SBF. The temperature during this treatment also varied compared to chapter 2 for the efficient deposition of the AN. 3Y-TZP samples, which were first chemically etched with hydrofluoric (HF) acid, were soaked in the two types of prepared Ca-P solutions and then immersed in SBF to investigate the apatite forming ability. Finally, the effect of HF etching and the role of the Mg ions on the adhesive strength of the hydroxyapatite layer to HF-etched 3Y-TZP surface was evaluated.

In chapter 4, the preparation of bioactive PVDF is presented. A similar type of AN preparation using 2.0SBF was considered as in chapter 2, and the AN-PVDF composite films were fabricated using the solvent casting technique. Finally, apatite forming ability was checked using SBF immersion and the effect of soaking period on the thickness of the hydroxyapatite layer was also analyzed.

In chapter 5, the author presents a comparative study of the bioactivity of PCL and PVDF thin films incorporated with AN. A similar approach was utilized for the fabrication of AN-PCL thin films, as mentioned in chapter 3 for the AN-PVDF thin films. A significant difference in apatite forming ability was found with respect to the soaking period in the SBF and weight percentage of AN in PCL and PVDF, respectively. This point was further clarified by analyzing the surface properties of the PCL and the PVDF films.

In chapter 6, the summary of the content of the above chapters is presented, considering the general conclusion of the present thesis.

1.8 **References**

[1] K. Fukai, H. Ogawa, P. Hescot, Oral health for healthy longevity in an ageing society: maintaining momentum and moving forward, Int. Dent. J., 67 (2017), 3-6.

[2] S. Wu, X. Liu, K.W.K. Yeung, C. Liu, X. Yang, Biomimetic porous scaffolds for bone tissue engineering, Mater. Sci. Eng. R. Rep., 80 (2014), 1-36.

[3] A.S. Greenwald, S.D. Boden, R.L. Barrack, M.P. Bostrom, V.M. Goldberg, M. Yaszemski, C.S. Heim, The evolving role of bone-graft substitutes, Proceedings of the American Academy of Orthopaedic Surgeons, 77th Annual Meeting (2010), p. 6.

[4] M.M. Stevens, Biomaterials for bone tissue engineering, Mater. Today, 11 (2008), 18-25.

[5] K. Rezwana, Q. Z. Chena, J. J. Blakera, A. R. Boccaccini, Biodegradable and bioactive porous polymer/inorganic composite scaffolds for bone tissue engineering, Biomaterials, 27 (2006), 3413-3431.

[6] K.C. Dee, R. Bizios, Mini-review: Proactive biomaterials and bone tissue engineering, Biotechnol. Bioeng., 50 (1996), 438-442.

[7] K. J. L. Burg, S. Porter, J. F. Kellam, Biomaterial developments for bone tissue engineering, Biomaterials, 21 (2000), 2347-2359.

[8] D.F. Williams, B. In the Williams Dictionary of Biomaterials Liverpool University Press, Liverpool, 33-54, 1999.

[9] L.L. Hench, R. J. Splinter, W. C. Allen, T. K. Greenlee, Bonding mechanisms at the interface of ceramic prosthetic materials, J. Biomed. Mater. Res., 5 (1971), 117-141.

[10] J. Chevalier, L. Gremillard, Ceramics for medical applications: A picture for the next 20 years, J. Eur. Ceram. Soc., 29 (2009),1245-1255.

[11] W. Rieger, Ceramics in orthopedics - 30 years of evolution and experience, pp. 283-294. In: World tribology forum in arthroplasty. Ed. by C. Rieker, S. Oberholzer, U. Wyss, Hans Huber, Bern, Switzerland, 2001.

[12] J.R. Davis, Overview of biomaterials and their use in medical devices, pp. 1-5. In: Handbook of materials for medical devices. Ed. by J.R. Davis, ASM International, Materials Park, Ohio, 2003.

[13] I.G. Turner, Ceramics and glasses, pp. 3-39. In: Biomedical materials. Ed. by R. Narayan, Springer, New York, 2009.

[14] L.L. Hench, Bioceramics, J. Am. Ceram. Soc., 81 (1998), 1705-1728.

[15] L.L. Hench, Chronology of bioactive glass development and clinical applications, New Journal of Glass and Ceramics, 3 (2013), 67-73.

[16] H. Oonishi, L.L. Hench, J. Wilson, F. Sugihara, E. Tsuji, M. Matsuura, S. Kin, T. Yamamoto, S. Mizokawa, Quantitative comparison of bone growth behavior in granules of Bioglass®, A-W glass-ceramic, and hydroxyapatite, J. Biomed. Mater. Res., 51 (2000), 37-46.

[17] H. Oonishi, L.L. Hench, J. Wilson, F. Sugihara, E. Tsuji, S. Kushitani, H. Iwaki, Comparative bone growth behavior in granules of bioceramic materials of various sizes, J. Biomed. Mater. Res., 44 (1999), 31-43.

[18] W.G. Billotte, Ceramic Biomaterials, pp. 21-55. In: Biomaterials Principles and Applications. Ed. by J. B. Park, J. D. Bronzino, CRC Press, Boca Raton, 2002.

[19] L.L. Hench, Ö. Andersson, Bioactive Glasses, pp. 25-40. In: An introduction to bioceramics, Advanced Series in Ceramics 2. Ed. by L.L. Hench, world scientific, Singapore, 1993.

[20] G. Heness, & B. B..Nissan, Innovative bioceramics, Mater. Forum, 27 (2003), 104-114.

[21] L.L. Hench, J.K. West, Biological applications of bioactive glasses, Life Chem. Reports, 13 (1996), 187-241.

[22] L.L. Hench, I.D. Xynos, L.D. Buttery, J.M. Polak, Bioactive materials to control cell cycle, Mater. Res. Innovations, 3 (2000), 313-323.

[23] I.D. Xynos, M.V. Hukkanen, J.J. Batten, L.D. Buttery, L.L. Hench, J.M. Polak, Bioglass 45S5 stimulates osteoblast turnover and enhances bone formation In vitro: implications and applications for bone tissue engineering, Calcif. Tissue Int., 67, 321-329, 2000.

[24] O.H. Andersson, K.H. Karlsson, K. Kangasniemi, Calcium phosphate formation at the surface of bioactive glasses in vivo, J. Non-Cryst. Solids, 119 (1990), 290-296.

[25] L.L. Hench, J. Wilson, Surface-active biomaterials, Science, 226 (1984),630-636.

[26] L.L. Hench, Bioceramics-from concept to clinic, J. American Ceramic. Society, 47 (1991), 1487-1510.

[27] W. Cao, L. L. Hench, Bioactive materials, Ceram. Inter., 22 (1996), 493-507.

[28] D.M. Liu, T. Troczynski, W.J.T. Seng, Water based sol–gel synthesis of hydroxyapatite: process development, Biomaterials, 22 (2001),1721-1730.

[29] K. DeGroot, C.P.A.T. Klein, J.G.C. Wolke, J.M.A. Blieck-Hogervorst, Chemistry of calcium phosphate bioceramics, pp. 3-16. In: CRC Handbook of Bioactive Ceramics, Vol II, Calcium Phosphate and Hydroxylapatite Ceramics. Ed.by T. Yamamuro, L.L. Hench, J. Wilson, CRC press, Boca Raton, 1990.

[30] M.I. Kay, R. A. Young, A.S. Posner, Crystal Structure of Hydroxyapatite, nature, 204 (1964), 1050-1052.

[31] J.C. Elliott, P.E. Mackie, R.A. Young, Monoclinic hydroxyapatite, Science, 180 (1973), 1055-1057.

[32] H. Morgan, R. M. Wilson, J. C. Elliott, S. E. P. Dowker, P. Anderson, Preparation and characterisation of monoclinic hydroxyapatite and its precipitated carbonate apatite intermediate, Biomaterials, 21 (2000), 617-627.

[33] J.C. Elliott, Hydroxyapatite and nonstoichiometric apatites, pp. 111-175. In: Structure and chemistry of the apatites and other calcium orthophosphates. Ed. by J.C. Elliott, Elsevier Science, Amsterdam 2013.

[34] H. Aoki, in Medical applications of hydroxyapatite, pp. 13-74, Ishiyaku Euro America, St. Louis, (1994)

[35] M. Wang, Materials selection and scaffold fabrication for tissue engineering in orthopaedics, pp.263-275. In: Advanced Bioimaging Technologies in Assessment of the Quality of Bone and Scaffold Materials,

Part 1. Ed. by: L. Qin, H.K. Genant, J.F. Griffth, K. Suileung, Springer, berlin, Heidelberg, 2007.

[36] P. Ducheyne, Q. Qiu, Bioactive ceramics: the effect of surface reactivity on bone formation and bone cell function, Biomaterials, 20 (1999), 2287-2303.

[37] S. Miao, W. Weng, K. Cheng, P. Du, G. Shen, G. Han, S. Zhang, Sol–gel preparation of Zn-doped fluoridated hydroxyapatite films, Surf. Coat. Technol., 198 (2005), 223-226.

[38] R.Z. LeGeros, Formation and Stability of Synthetic Apatites: Effect of Some Elements. pp. 82-107. In: Calcium phosphates in oral biology and medicine, Monographs in oral science, Ed. by R. Z. LeGeros, 1991.

[39] K. de Groot, Bioceramics of calcium phosphate, CRC press, Boca Raton, Florida (1983).

[40] K.S. Katti, Biomaterials in total joint replacement, Colloids Surf. B, 39 (2004),133-142.

[41] M. Neo, S. Kotani, T. Nakamura, T. Yamamuro, C. Ohtsuki, T. Kokubo, Y. Bando, A Comparative Study of Ultrastructures of the Interfaces Between Four Kinds of Surface-Active Ceramic and Bone, J. Biomed. Mater. Res., 26 (1992),1419-1432.

[42] M. Neo, T. Nakamura, C. Ohtsuki, T. Kokubo, T. Yamamuro, Apatite Formation on Three Kinds of Bioactive Material at an Early Stage in Vivo: A Comparative Study by Transmission Electron Microscopy J. Biomed. Mater. Res., 27 (1993), 999-1006.

[43] J.R. Jones, Bioactive glass, pp.266-283. In: Bioceramics and their Clinical Applications, Ed. By T. Kokubo, Woodhead publishing, UK ,2008.

[44] B.V. Rejda, J.G. Peelen, K. de Groot, Tri-calcium Phosphate as a Bone Substitute, J. Bioeng., 1 (1977), 93-97.

[45] C. Rey, C. Combes and C. Drouet, Tricalcium phosphate-based ceramics, pp. 326-366. In: Bioceramics and their Clinical Applications, Ed. By T. Kokubo, Woodhead publishing, UK, 2008.

[46] U.M. Gross, C. Müller-Mai, C. Voigt, Ceravital® Bioactive Glass-Ceramics, pp. 105-124. An Introduction to Bioceramics. Ed. by L.L. Hench and J. Wilson, World Scientific, Singapore,1993.

[47] W. Höland, W. Vogel, Machinable and Phosphate Glass-Ceramics. pp. 125-137. In: An Introduction to Bioceramics. Ed. by L.L. Hench and J. Wilson, World Scientific, Singapore,1993.

[48] T. Kokubo, Bioactive glass ceramics: properties and applications, Biomaterials, 12 (1991), 155-163.

[49] T. Kokubo, M. Shigematsu, Y. Nagashima, M. Tashiro, T. Nakamura, Yamamuro, S. Higashi, Apatite- and Wollastonite-Containg Glass-Ceramics for Prosthetic Application, Bulletin of the Institute for Chemical Research, Kyoto University 60(3-4), (1982), 260-268.

[50] T. Kokubo, Surface chemistry of bioactive glass-ceramics, J. Non-Cryst. Solids., 120 (1990), 138-151.

[51] T. Kokubo, A/W Glass-ceramic: Processing and properties. Pp. 284-301. In: An Introduction to bioceramics. Ed. by L.L. Hench, J. Wilson, World Scientific, Singapore,1993.

[52] P.N. De Aza, A.H. De Aza, P. Pena, S. De Aza, Bioactive glasses and glass-ceramics, Bol. Soc. Esp. Ceram. 46 (2007), 45-55.

[53] W. Höland, W. Vogel, K. Naumann, J. Gummel, Interface reactions between machinable bioactive glass-ceramics and bone, J. Biomed. Mater. Res., 19 (1985), 303-312.

[54] T. Kitsugi, T. Nakamura, T. Yamamura, T. Kokubu, T. Shibuya, M. Takagi, SEM-EPMA observation of three types of apatite-containing glass-ceramics implanted in bone: The variance of a Ca-P-rich layer, J. Biomed. Mater. Res., 21 (1987), 1255-1271.

[55] T. Kitsugi, T. Yamamuro, T. Nakamura, T. Kokubo, Bone bonding behavior of MgO-CaO-SiO_2-P_2O_5-CaF_2 glass (Mother glass of A.W-glass-ceramics), J. Biomed. Mater. Res., 23 (1989), 631-648.

[57] K. Ohura, T. Nakamura, T. Yamamuro, T. Kokubo, Y. Ebisawa, Y. Kotoura, M. Oka, Bone-bonding Ability of P_2O_5-free CaO.SiO_2 Glasses, J. Biomed. Mater. Res. 25 (1991), 357-365.

[58] C. Ohtsuki, H. Kushitani, T. Kokubo, S. Kotani, T. Yamamuro, Apatite formation on the surface of Ceravital-type glass-ceramic in the body, J. Biomed. Mater. Res. 25 (1991),1363-1370.

[59] C. Loty, J.M.Sautier, H. Boulekbache, T. Kokubo, H.M. Kim, N. Forest, In vitro bone formation on a bone-like apatite layer prepared by a biomimetic process on a bioactive glass–ceramic, J. Biomed. Mater. 49 (2000), 423-434.

[60] T. Kokubo, Recent progress in glass-based materials for biomedical applications, J. Ceram. Soc. Japan, 99 (1991), 974-982.

[61] A. Rabiei, S. Sandukas, Processing and evaluation of bioactive coatings on polymeric implants, J. Biomed. Mater. Res. Part A, 101 (2013), 2621-2629.

[62] A.R. Boccaccinia, M. Erol, W.J. Stark, D. Mohn, Z. Hong, J. F. Mano, Polymer/bioactive glass nanocomposites for biomedical applications: A review, Compos. Sci. Technol.,70 (2010), 1764-1776.

[63] A. Sola, D. Bellucci, V. Cannillo, A. Cattini, Bioactive glass coatings: a review, Surf. Eng., 27 (2011), 560-572.

[64] B.G.X. Zhang, D.E Myers, G.G Wallace, M. Brandt, P.F.M. Choong, Bioactive coatings for orthopaedic implants-recent trends in development of implant coatings, Int. J. Mol. Sci. 15 (2014), 878-921.

[65] A. Sáenz, E. Rivera, W. Brostow, V.M. Castano, Ceramic biomaterials: an introductory overview, J. Mater. Educ., 21 (1999), 267-276.

[66] Y. Yang, K.H. Kim, J. L. Ong, A review on calcium phosphate coatings produced using a sputtering process-an alternative to plasma spraying, Biomaterials, 26 (2005), 327-337.

[67] W.S.W. Harun, R.I.M. Asri, J. Alias, F.H. Zulkifli, K. Kadirgama, S.A.C. Ghani, J.H.M. Shariffuddin, A comprehensive review of hydroxyapatite-based coatings adhesion on metallic biomaterials, Ceram. Int., 44 (2018), 1250-1268.

[68] S. Bose, S. Tarafder, A. Bandyopadhyay, Hydroxyapatite coatings for metallic implants, in pp. 143-157. In: Hydroxyapatite (Hap) for Biomedical Applications, Ed. by M. Mucalo, Woodhead Publishing, UK, 2015.

[69] P. Habibovic, F. Barrère, C. A. Van Blitterswijk, K. de Groot Pierre Layrolle, Biomimetic Hydroxyapatite Coating on Metal Implants, J. Am. Ceram. Soc., 85 (2002), 517-522.

[70] N. Koju, P. Sikder, Y. Ren H. Zhou, S.B Bhaduri, Biomimetic coating technology for orthopedic implants, Curr. Opin. Chem. Eng, 15 (2017), 49-55.

[71] T.Kokubo, H. Takadama, How useful is SBF in predicting in vivo bone bioactivity?, Biomaterials, 30 (2009), 2175-2179.

[72] T. Kokubo, H. Takadama, Simulated body fluid (SBF) as a standard tool to test the bioactivity of implants, pp. 97-109. In: Handbook of Biomineralization: Biological Aspects and Structure Formation. Ed. by E. Beuerlein, Wiley-VCH, Germany,2007.

[73] H. Takadama, T. Kokubo, In vitro evaluation of bone bioactivity, pp. 165-182. In: Bioceramics and their Clinical Applications, Ed. By T. Kokubo, Woodhead publishing, UK, 2008.

[74] T. Kokubo, H. Kushitani, S. Sakka, T. Kitsugi, T. Yamamuro, Solutions able to reproduce in vivo surface-structure changes in bioactive glass-ceramic A-W, J. Biomed. Mater. Res., 24 (1990), 721-34.

[75] Y. Abe, M. Kawashita, T. Kokubo, T. Nakamura, Effects of solution on apatite formation on substrate in biomimetic process, J. Ceram. Soc. Japan, 109 (2001), 106-109.

[76] M. Tanahashi, T. Yao, T. Kokubo, M. Minoda, T. Miyamoto, T. Nakamura, T. Yamamuro, Apatite formation on organic polymers by biomimetic process using Na_2O-SiO_2 glasses as nucleating agent, J. Ceram. Soc. Japan, 102 (1994), 822-829.

[77] M. Tanahashi, T. Yao, T. Kokubo, M. Minoda, T. Miyamoto, T. Nakamura, T. Yamamuro, Apatite coated on organic polymers by biomimetic process: improvement in its adhesion to substrate by NaOH treatment, J. Appl. Biomater., 5 (1994) 339-347.

[78] G.J. Liu, F. Miyaji, T. Kokubo, H. Takadama, T. Nakamura, A. Murakami. Apatite-organic polymer composites prepared by a biomimetic process: improvement in adhesion of the apatite layer to the substrate by ultraviolet irradiation, J. Mater. Sc.i Mater. Med., 9 (1998), 285-290.

[79] T. Kokubo, M. Hanakawa, M. Kawashita, M. Minoda, T. Beppu, T. Miyamoto, T. Nakamura, Apatite formation on non-woven fabric of carboxymethylated chitin in SBF, Biomaterials, 25 (2004). 4485-4488.

[80] M. Tanahashi, T. Yao, T. Kokubo, M. Minoda, T. Miyamoto, T. Nakamura & T. Yamamuro, Apatite coated on organic polymers by biomimetic process: improvement in adhesion to substrate by HCl treatment. J. Mater. Sci.: Mater. Med., (1995), 319-326.

[81] T. Yao, M. Hibino, T. Yabutsuka, US Patent, 8,512,732 (2013), Japanese Patent 5, 252, 399 (2013).

[82] T. Yao, M. Hibino, S. Yamaguchi and H. Okada, US Patent, 8,178,066 (2012), Japanese Patent 5, 261, 712 (2013).

[83] K. Masamoto, S. Fujibayashi, T. Yabutsuka, T. Hiruta, B. Otsuki, Y. Okuzu, K. Goto, T. Shimizu, Y.Shimizu, C. Ishizaki, K. Fukushima, T. Kawai, M. Hayashi, K. Morizane, T. Kawata, M. Imamura, S. Matsuda, In vivo and in vitro bioactivity of a "precursor of apatite" treatment on polyetheretherketone, Acta Biomater., 91 (2019), 48-59.

[84] T. Yabutsuka, K. Fukushima, T. Hiruta, S. Takai, T.Yao, Fabrication of bioactive fiber-reinforced PEEK and MXD6 by incorporation of Precursor of apatite, J. Biomed. Mater. Res B, 106 (2017), 2254-2265.

[85] T. Yabutsuka, I. Fukushima, T. Hiruta, S. Takai, T. Yao, Effect of pores formation process and oxygen plasma treatment to hydroxyapatite formation on bioactive PEEK prepared by incorporation of precursor of apatite, Mater. Sci. Eng., 81 (2017), 349-358.

[86] C. Piconi, G. Maccauro, Zirconia as a ceramic biomaterial, Biomaterials, 20 (1999), 1-25.

[87] W. Burger, H.G. Richter, C. Piconi, R. Vatteroni, A. Cittadini, M. Boccalari, New Y-TZP powders for medical grade zirconia, J. Mater. Sci.: Mater. Med., 8 (1997), 113-118.

[88] R.H. Hannink, P.M. Kelly, B.C. Muddle, Transformation toughening in zirconia-containing ceramics, J. Am. Ceram. Soc., 83 (2000), 461-487.

[89] R.C. Garvie, R.H. Hannink, R.T. Pascoe, Ceramic steel?, Nature, 258 (1975), 703-704.

[90] L. Sennerby, A. Dasmah, B. Larsson, M. Iverhed, Bone tissue responses to surface-modified zirconia implants: a histomorphometric and removal torque study in the rabbit. Clin. Implant Dent. R., 7 (2005), 13-20.

[91] J.D. Langhoff, K. Voelter, D. Scharnweber, M. Schnabelrauch, F. Schlottig, T. Hefti, K.; Kalchofner, K. Nuss, B. von Rechenberg, Comparison of chemically and pharmaceutically modified titanium and zirconia implant surfaces in dentistry: a study in sheep., Int. J. Oral. Max. Impl., 37 (2008), 1125-1132.

[92] M. Uchida, H.M.; Kim, T. Kokubo, M. Nawa, T. Asano, K. Tanaka, T. Nakamura, Apatite-forming ability of a zirconia/alumina nano-composite induced by chemical treatment. J. Biomed. Mater. Res., 60 (2002), 277-282.

[93] M. Dehestani, D. Zemlyanov, E. Adolfsson, L.A. Stanciu, Improving bioactivity of inert bioceramics by a novel Mg-incorporated solution treatment. App.l. Surf. Sci., 425 (2017), 564-575.

[94] H. Kawai, The Piezoelectricity of poly(vinylidene Fluoride), Jpn. J. App.l. Phys., 8 (1969), 975-976.

[95] G.W. Hastings, F.A. Mahmud, Electrical effects in bone, J. Biomed. Eng., 10 (1988), 515-521.

[96] J. Ficat, G. Escourron, M.J. Fauran, R. Durroux, P. Ficat, C. Lacabanne, F. Micheron, Osteogenesis induced by bimorph polyvinylidene fluoride films, Ferroelectrics, 51 (1983), 121-128.

[97] C. Ribeiro, V. Sencadas, D.M. Correia, S.L. Méndez, Piezoelectric polymers as biomaterials for tissue engineering applications, Colloids Surf. B, 136 (2015), 46-55.

[98] A.H. Rajabi, M. Jaffe, T.L. Arinzeh, Piezoelectric materials for tissue regeneration: A review, Acta Biomaterialia, 24 (2015),12-23.

[99] N. Bölgen, Y.Z. Menceloglu, K. Acatay, I. Vargel, E. Piskin, In vitro and in vivo degradation of non-woven materials made of poly(epsilon-Caprolactone) nanofibers prepared by electrospinning under different conditions, J. Biomater. Sci. Polym., 16 (2005), 1537-1555.

Chapter 2

Fabrication of Bioactive Zirconia by Doubled Sandblasting Process and Incorporation of Apatite Nuclei

2.1 **Introduction**

Zirconia (ZrO_2) is known as ‘ceramic steel’ owing to its superior toughness, strength, fatigue and wear resistance. As a biomaterial, zirconia is biologically inert and biocompatible showing no adverse reaction with tissues or cytotoxicity and are widely used as ball head of total hip replacements (THR) [1]. Hence, the impartation of bone bonding ability to zirconia makes it more attractive to be widely used as dental or orthopedic implant materials.

An effective approach is to provide biological interaction between the non-bioactive implant with the host tissue is to coat the surface of the implant with suitable bioactive materials [2]. Biomimetic coating of various materials such as calcium phosphates, hydroxyapatite, and bioactive glass makes the connection between the host bone and the implant which helps for the tissue regeneration [3]. These surface treatments help to attain bioactivity without affecting the mechanical and chemical integrity of the material.

A suitable method for the deposition of calcium phosphate on the surface of non-bioactive materials is simulated body fluid (SBF) treatment. SBF has inorganic ion concentration similar to human blood plasma. When either the pH or temperature of SBF is raised, fine particles of calcium phosphate are precipitated in the fluid. It is reported that these particles actively induce

Table 1 Ion concentration of simulated body fluid (SBF), 2.0SBF and human blood plasma.

	Ion concentration / mM		
	SBF	2.0SBF	Blood plasma
Na^+	142.0	284.0	142.0
K^+	5.0	10.0	5.0
Ca^{2+}	2.5	5.0	2.5
Mg^{2+}	1.5	3.0	1.5
Cl^-	147.8	295.6	103.0
HCO_3^-	4.2	8.4	27.0
HPO_4^{2-}	1.0	2.0	1.0
SO_4^{2-}	0.5	1.0	0.5

hydroxyapatite formation in SBF and are named as apatite nuclei (AN) [4,9]. In previous studies, various bioactive polymers, ceramics and metals have been successfully prepared through biomimetic AN surface treatment [5,6]. It was found that for stainless steel (SUS316L) the surface roughness and surface area greatly affect hydroxyapatite formation in SBF and its adhesion to the surface of the specimen [7]. In the case of doubled sandblasting process in which the surface of the stainless-steel specimens was subsequently subjected to two different kind of particles having a significant difference in diameters increased the surface area and the surface roughness of the specimens compared with specimens subjected to single kind of particles [6].

In this chapter, the author presents the work aimed to introduce bioactivity to doubled sandblasted zirconia specimens by a surface biomimetic treatment of AN and tested their in vitro hydroxyapatite-forming ability through SBF treatment.

2.2 **Materials and Methods**

2.2.1 *Preparation of SBF*

Reagent-grade NaCl, $NaHCO_3$, KCl, $K_2HPO_4 \cdot 3H_2O$, $MgCl_2 \cdot 6H_2O$, $CaCl_2$ and Na_2SO_4 were dissolved in ultrapure water. By this treatment, SBF with the ion composition as shown in Table 1 was prepared and buffered at pH 7.40 with tris(hydroxymethyl)aminomethane and 1 M HCl at 36.5 °C [8].

2.2.2 *Preparation of zirconia specimens*

Zirconia plates (AS ONE Corporation, Osaka, Japan) were cut into 2 mm thick specimens using a diamond wheel. Then the specimens were sintered at 1450 °C for 2 hours to increase the strength and toughness. The surface of

zirconia specimens was treated by the doubled sandblasting process using alumina grinding particles with 14.0 μm and subsequently 3.0 μm for average particle size, respectively to increase the surface roughness and area. After the sandblasting process, the specimens were thoroughly cleansed in distilled water by ultrasonication technique. The surface morphology was observed by SEM imaging and EDX analysis before and after the sandblasting treatment.

2.2.3 *AN treatment*

AN were prepared from a SBF, which has a doubled concentration of inorganic ions compared to conventional SBF as mentioned in Table 1 and hence was named as 2.0SBF to differentiate it from the conventional SBF. When pH of 2.0SBF containing zirconia, specimens was raised to 8.2 at 36.5 °C and subsequently held at a constant temperature of 36.5 °C for 1 day, particles of AN precipitated out from the solution into the micrometers sized cavities of the roughened surface on the blasted zirconia specimens. The surface of the specimens was characterized by SEM imaging and EDX analysis for AN precipitation.

2.2.4 *Evaluation of bioactivity*

The bioactivity of the specimens was evaluated by SBF test. The specimens were immersed in the physiological SBF (pH 7.4 at 36.5 °C) for 1 day and 3 days, respectively. After the test, the surface of the specimens was analyzed by thin film X-ray diffraction (XRD; Rint 2500, Rigaku, Japan), scanning electron microscopy (SEM; SU6600, Hitachi High- Technologies, Japan) and energy dispersive X-ray analysis (EDX; XFlash® 5010, Bruker, Germany). The TF-XRD measurements were conducted using CuKα radiation.

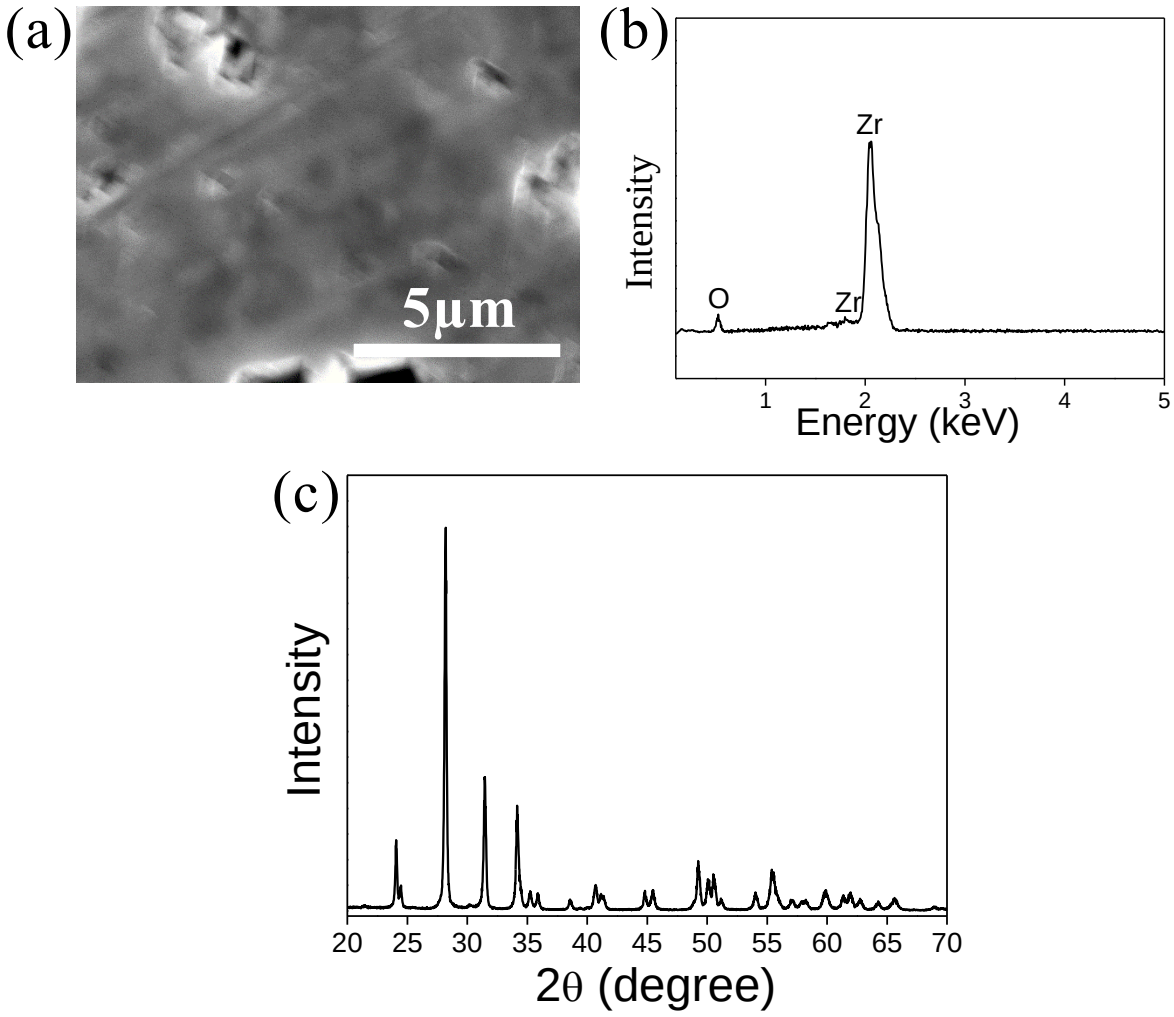

Figure 1 (a) SEM image, (b) EDX profile and (c) XRD plot of the surface of the as-purchased zirconia.

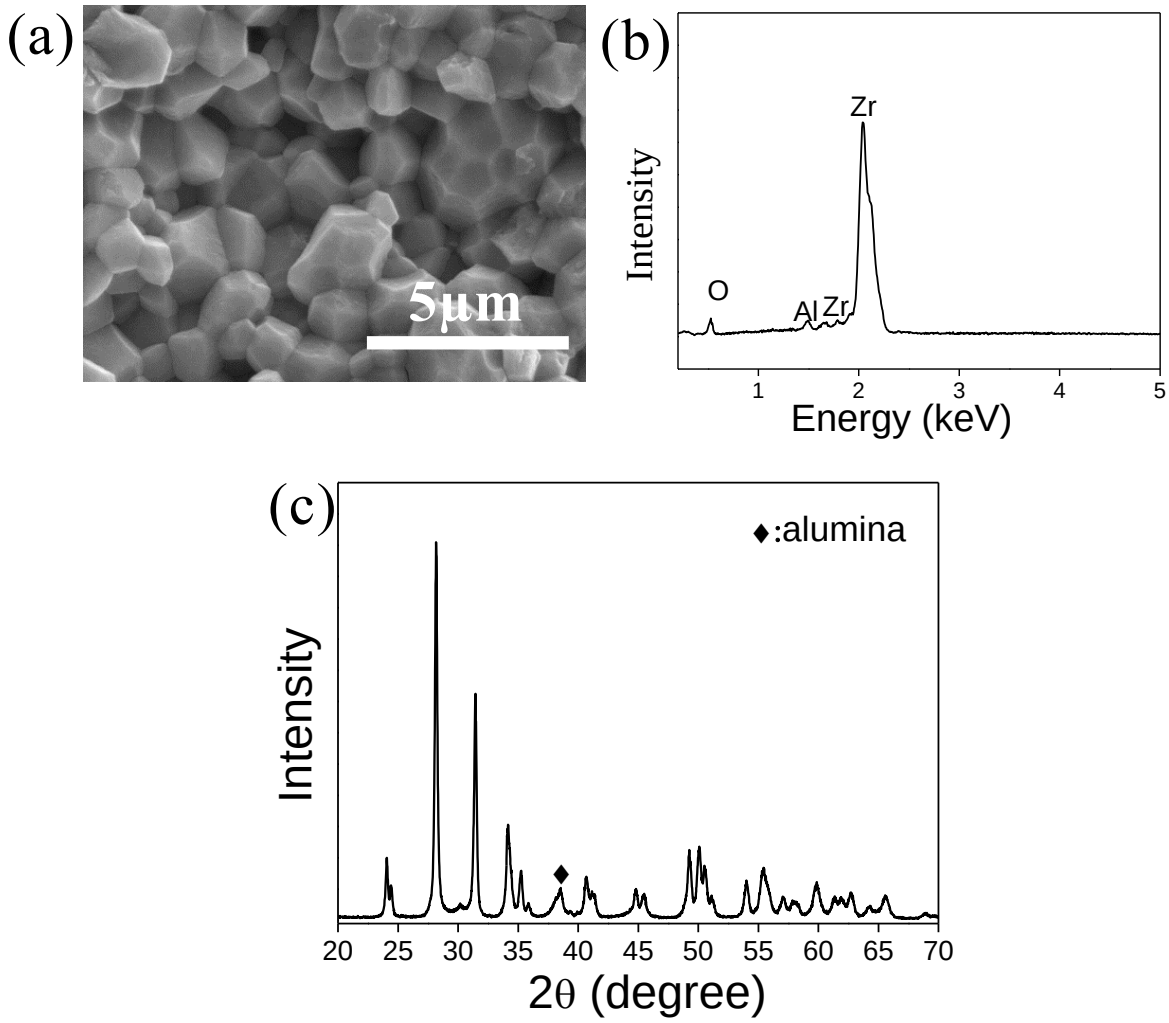

Figure 2 (a) SEM image, (b) EDX profile and (c) XRD plot of the zirconia specimen after the sandblasting treatment.

2.3 **Results and Discussion**

Figure 1 shows the SEM image, EDX profile and XRD plot for the as-purchased zirconia specimen after diamond cutting. SEM image in Figure 1(a) revealed a relatively smooth surface of the specimen compared to specimen after sandblasting treatment in Figure 2(a) shown. In the EDX profile, peaks of Zr and O were obtained from the specimen. Zirconia has three different crystalline phases at different temperatures, monoclinic, tetragonal and cubic. At low temperatures, the most stable phase of zirconia has a monoclinic [10]. The XRD plot in Figure 1(c) shows that the specimens have predominantly monoclinic phase.

Figure 2 shows the SEM image, EDX profile and XRD plot of the zirconia specimen after sandblasting treatment. Alumina particles with 14.0 μm and subsequently 3.0 μm in average particle size were used for the sandblasting. From the SEM image, it is clearly observed that the surface of the specimen was significantly roughened by the sandblasting treatment forming dense cavities of few microns in size. In addition to Zr and O peaks, Al peak was also observed in the EDX profile. The XRD plot showed the monoclinic phase of zirconia with a distinct peak at 38.5° representing α-phase alumina, however, it is difficult to distinguish other peaks as it coincides with zirconia peaks. Alumina peak is observed is due the remained alumina particles after ultrasonication treatment.

Figure 3 compares the SEM image and EDX profile of the fine polished and doubled sandblasted zirconia specimens after the AN treatment. Spherical particles were found to be evenly deposited in the cavities of roughened surface of the doubled sandblasted specimen. Ca peak was newly observed in

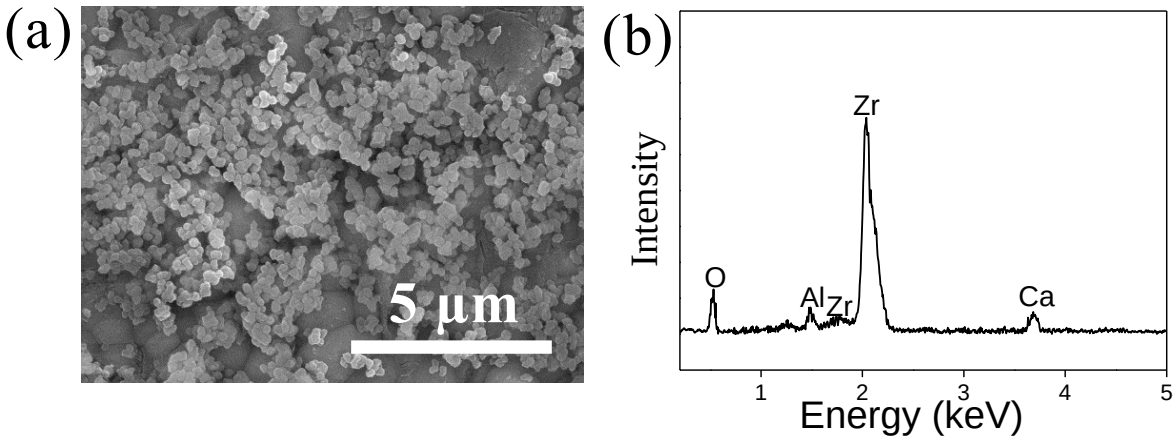

Figure 3 (a) SEM image and (b) EDX profile of the doubled sandblasted zirconia specimens after AN treatment.

the EDX profile for the sandblasted specimen. However, it was difficult to distinguish the P peak as it coincides with the Zr peak. Hence, it can be concluded the AN treatment led to the successful deposition of AN particles into the micrometers sized cavities of the roughened surface of the doubled sand blasted specimens whereas smooth surface of fine polished specimens did not deposit AN.

Figure 4 compares the SEM images and EDX profiles of the doubled sandblasted zirconia specimens after 1 day and 3 days immersion in SBF, respectively. In the SEM images (a, c), flake-like crystallites, which characterize bone-like apatite formed in SBF, were observed covering the surface of the specimens. In the EDX profiles (b, d), a highly intensified Ca peak is observed from the specimen for the 1 day soaking period which further increased for 3 days soaking period.

Figure 5 compares the XRD plots of doubled sandblasted zirconia specimens before and after immersion in the SBF. Although a peak at 31.7° which is the most prominent peak representing hydroxyapatite was difficult to distinguish as it coincides with zirconia peak, a peak of hydroxyapatite was detected at 26° in addition to zirconia and alumina peaks. The intensity of the peak was higher for specimens soaked for 3 days in SBF compared to 1 day. This suggests the increase in thickness of the hydroxyapatite layer, which complements the EDX results described in Figure 4(b, d). Taking SEM, EDX and XRD results into consideration, it is concluded that the precipitated AN induced hydroxyapatite formation within 1 day and subsequently crystal growth of the induced hydroxyapatite proceeded in SBF such as other related bioactive materials reported in our previous papers [6,7,11].

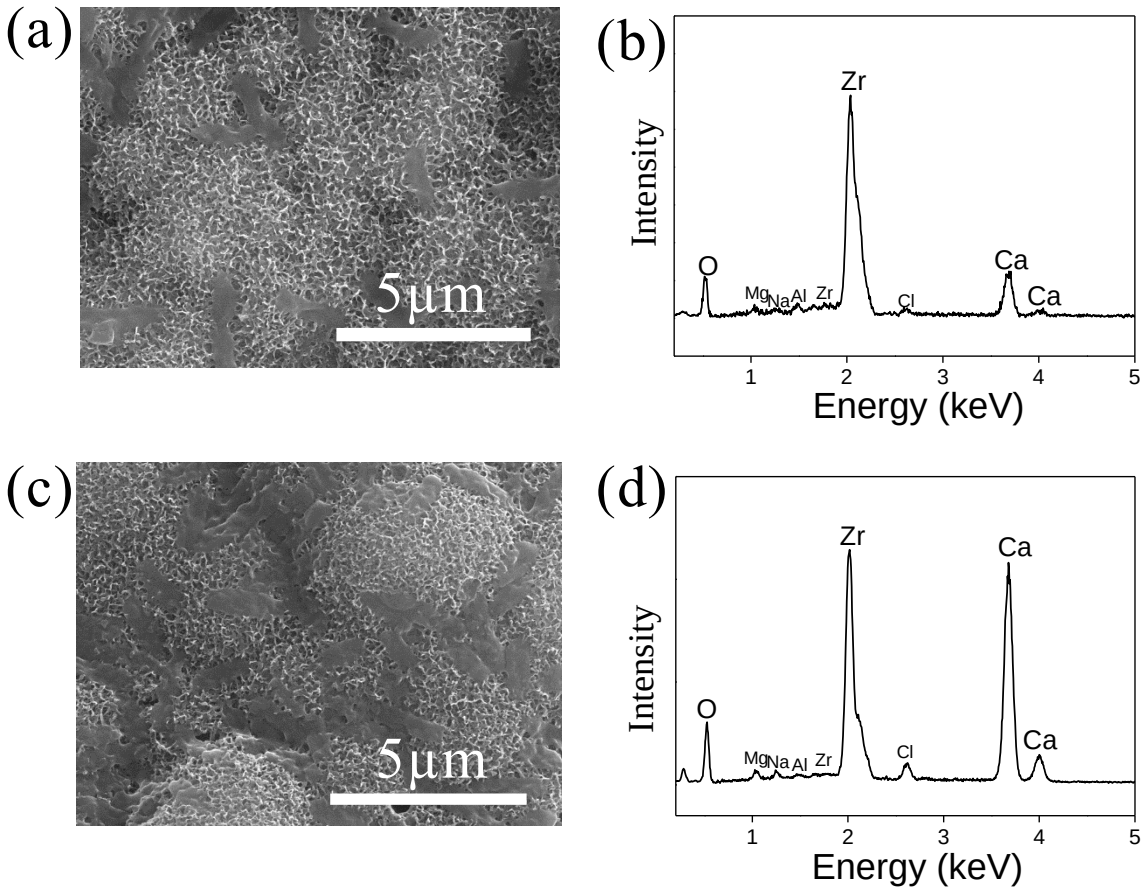

Figure 4 (a, c) SEM images and (b, d) EDX profiles of the AN precipitated zirconia specimen after (a, b) 1 day and (c, d) 3 days immersion in SBF, respectively.

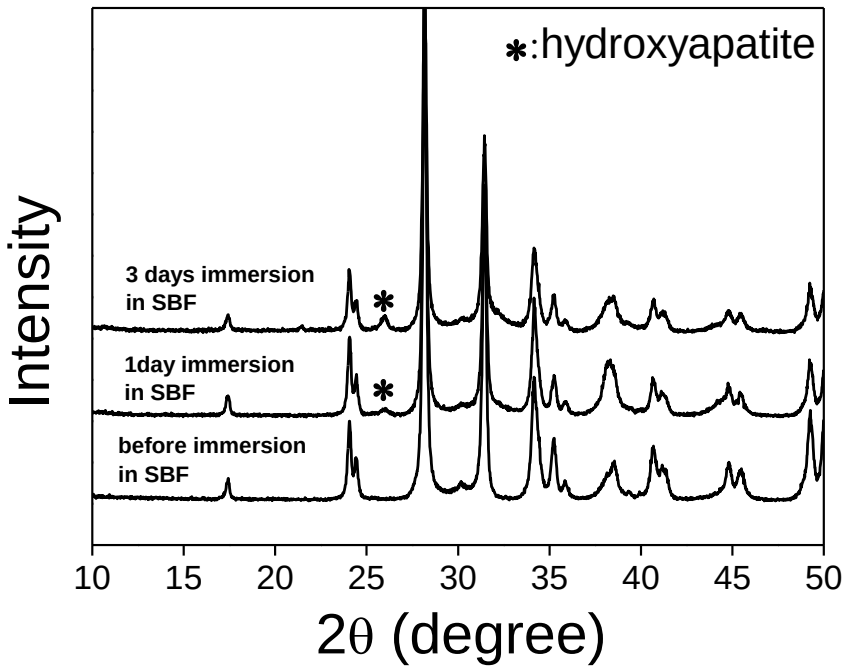

Figure 5 Comparison of XRD plots of zirconia specimens before and after immersion in SBF for 1 day and 3 days.

2.4 **Conclusion**

AN were successfully incorporated on the surface of the zirconia specimens, through the formation of micrometers sized cavities by the doubled sandblasting method. Hydroxyapatite formation was observed in 1 day on the surface of the sandblasted specimens after immersion in SBF. The increase in soaking time period in SBF increased the quantity of hydroxyapatite deposited onto the surface of these specimens as observed from EDX and XRD analysis. Bioactivity was successfully induced to the bioinert zirconia by incorporation AN.

2.5 **References**

[1] J. Chevalier, What future for zirconia as a biomaterial?, Biomaterials, 27 (2006) 535-543.

[2] Y. Abe, T. Kokubo, T. Yamamuro, Apatite coating on ceramics, metals and polymers utilizing a biological process, J. Mater. Sci., 1 (1990), 233-238.

[3] M. Bohner, L. Galea, N. Doebelin, Calcium phosphate bone graft substitutes: Failures and hopes, J. Eur. Ceram. Soc., 32 (2012) 2663-2671.

[4] T. Yao, M. Hibino, S. Yamaguchi and H. Okada, US Patent, 8, 178, 066 (2012), Japanese Patent 5, 261, 712 (2013).

[5] T. Yao, M. Hibino, T. Yabutsuka, US Patent, 8, 512, 732 (2013), Japanese Patent 5, 252, 399 (2013).

[6] T. Yabutsuka, H. Mizutani, S. Takai, T. Yao, Fabrication of bioactive Co-Cr-Mo-W alloy by using doubled sandblasting process and apatite nuclei treatment, Trans. Mat. Res. Soc. Japan, 43 (2018) 143-147.

[7] T. Yabutsuka, R. Karashima, S. Takai, T. Yao, Effect of doubled sandblasting process and basic simulated body fluid treatment on fabrication of bioactive stainless steels. Materials, 11 (2018), 1334.

[8] T. Kokubo, H. Takadama, How useful is SBF in predicting in vivo bone bioactivity? Biomaterials, 27 (2006), 2907-2915.

[9] T. Yao, T. Yabutsuka, Japanese Patent, 6, 071, 895 (2017).

[10] J. Chevalier, L. Gremillard, A. V. Virkar, D. R. Clarke, The tetragonal-monoclinic transformation in zirconia: Lessons learned and future trends, J. Am. Ceram. Soc., 92 (2009), 1901-1920.

[11] T. Yabutsuka, K. Fukushima, T. Hiruta, S. Takai, T. Yao, Fabrication of bioactive fiber reinforced PEEK and MXD6 by incorporation of precursor of apatite, J. Biomed. Mater. Res. B Appl. Biomater., 106 (2018), 2254-2265.

Chapter 3

Role of Magnesium and the Effect of Surface Roughness on the Hydroxyapatite-Forming Ability of Zirconia Induced by Biomimetic Aqueous Solution Treatment

3.1 Introduction

Zirconia is a highly considered biocompatible ceramic, also known as the "ceramic steel" due to its outstanding mechanical properties [1,2]. This makes it highly suitable for orthopedic applications such as femoral heads and acetabular cups, and, in dentistry, it is used as crowns, implants, and abutments [2,3]. Zirconia exists in three crystal forms monoclinic, cubic, and tetragonal. Pure zirconia is in the monoclinic phase at room temperature. When mixed with ≈3 mol% yttria, zirconia is stabilized into the tetragonal phase and known as yttria-stabilized zirconia or tetragonal zirconia polycrystal (3Y-TZP). 3Y-TZP shows excellent fracture toughness and flexural strength, which is due to the phase transformation toughening that enhances resistance to the propagating crack. As the 3Y-TZP surface is subjected to stress, the crack stress field leads to phase transformation from tetragonal to monoclinic. This phase change causes a volumetric change that seals the advancing crack [1,4]. Another noteworthy characteristic of zirconia is its aesthetic value of being white in color, which is in contrast to metals that can cause metallic discoloration [5,6].

A bioactive material is defined as "a material that elicits a specific biological response at the interface of the material, which results in the formation of a bond between the tissues and the material" [7]. When a bioinert

material is grafted into the bone defect, it spontaneously gets coated with non-calcified fibrous tissues. This isolates it from the surrounding living tissue, which is a normal immune response of the human body against exogenous substances [8,9]. Hench discovered 45S5 Bioglass in the year, 1969, which had the ability to form an interfacial bond between the tissue and the implant. This interesting feature of bioactive glasses as described by Hench is due to the formation of carbonated hydroxyapatite when exposed to the physiological fluid [10]. Since then, a great deal of effort has been put to the development of novel bioactive materials. In the field of orthopedics, ceramic biomaterials such as bioglass and calcium phosphate-based materials such as hydroxyapatite (HAp) are highly considered due to their inherent bioactive nature [11,12]. Hence, one of the best approaches to induce bioactivity to a bioinert material is to coat it with suitable bioactive material, such as HAp.

For bioinert ceramics and metallic materials, various techniques such as sputtering, electrophoretic deposition, and plasma spraying have been employed to provide a suitable HAp coating. However, these methods require a high-temperature treatment or are expensive [13,14]. High-temperature treatment starting from 850 °C results in dehydroxylation of HAp that creates vacancies in the lattice and leads to the formation of oxyhydroxyapatite. After further heating beyond the temperature of 1050 °C, HAp starts to decompose into other variants of calcium phosphates such as tetracalciumphosphate, tricalciumphosphate, and CaO [15]. These variants have faster dissolution and degradation rates compared to HAp which decreases the chemical stability in the body for a longer period [16].

Kukobo et. al. developed simulated body fluid (SBF), which has an ionic concentration and a pH similar to human blood plasma. SBF can mimic the

formation of HAp on the surface of a bioactive material similar to the living body. Kukobo's method has widely been used to test and predict the bioactivity of a material [17,18]. Biomimetic calcium phosphate-based coatings utilizing SBF or modified SBF treatments are the simplest methods to impart bioactivity to bioinert material as it requires low processing temperatures and the HAp formed in biomimetic coating resembles the bone's HAp [19-23].

Various studies have been performed on in-vitro bioactivity assessment of surface coated zirconia or zirconia composites in SBF. These studies reported bone-like apatite formation ranging from 3 days to 4 weeks of immersion in the SBF [24-30]. Magnesium (Mg) is a biofunctional cation present, abundantly, in the human body, which promotes bone cells activation and proliferation. It also influences bone strength, mineralization, and growth [31,32]. Many studies have also investigated the role of Mg in enhancing osteointegration [33-36].

In this chapter author reports the fabrication of the bioactive 3Y-TZP by treating it with calcium and phosphate ions-containing biomimetic aqueous solution (Ca-P solution), which also included Mg ions in a very short immersion period of 1 day in the SBF. Hydrofluoric acid (HF) etching was performed on the 3Y-TZP surface to enhance the surface roughness. Then the samples were treated with two different types of Ca-P solutions one with and the other without Mg ions, to analyze the effect of Mg ions on the HAp layer formed in the SBF. SBF immersion test was carried out in order to investigate the HAp-forming ability of thus-treated 3Y-TZP. Furthermore, the effect of the Mg ion on the adhesive strength of the HAp layer on the etched 3Y-TZP surface was also investigated.

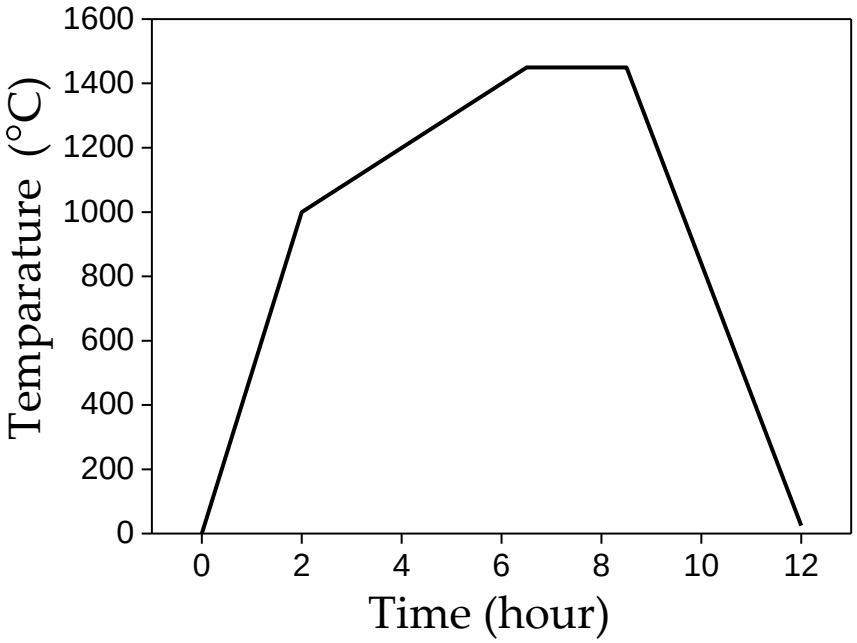

Figure 1 Sintering graph for 3Y-TZP samples.

3.2 **Materials and Methods**

3.2.1 *Outline of the Experimental Procedure*

The experimental procedure consisted of the following steps. First, HF etching was performed on the polished 3Y-TZP surface. Then, 3Y-TZP samples were subjected to two types of Ca-P solution treatments. SBF immersion test of both types of Ca-P solution treated samples was carried to check the HAp-forming ability. Finally, the adhesive strength of the formed apatite layer was evaluated.

3.2.1.1 *Fabrication of the Roughened 3Y-TZP Samples*

Dental-grade 3Y-TZP (KZR-CAD ZR, Yamakin Co. Ltd., Osaka, Japan) was cut into 2 mm thick samples using a diamond wheel. Sintering was performed according to prerequisite instructions provided by the manufacturer, the 3Y-TZP samples were sintered at peak sintering temperature of 1450 °C as shown in Figure 1, the sintering cycle consisted of four steps. First, the samples were heated from room temperature to 500 °C in 2 h (≈4 °C·min^{-1}). Next, the temperature was raised from 500 °C to the peak temperature in 4.5 h (≈3.5 °C·min^{-1}). Then, dwelling at the peak sintering temperature was done for two hours. Finally, the samples were gradually allowed to cool down. After sintering the samples were polished using #400 abrasive-coated paper. Then, HF etching was performed by immersing the 3Y-TZP samples in HF (~55% concentration, Stella Chemifa Co., Ltd. Izumi factory, Osaka, Japan) at room temperature for 10 min. The obtained samples were ultrasonically cleansed for 10 min each in acetone and distilled water, respectively, and were air-dried. Finally, surface analysis and surface

Table 1 Name of solutions, concentration of the dissolved reagents in each Ca-P solution, and name of the precipitated calcium phosphate particles.

$K_2HPO_4 \cdot 3H_2O$ [mM]	$MgCl_2 \cdot 6H_2O$ [mM]	$CaCl_2$ [mM]	Name of Precipitated Calcium Phosphate Particles
1.0	0	2.5	“Mg0” particles
1.0	1.5	2.5	“Mg1.5” particles

roughness measurement of the samples before and after the HF etching treatment as described in the Section 3.2.2.1.

3.2.1.2 *Ca-P Solution Treatments*

Two types of Ca-P solutions were prepared in distilled water containing $K_2HPO_4 \cdot 3H_2O$, $MgCl_2 \cdot 6H_2O$ and $CaCl_2$ as mentioned in Table 1 at 25.0 °C and a pH 8.2 using tris(hydroxymethyl)aminomethane (THAM; Hayashi Pure Chemical Ind., Ltd., Osaka, Japan). One solution containing Mg ions and was named as “Mg1.5” solution while the other which did not contain Mg ions was named as “Mg0” solution. The concentration of the “Mg1.5” solution contained similar concentrations of Ca^{2+}, Mg^{2+}, and phosphate ions as compared to the conventional SBF, while “Mg0” solution only contained Ca^{2+} and phosphate ions also similar to conventional SBF [17,18]. The rest of the ions were removed from the solution to distinguish the effect of Mg ions on the HAp formed in the SBF. The HF-etched 3Y-TZP samples were soaked in these solutions at 70 °C for 1 day. After 1 day, white particles were observed to be precipitated in both types of solutions, which were denoted as “Mg0” and “Mg1.5” particles, respectively. Then, the 3Y-TZP samples were removed from the solution and the remaining white precipitates were collected by vacuum filtration using 0.025 μm membrane filter (Merck Millipore, Burlington, MA, USA).

3.2.1.3 *HAp-Forming Ability*

After the Ca-P solution treatments the 3Y-TZP samples were immersed in the SBF to test the HAp-forming ability for 1 and 7 days. The SBF solution was replenished after 3 days. The SBF was prepared by the method reported

by Kokubo et. al. [17,18] and buffered at pH = 7.4, 36.5 °C by disillusion of THAM.

3.2.1.4 *Analysis*

The surface of the samples mentioned in the Section 3.2.1.1 and 3.2.1.3 and collected Ca-P particles mentioned in Section 3.2.1.2 were analyzed by high-vacuum field emission scanning electron microscopy (SEM; SU6600, Hitachi High-Technologies Corporation, Tokyo, Japan), energy dispersive X-ray spectrometry (EDS; XFlash® 5010, Bruker, Billerica, MA, USA), thin film X-ray diffraction (XRD; Rint 2500, Rigaku Corporation, Tokyo, Japan), and Fourier transform infrared spectroscopy (FTIR; FT-720, Horiba, Ltd., Kyoto, Japan). Before SEM and EDX observation the samples were coated with Au using sputtering method. For SEM analysis acceleration voltage of 20 kV, emission current of 32 μA and secondary electron detector was used. For the EDX an acceleration voltage of 20 kV and emission current of 32 μA was used. After the SEM and EDX analysis, XRD measurement of the same samples were performed to compare the surface morphology and composition with corresponding crystalline phase from 2θ range of 20°–80° using angle step of 1°. min^{-1}. FTIR analysis was done using Attenuated total reflectance (ATR).

3.2.2 *Evaluation of Materials Properties*

3.2.2.1. *Surface Roughness Measurement*

Surface roughness of the surface of the samples before and after the HF etching mentioned in Section 3.2.1.1 was compared by ultra-precision point autofocus laser probe 3D measuring instrument (NH-3SP, Mitaka Kohki Co.,

Ltd., Tokyo, Japan). In this measurement, heights at 10,021 points in 10 by 10 μm^2 of base area were probed and root mean square surface roughness (S_q) was calculated from the probed information. One sample was used for each condition.

3.2.2.2 *Evaluation of Ca/P Atomic Ratio and Mg Release*

Measurement of inductively coupled plasma atomic emission spectroscopy (ICP; ICP7510, Shimadzu Corporation, Kyoto, Japan) was carried out to find out the concentration ($ppm \cdot mL^{-1}$) of the Ca, P, and Mg present in the Ca-P particles precipitated in the "Mg0" or "Mg1.5" solution. The obtained results were used to calculate the Ca/P and Mg/Ca ratio for each type of mentioned particles and compared with Ca/P and Mg/Ca ratio of the commercially obtained HAp (Fujifilm Wako Pure Chemical, Osaka, Japan). For this, both types of Ca-P particles along with commercially obtained HAp were dissolved 1 M HCl (Fujifilm Wako Pure Chemical, Osaka, Japan) at a concentration of 0.1 $mg \cdot mL^{-1}$. Three samples of solutions for each type of the mentioned particles were used for concentration measurement of the respective ions. Release of Mg ions from "Mg1.5" particles in 0.01 M phosphorus buffered saline (PBS, pH = 7.2~7.4 at 25 °C, Fujifilm Wako Pure Chemical) was also measured. Similarly, the "Mg1.5" particles were dispersed in PBS at a concentration of 0.1 $mg \cdot mL^{-1}$ and stored at the physiological temperature of 36.5 °C. The particles were filtered using vacuum filtration using 0.025 μm membrane filter and concentration of Mg ions released in PBS was measured at the various time period. Three samples of solutions were prepared for measurement of concentration of Mg ions at each time period. One-way analysis of variance (ANOVA) followed by Tukey's multiple comparison tests

was carried out to calculate *p* values and to evaluate significant difference between Ca/P ratios for HAp, “Mg0”, and “Mg1.5” particles.

3.2.2.3 *Adhesive Strength Test*

The bonding strength between the HF-etched 3Y-TZP samples and the formed HAp film was examined and compared with polished 3Y-TZP samples after 14 days SBF immersion by a modified ASTM C633 method [37–39]. Two sets each containing three samples for polished 3Y-TZP samples treated with “Mg0” and “Mg1.5” solutions, respectively, and two sets each containing five samples for HF-etched 3Y-TZP samples treated with “Mg0” and “Mg1.5” solutions, respectively, were tested. The surfaces of the samples were attached to the SUS jigs (10 by 10 mm^2) using Araldite® glue (Nichiban Co., Ltd., Tokyo, Japan) and the tensile load was applied at 1 $mm \cdot min^{-1}$ of cross-head speed until fracture occurred at the HAp film and the samples interface using a universal testing machine (Model AGS-H Autograph, Shimadzu Corporation, Kyoto, Japan). Finally, the fractured surface was analyzed by SEM and EDX surface scanning to find out the mechanism of the fracture. One-way ANOVA followed by Tukey’s multiple comparison tests was carried out to calculate *p* values and to evaluate significant difference between adhesive strength for each type of the above-mentioned conditions.

3.3 **Results and Discussion**

Figure 2 compares the effect of HF etching on the 3Y-TZP surface. In this study, the samples were subjected to HF etching treatment for 10 min aimed to enhance the roughness of the 3Y-TZP surface. As it can be observed from the SEM and 3D images in Figure 2 (a-d) that the surface got highly roughened

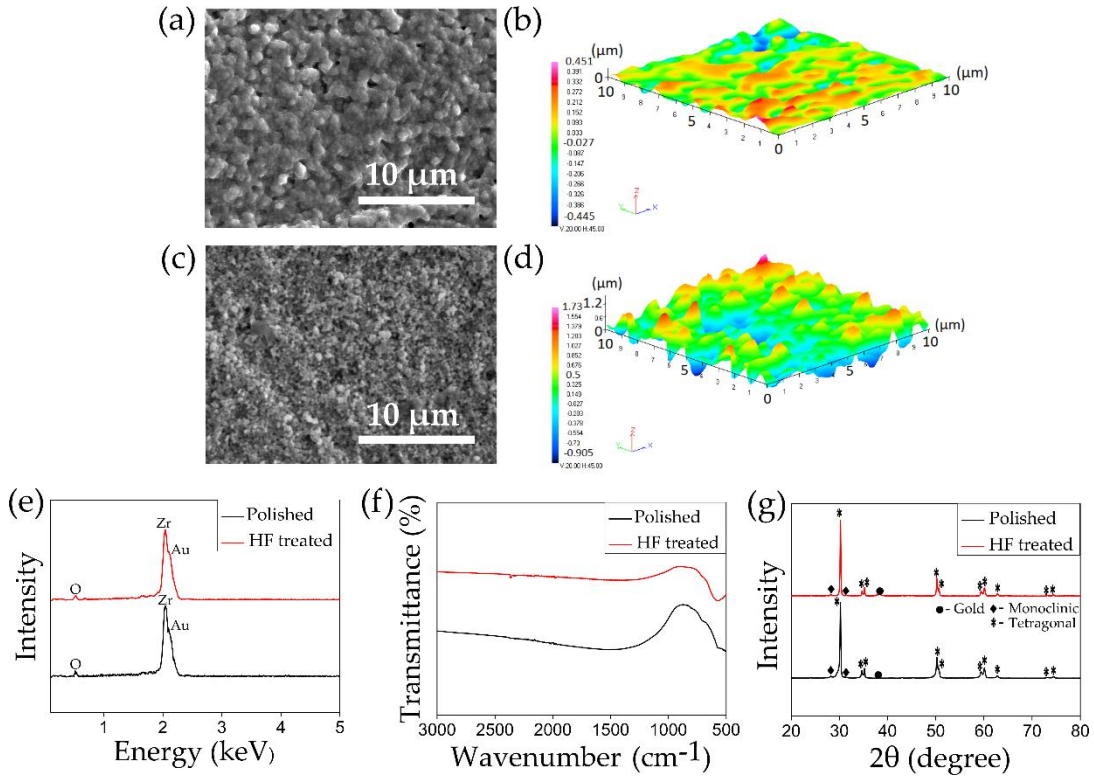

Figure 2 (a,c) SEM images and (b,d) 3D images of (a,b) polished and (c,d) hydrofluoric acid (HF)-treated tetragonal zirconia polycrystal (3Y-TZP) surface. (e) EDX, (f) FTIR, and (g) XRD plots comparing 3Y-TZP samples before (polished) and after HF etching.

after the treatment. The S_q value rose from ~0.126 μm to ~0.401 μm before and after the HF etching. In the EDX spectra as shown in Figure 2 (e) peaks representing Zr and O was detected and in the FTIR spectra, as shown in Figure 2 (f), peak at ~500 cm^{-1} was observed, which is fundamental infrared frequency attributable to ZrO_2. XRD patterns as depicted in Figure 2 (g), both before and after the HF etching revealed the presence of the tetragonal phase predominantly, a small characteristic peak representing the monoclinic phase was detected at 28.1°. 3Y-TZP is highly chemically stable, the peaks in the EDX, FTIR, and XRD plots before and after the HF treatment showed no significant change, which means that there was no change in the elemental composition. Noro et al. showed the effect of various surface treatments on the roughness of the 3Y-TZP surface. It was observed that a combination of sandblasting and HF etching (~44%) for 15 min resulted in a highly roughened surface with superhydrophilic properties [40]. Noro's work and the experimental methodology in the present study shows the effectiveness of the HF treatment in enhancing surface roughness of the 3Y-TZP.

Figure 3 represents the SEM images, EDX, FTIR, and XRD plots of both types of Ca-P particles. In the SEM images, coarse particles with uneven shape and size were observed for "Mg0" particles while fine spherical particles having size around 1–2 μm were observed in the case of "Mg1.5" particles. As was observed from strong peaks from PO_4^{3-} of P = O stretching at 1050cm^{-1} and 580 cm^{-1} in FTIR spectra and strong Ca and P peaks in the EDX spectra, both types of particles were composed of calcium phosphate. A Mg peak was observed in the EDX spectrum only for the case of "Mg1.5" particles that indicated the incorporation of Mg in the particles. In the Figure 3 (e) the

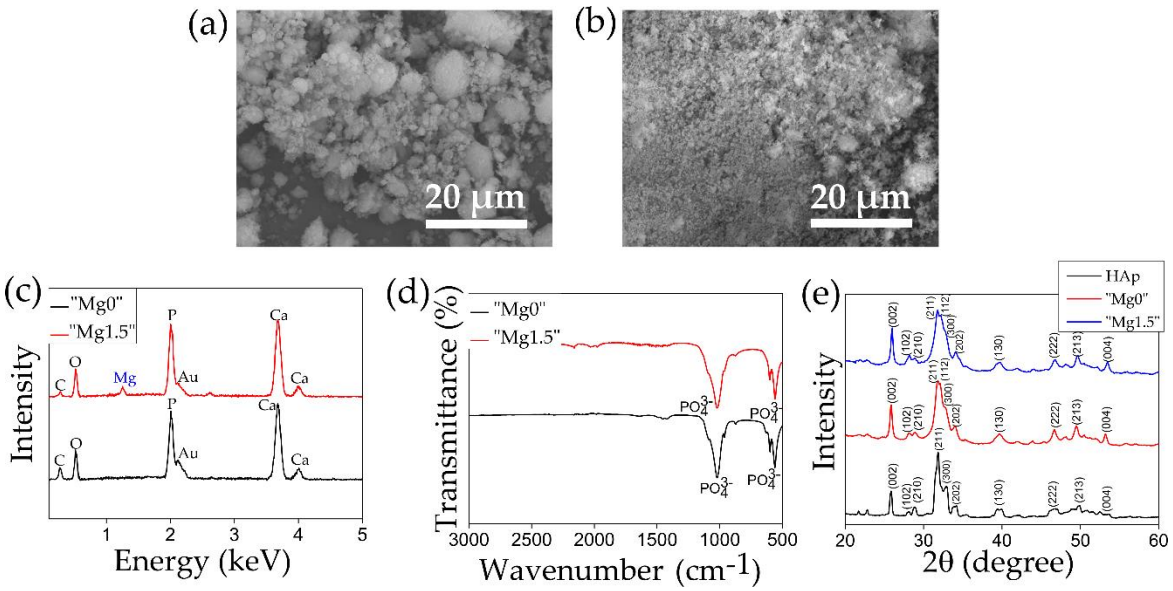

Figure 3 SEM images of (a) “Mg0” and (b) “Mg1.5” particles. (c) EDX and (d) FTIR plots comparing properties of “Mg0” and “Mg1.5” particles. (e) XRD plots comparing properties of “Mg0” and “Mg1.5” particles with commercially obtained HAp.

XRD patterns of “Mg0” and “Mg1.5” were compared with the commercially obtained HAp. Both “Mg0” and “Mg1.5” particles patterns resembled that of typical HAp, however, slightly broader peaks suggested that these particles were slightly less crystalline compared to HAp.

The formation of HAp in an aqueous solution from the constituent ions can be described by the following chemical equilibrium.

$$10Ca^{2+} + 6PO_4^{3-} + 2OH^- \rightleftharpoons Ca_{10}(PO_4)_6(OH)_2 \quad (1)$$

Considering the equation ionic activity product (IP) of the apatite in the solution can be described by the following formula, where “γ” is the activity coefficient and “[ ]” is the concentration of each ion.

$$IP \rightleftharpoons (\gamma Ca^{2+})^{10}(\gamma PO_4^{3-})^6(\gamma OH^-)^2 \times [Ca^{2+}]^{10}[PO_4^{3-}]^6[OH^-]^2 \quad (2)$$

Conventional SBF at a physiological condition, i.e., pH 7.40, and 36.5 °C, is supersaturated with respect to HAp. However, because of the high energy obstacles with respect to the HAp formation, the HAp formation is only induced in certain active surfaces as in the case of bioactive materials [41]. The rate of precipitation and the properties of precipitated Ca-P particles such as crystallinity and phase are strongly dependent on the physical parameters such as temperature and pH, and, also, the concentration of the constituent ions in the aqueous solution. In this work, the concentration of the respective ions (Ca, Mg, and phosphate) in the both types of aqueous solution were kept the same as the conventional SBF. The pH of the aqueous solution was raised to 8.2, which presumably resulted in the increase of IP value because of the increase in the OH^- concentration. Initially, the temperature was maintained

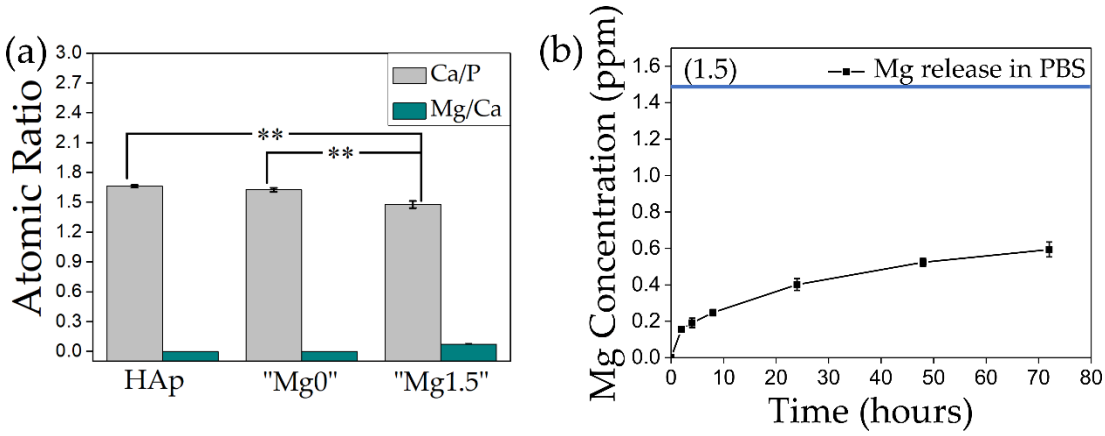

Figure 4 (a) Comparison of Ca/P and Mg/Ca atomic ratio of "Mg0" and "Mg1.5" particles with commercially available HAp particles. In (a), the symbol "**" indicates $p < 0.01$, and no symbol indicates $p > 0.05$ by one-way ANOVA followed by the Tukey's tests. (b) release behavior of Mg ions from "Mg1.5" particles in the PBS. In (b), blue straight line shows 1.503 ppm which was assumed concentration if all the Mg contained in the "Mg1.5" particles had been released to the phosphorus buffered saline (PBS).

at 25 °C during the preparation of the solution to slow the precipitation of particles and then raised and held at 70 °C to accelerate the precipitation. This method successfully resulted in the formation of Ca-P particles in a 1 day time period from both types of solutions.

HAp crystallization is greatly affected by the presence of additional ion besides Ca^{2+} and PO_4^{3-} or HPO_4^{2-} such as Mg which results in the reduction of Ca/P ratio and decrease in crystal size. Bigi et. al. reported that the decrease in the crystal size was highly significant even at the lower Mg percentage, and crystal size decreases with the increase in Mg concentration up to 35 atomic percentage in respect of the total metal ions. At a concentration between 35 to 50 atomic percentage of Mg, the particles are amorphous and more than 50 percent results in the formation of different crystalline phases [42].

Figure 4 shows the results of ICP measurements. ICP measurement was performed to measure the concentration of Ca/P and Mg/Ca ratios in both types of Ca-P particles and compared against the commercially available HAp as represented in Figure 4a. The error bar shows the standard deviation obtained from the three samples used for concentration measurement for each type of particles. By applying one-way ANOVA followed by the Tukey's tests, Ca/P ratios of HAp and "Mg0" particles showed no statistical significance ($p > 0.05$). In contrast, statistical comparison of Ca/P ratio of HAp or "Mg0" particles with "Mg1.5" particles showed statistical significance ($p < 0.01$). It was difficult to compare the statistical significance of Mg/Ca ratio due to significantly low value and detection limitation. Mg ions incorporation in "Mg1.5" particles resulted in the significant decrease of Ca/P ratio. Compared against HAp Ca/P atomic ratio of 1.66, for "Mg0" and "Mg1.5" particles Ca/P ratio was found to be ~1.625 and ~1.478, respectively. For "Mg1.5" particles,

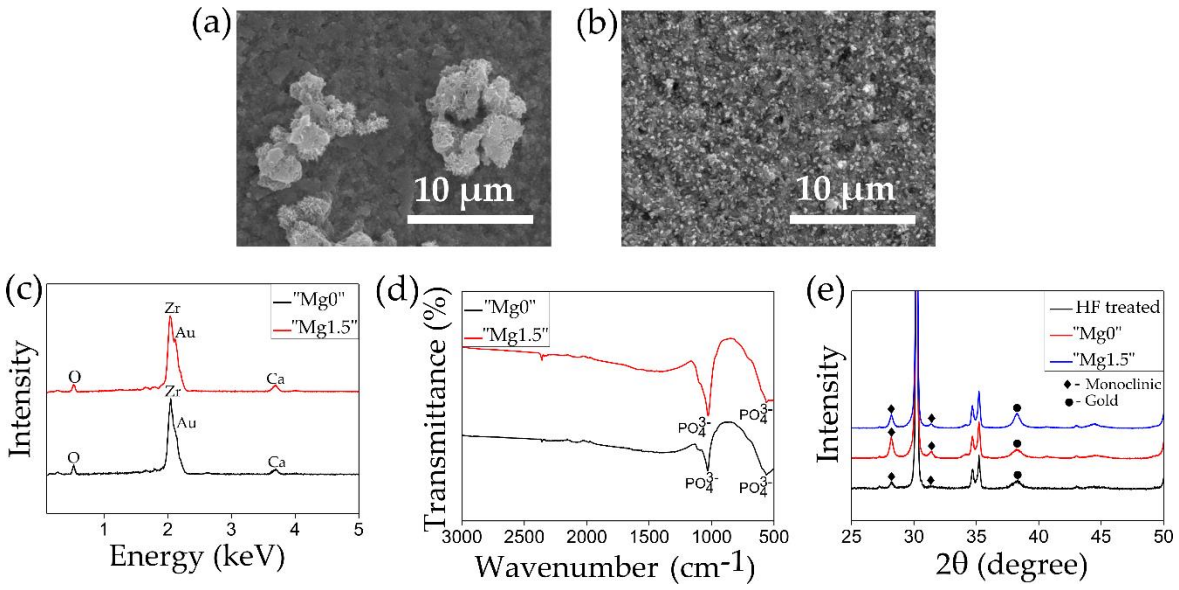

Figure 5 SEM images of HF-etched 3Y-TZP samples after (a) “Mg0” and (b) “Mg1.5” solution treatments. (c) EDX and (d) FTIR comparing properties of the HF-etched 3Y-TZP samples after “Mg0” or “Mg1.5” solution treatments. (e) XRD plots of HF-etched 3Y-TZP samples before and after “Mg0” or “Mg1.5” solution treatments.

the Mg/Ca atomic ratio was found to be ~0.0728 which is low, however, it significantly decreased the particle size as observed from the SEM images shown in Figure 3 (a,b). As it was mentioned in the explanation of the XRD peaks of both “Mg0” and Mg”1.5” particles in Figure 3 (e), the slight decrease in the crystallinity of the particles was attributed to the decreased Ca/P ratio as compared to commercial HAp as represented in Figure 4 (a).

Similarly, the release of Mg ions was measured from 0.1 mg of “Mg1.5” particles in 1 mL of PBS (at 36.5 °C) starting from 2 h to 3 days and at different time periods in between, as shown in Figure. 4b. The error bar represents the standard deviation obtained from three samples prepared for measurement of the concentration of Mg ions released from Mg”1.5” particles in PBS at respective time periods. When the same amount (0.1 mg) of “Mg1.5” particles were dissolved in same volume (0.1 mL) of 1M HCl to evaluate total Mg contained in the “Mg1.5” particles, the concentration of Mg ions in “Mg1.5” particles was found to 1.503 ppm. As it can be observed from the graph that a significant amount of Mg ions was released in 2 h and about ~26.6% of Mg ions were released from the particles in the PBS in 1 day and then Mg ions were continuously released. This result indicated that the “Mg1.5” particles showed sustained release of Mg ions in biological environment.

Figure 5 shows the SEM images, EDX and FTIR plots on the surface of the HF-etched 3Y-TZP samples after the 1 day Ca-P solution treatments. As it can be observed in the SEM images, “Mg0” solution treatment resulted in the deposition of coarse particles, of uneven shape and size in clusters, while in the case of “Mg1.5” solution treated samples, the 1–2 μm sized particles were homogenously deposited throughout the surface of the substrate. Such difference in the particle size was corresponded to the results of comparative

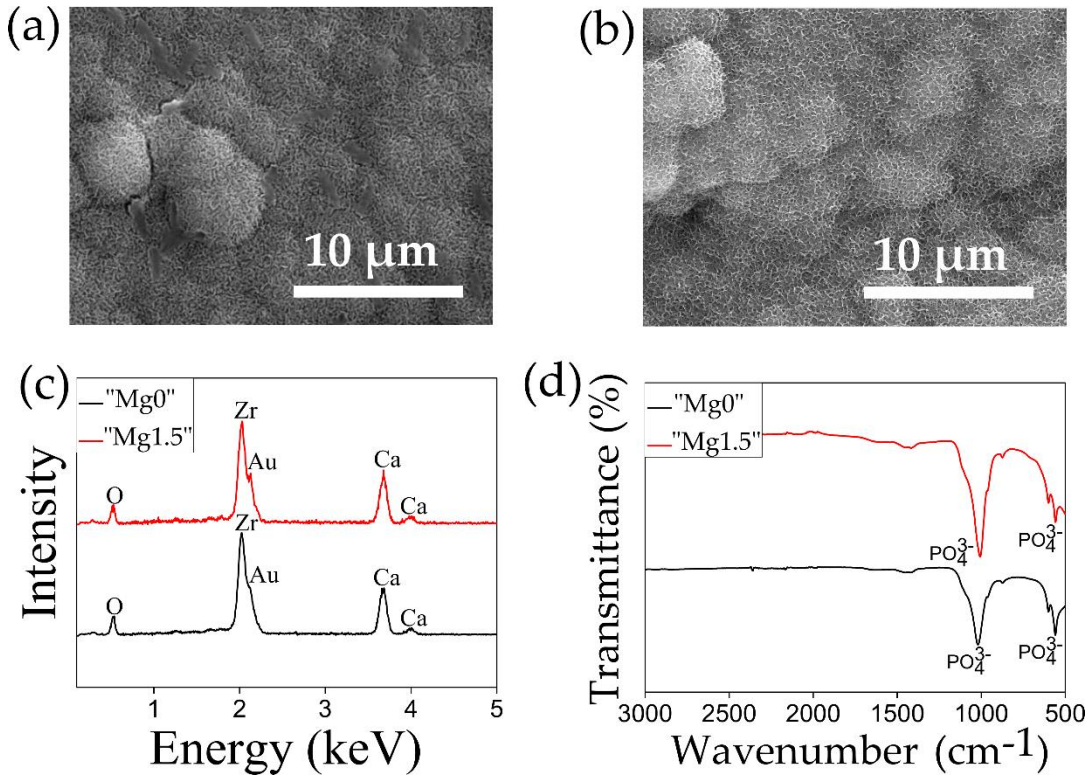

Figure 6 SEM images of (a) “Mg0” solution and (b) “Mg1.5” solution-treated 3Y-TZP samples after 1 day SBF immersion. (c) EDX and (d) FTIR plots comparing properties of “Mg0” solution and “Mg1.5” solution-treated 3Y-TZP samples after 1 day SBF immersion.

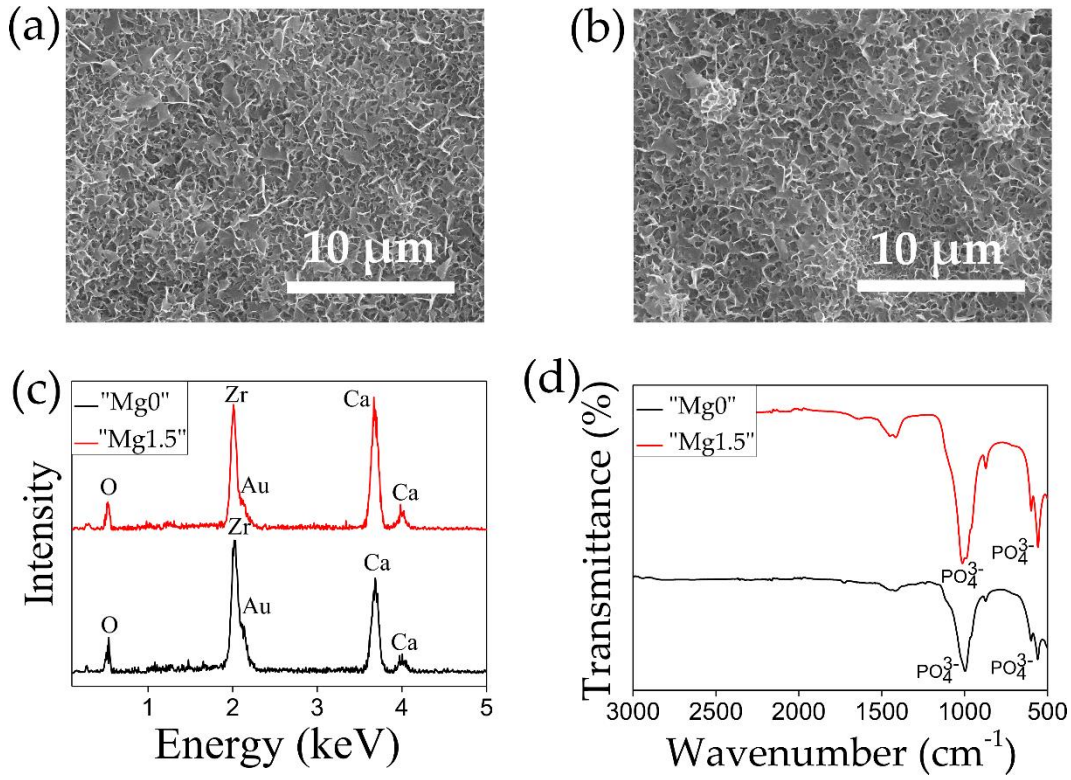

Figure 7 SEM images of (a) “Mg0” solution and (b) “Mg1.5” solution-treated 3Y-TZP samples after 1 day SBF immersion. (c) EDX and (d) FTIR plots comparing properties of “Mg0” solution and “Mg1.5” solution-treated 3Y-TZP samples after 3 days SBF immersion.

observation of the filtered “Mg0” and “Mg1.5” particles as shown in Figure 3. Small Ca peak was detected from both types of particles in the EDX spectra while P peak was difficult to distinguish as it coincided with the Zr peak. In the FTIR spectra for both types of solution treated samples, the strong peaks of P=O stretching from PO_4^{3-} at 1050 cm^{-1} and 580 cm^{-1} were observed. Comparing the XRD plots before (after HF treatment) and after the Ca-P solutions treatments, no significant difference was observed. The characteristics peaks of HAp at 26° and 32° were not observed, which was due to the formation of isolated and fewer number of Ca-P particles rather than a continuous layer leading to insufficient surface coverage. On the other hand, the peak at 28.1° representing the monoclinic phase of zirconia became more prominent. It is considered that this was due to the exposure to water, which caused tetragonal to monoclinic transformation in zirconia, a phenomenon known as low-temperature degradation [43,44]. The Au peak detected in the XRD is from the deposition of Au layer for the SEM observation of the same samples. In this study, both types of Ca-P solution treatments were designed to efficiently deposit Ca-P particles on the substrate. It is noteworthy to observe that the inclusion of Mg led to the nucleation of small and fine particles homogeneously throughout the substrate.

Figures 6 and 7 shows SEM images, EDX, and FTIR plots of both the types of HF-etched and subsequently Ca-P solution-treated 3Y-TZP samples after 1 day and 7 days of SBF immersion. From the SEM images, it can be observed that flake-like crystallites representing bone-like apatite, covered the whole surface of the 3Y-TZP samples for both types of Ca-P solution treatments irrespective of the Mg inclusion in the solution. Similarly, P=O stretching peaks at 1050 cm^{-1} and 580 cm^{-1} in the FTIR plots and high intensity Ca peak

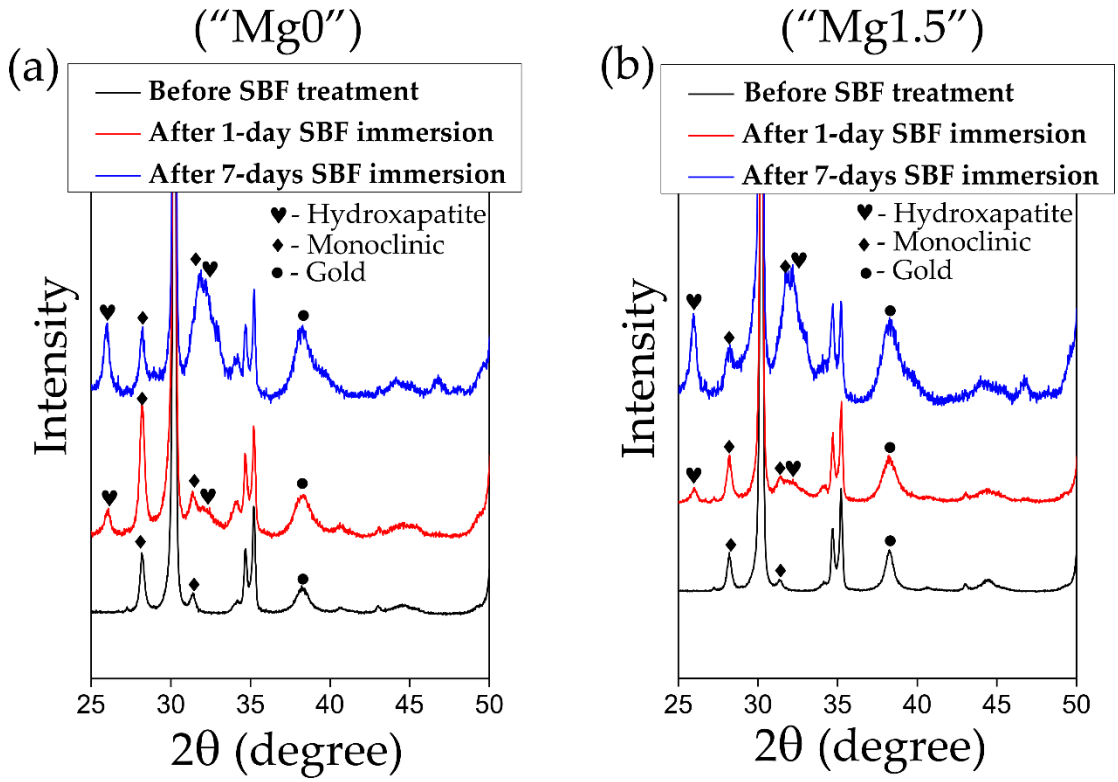

Figure 8 XRD plots comparing properties of (a) "Mg0" solution and (b) "Mg1.5" solution-treated 3Y-TZP samples before and after 1 day or 7 days SBF immersion.

observed in the EDX plots were observed for both types of solution treated samples.

Figure 8 compares XRD plots of 3Y-TZP samples after 1 day and 7 days SBF immersion with both types of “Mg0” solution and Mg”1.5” solutions-treated samples to clarify the formation of HAp. In the XRD plots, characteristics peaks of HAp at 26° and 32° were detected for both types of solution treated samples for 1 day SBF immersion which got further intensified after 7 days SBF immersion. This means that both the types of solution treatments induced high HAp-forming ability to 3Y-TZP in 1 day SBF immersion. Compared to a similar work [30], in the present study short induction time for the HAp formation can be attributed to good deposition of Ca-P particles. These particles increased the degree of supersaturation of the Ca ions in the SBF solution at the vicinity of the 3Y-TZP surface accelerating the formation of the HAp.

Figure 9 shows the average adhesive strength of the HAp layer to the HF-etched 3Y-TZP samples compared to fine polished 3Y-TZP samples. In this figure “Pol” refers to polished and “HF” refers to HF etched 3Y-TZP samples. The error bar in the figure represents the standard deviation. By applying one-way ANOVA followed by the Tukey’s tests, statistical comparison of adhesive strength of Pol “Mg0” and Pol “Mg1.5” ($p > 0.05$) samples showed no statistical significance. Whereas, adhesive strength of HF “Mg1.5” samples compared statistically with Pol “Mg0”, Pol “Mg1.5”, or HF “Mg0” ($p < 0.01$) showed statistical significance. Statistical comparison of adhesive strength of Pol “Mg0” and HF “Mg0” ($p < 0.01$) or Pol “Mg1.5” and HF “Mg0” ($p < 0.05$) also showed statistical significance. In the case of the polished 3Y-TZP samples, the adhesive strength was found to be very low irrespective of the

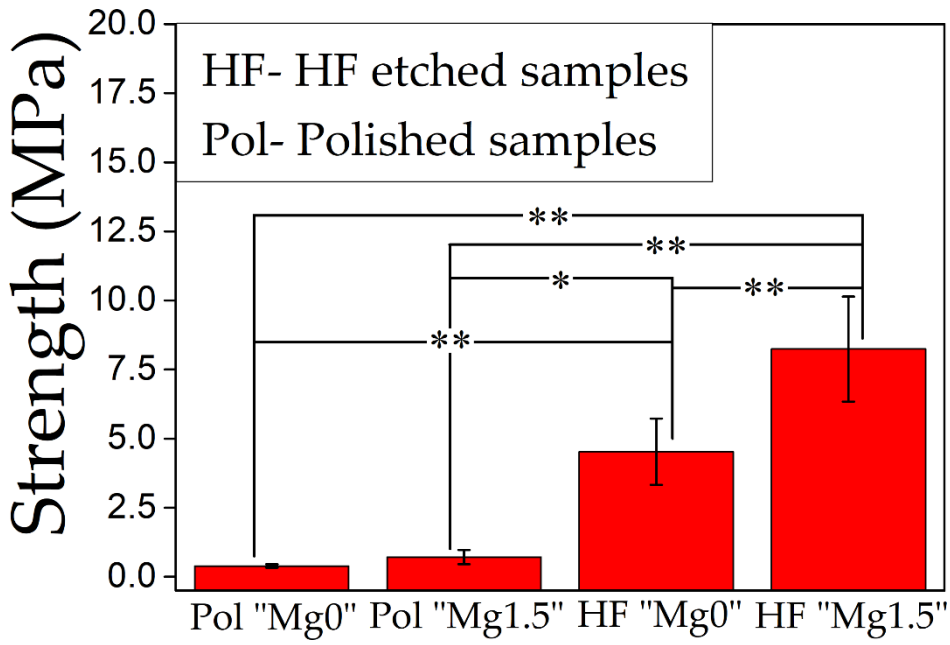

Figure 9 Comparison of adhesive strength of the HAp layer on only polished (Pol) and HF-etched and subsequently "Mg0" solution-treated and "Mg1.5" solution-treated 3Y-TZP formed by 14 days SBF immersion. The symbol "**" indicates $p < 0.01$, "*" indicates $p < 0.05$ and the no symbol indicates $p > 0.05$ by one-way ANOVA followed by the Tukey's tests.

condition of Ca-P solution treatments. While the HF treatment resulted in a significant increase in the adhesive strength of the HAp layer to the 3Y-TZP surface compared to polished samples, for both types of Ca-P solution-treated samples which was due to improvement of interlocking effect [45]. The important point to note is that the adhesive strength of the HAp layer to the HF-etched 3Y-TZP surface for “Mg1.5” solution treated samples were also significantly higher compared to “Mg0” solution treated HF-etched 3Y-TZP samples. This concludes that HF treatment contributed to the improvement of the adhesive strength of the HAp film. Incorporation of Mg ions in the Ca-P solution further contributed to improvement of the adhesive strength of the HAp layer. However, this contribution of Mg ion was very small or unnoticeable without the HF treatment. To understand the difference in the mechanism of failure, SEM and EDX analysis of the fractured surface of HF-etched 3Y-TZP samples were performed.

In Figure 10, the SEM images and EDX elemental mapping images for Ca of fractured surfaces of “Mg0” and “Mg1.5” solutions treated HF-etched 3Y-TZP samples are shown, respectively. In the case of “Mg0” solution treated HF-etched 3Y-TZP samples, for the part of the surface attached to jig, HAp layer was removed and the surface of the 3Y-TZP was exposed after the fracture. While, in the case of “Mg1.5” solution treated HF-etched 3Y-TZP samples, for the part of the surface attached to jig, broken surface of HAp layer was observed after the fracture. Adhesive and cohesive failure are two common modes of failure between two different types of bonded materials. In the case of adhesive failure, the failure is at the interface while in the case of cohesive failure the material breaks itself which is the HAp layer in this study as depicted in Figure 11.

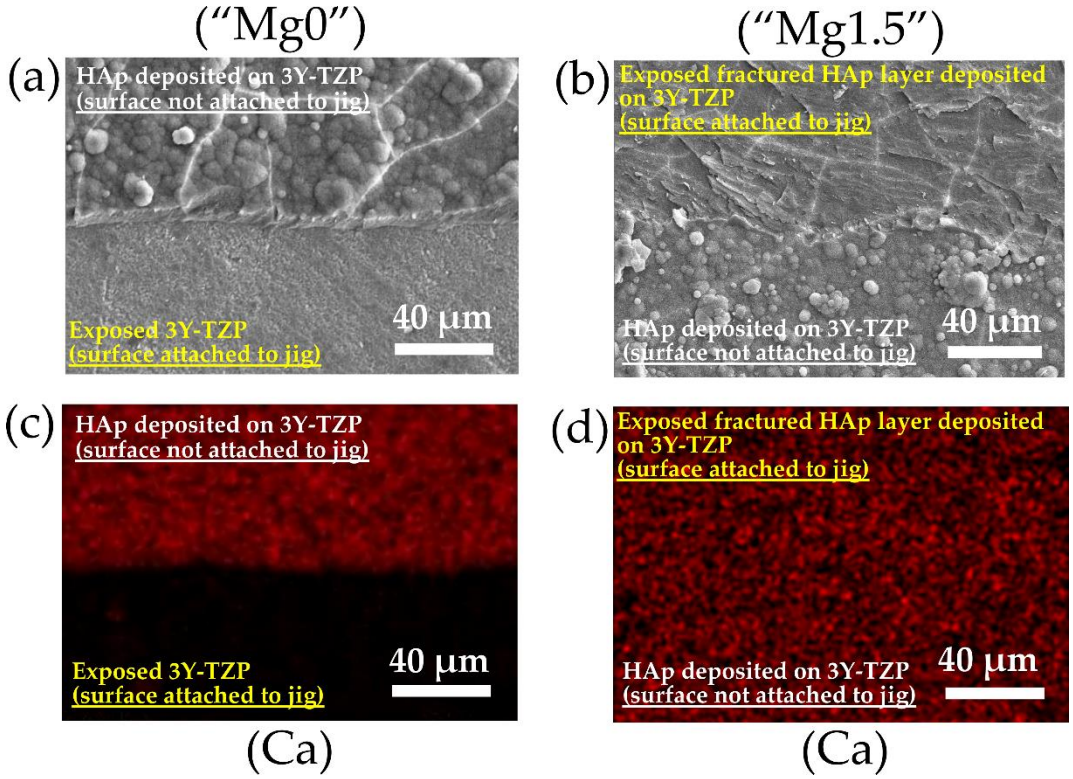

Figure 10 SEM images and EDX elemental mapping images of the surface of (a,c) "Mg0" and (b,d) "Mg1.5" solution treated HF-etched 3Y-TZP samples after the adhesive strength test.

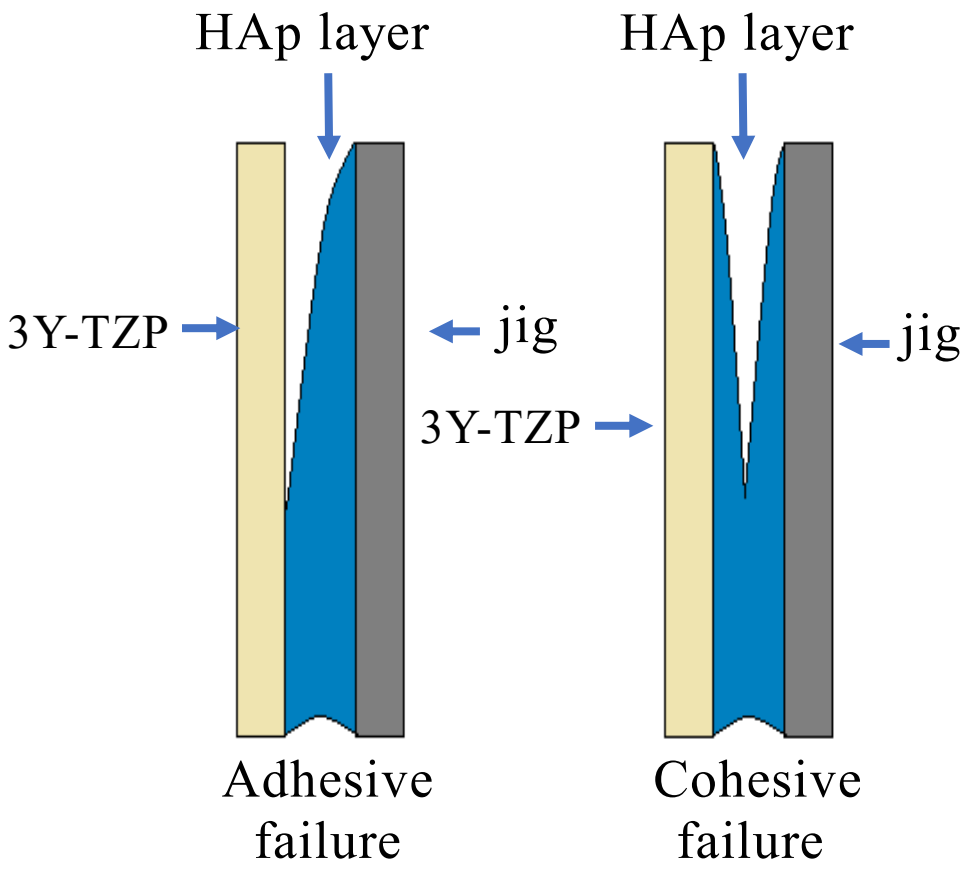

Figure 11 Schematic depicting adhesive and cohesive modes of failure related to the formed HAp layer.

Both the types of Ca-P solution-treated 3Y-TZP showed mixed modes of failures in different proportions. However, “Mg1.5” solution-treated HF-etched 3Y-TZP predominantly showed cohesive failure while “Mg0” solution-treated HF-etched 3Y-TZP showed adhesive failure.

Various studies have been reported the effect of Mg ion on the inhibition of Ca-P crystal growth [42,46–48]. Depending of the concentration of the Mg in the Ca-P particles, the Mg/Ca atomic ratio affects the particles morphology, crystallinity, and phase of the Ca-P particles. Incorporation of the Mg ion into the Ca-P particles results in the decrease of the Ca/P ratio. Mg ions replaces the Ca ions in the initial phase of amorphous Ca-P nuclei formation. This distorts the crystal structure by creating structural mismatch which prevent the growth of initial Ca-P nuclei into hydroxyapatite.

Barrere et. al. reported the development Ca-P coating on Ti6Al4V samples having rough surface (Ra = 0.80 μm) from supersaturated SBF (SBF × 5) solutions which had five times the concentration of ions compared the conventional SBF in a CO_2 atmosphere. Their study showed the effect of Mg ions on the precipitated Ca-P coatings. SBF with higher Mg concentration (SBF × 5, Mg × 8) resulted in the deposition of brushite or dicalcium phosphate dihydrate (DCPD). SBF solution without Mg (SBF × 5, Mg × 0) resulted in formation of carbonated apatite. At lower (SBF × 5, Mg × 3) and intermediate (SBF × 5) concentration of Mg resulted the deposition of amorphous carbonated Ca-P. It was concluded that Mg ions presence near the Ti6Al4V surface causes inhibition of the crystal growth of the apatite resulting in the formation of less crystallized tiny Ca-P globules. However, these tiny Ca-P structures causes stronger attachment of the Ca-P coating [49].

The present study was designed to quantitatively assess the effect of Mg ions on the enhancement of the adhesive strength of the HAp layer formed in the SBF. The physical parameters (temperature and pH) and concentration were controlled, and both types of Ca-P solution treatment either with or without Mg ions resulted in formation of slightly less crystallized HAp particles. Mg ions were incorporated in the Ca-P particles precipitated from "Mg1.5" Ca-P solution treatment, but Ma/Ca ratio was low to significantly affect the phase or crystallinity of precipitated Ca-P particles. However, Mg resulted in the decease of the particle size of precipitated particles and also led to the homogenous deposition of these particles on the 3Y-TZP substrate. Due the adequate deposition of the Ca-P particles, both of the solution treatments resulted in high HAp forming ability in the SBF. In the case of polished 3Y-TZP substrate due to the absence of any surface irregularity or micropores, both types of Ca-P solution treated samples resulted in the nucleation and growth of HAp crystals in the SBF on the surface without any strong adhesion. Whereas for the HF treated rough 3Y-TZP substrate, both types of Ca-P solution treatments resulted in the penetration of initially nucleated HAp crystals in SBF inside the surface irregularity or pores causing an enhancement of adhesive strength compared to polished samples. Furthermore, it is speculated that the sustained release of Mg ions from the particles deposited form "Mg1.5" solution near the vicinity of HF etched 3Y-TZP surface inhibited the growth of initially formed HAp crystal in the SBF. Being smaller in size these crystals were able penetrate more efficiently inside the surface pores or irregularities. These strongly penetrated crystals at the interface, fully developed into a dense HAp layer with increasing the immersion period in the SBF which increased the adhesion of the whole HAp layer. The results signify the importance of surface roughness and the

contribution of Mg ions in the designed biomimetic Ca-P solution treatment on enhancing the adhesive strength of formed HAp layer in the SBF.

3.4 **Conclusions**

This work dealt with the fabrication of bioactive 3Y-TZP by biomimetic Ca-P solution treatment. HF etching was performed to enhance the surface roughness of the 3Y-TZP samples and then the samples were treated with two different types of Ca-P solutions, one solution contained Mg ions while other did not. Both types of solution treatments resulted in the deposition of Ca-P particles with different morphologies on the 3Y-TZP surface. Mg ions significantly reduced the size of Ca-P particles. Likewise, both these types of Ca-P solution treated 3Y-TZP samples showed HAp-forming ability in 1 day SBF immersion. The adhesive strength of the HAp layer to the 3Y-TZP surface was significantly low for the polished samples compared to HF-etched samples. Moreover, the adhesive strength also varied for the type of Ca-P solution treatments, Mg incorporated Ca-P solution treatment resulted in significantly higher adhesive strength of HAp layer on the HF-etched 3Y-TZP compared to Ca-P solution treatment with no Mg ions. It is considered that the release of Mg ions near the vicinity of the 3Y-TZP surface resulted in the formation of finer HAp crystal which strongly adhered to the pores on the roughened surface. A combination of HF etching and inclusion of Mg ions in the Ca-P solution treatment designed to induce HAp-forming ability resulted in sufficiently higher adhesive strength of the HAp layer to the surface of the substrate.

3.5 **References**

[1] R.C. Garvie, R.H. Hannink, R.T. Pascoe, Ceramic steel? Nature, 258 (1975), 703-704.

[2] C. Piconi, G. Maccauro, Zirconia as a ceramic biomaterial, Biomaterials, 20 (1999), 1-25.

[3] W. Burger, H.G. Richter, C. Piconi, R. Vatteroni, A. Cittadini, M. Boccalari, New Y-TZP powders for medical grade zirconia, J. Mater. Sci.: Mater. Med., 8 (1997),113-118.

[4] R.H. Hannink, P.M. Kelly, B.C. Muddle, Transformation toughening in zirconia-containing ceramics, J. Am. Ceram. Soc., 83 (2000), 461-487.

[5] L. Sennerby, A. Dasmah, B. Larsson, M. Iverhed, Bone tissue responses to surface-modified zirconia implants: a histomorphometric and removal torque study in the rabbit, Clin. Implant Dent. R., 7 (2005), 13-20.

[6] J.D. Langhoff, K. Voelter, D. Scharnweber, M. Schnabelrauch, F. Schlottig, T. Hefti, K. Kalchofner, K. Nuss, B. von Rechenberg, Comparison of chemically and pharmaceutically modified titanium and zirconia implant surfaces in dentistry: a study in sheep, Int. J. Oral. Max. Impl., 37 (2008), 1125-1132.

[7] C. Wanpeng, L.L. Hench, Bioactive materials, Ceram. Int., 22 (1996), 493-507.

[8] M. Neo, T. Nakamura, C. Ohtsuki, T. Kokubo, T. Yamamuro, Apatite formation on three kinds of bioactive materials at an early stage in vivo: A

comparative study by transmission electronmicroscopy, J. Biomed. Mater. Res., 27 (1993), 999-1006.

[9] M. Neo, S. Kotani, Y. Fujita, T. Nakamura, T. Yamamuro, Y. Bando, C. Ohtsuki, T. Kokubo, Differences in ceramics-bone interface between surface-active ceramics and resorbable ceramics: A study by scanning and transmission electron microscopy, J. Biomed. Mater. Res., 26 (1992), 255-267.

[10] L.L. Hench, Bioceramics: From concept to clinic, J. Am. Chem. Soc., 74 (1991), 1487-1510.

[11] L.L. Hench, The story of Bioglass®. J. Mater. Sci. Mater. Med., 17 (2006), 967–978.

[12] H. Aoki, Medical applications of hydroxyapatite, Ishiyaku Euro America St. Louis, (1994),13-74.

[13] W.S.W. Harun, R.I.M. Asri, J. Alias, F.H. Zulkifli, K. Kadirgama, S.A.C. Ghani, J.H.M. Shariffuddin, A comprehensive review of hydroxyapatite-based coatings adhesion on metallic biomaterials, Ceram. Int., 44 (2018), 1250-1268.

[14] Y. Yang, K.H. Kim, J.L. Ong, A review on calcium phosphate coatings produced using a sputtering process-an alternative to plasma spraying, Biomaterials, 26 (2005), 327-337.

[15] K. Tonsuaadu, K.A. Gross, L. Pluduma, M. Veiderma, A review on the thermal stability of calcium apatites, J. Therm. Anal. Calorim., 110 (2012), 647-659.

[16] P. Ducheyne, S. Radin, L. King, The effect of calcium phosphate ceramic composition and structure on in vitro behavior. I. Dissolution, J. Biomed. Mater. Res., 27 (1993), 25-34.

[17] H. Takadama, T. Kokubo, In vitro evaluation of bone bioactivity, In: Bioceramics and Their Clinical Applications. pp.165-182. Ed. by T. Kokubo, Woodhead Publishing Limited, Cambridge, UK, 2008.

[18] T. Kokubo, H. Takadama, How useful is SBF in predicting in vivo bone bioactivity?, Biomaterials, 27 (2006), 2907-2915.

[19] P. Habibovic, F. Barrere, C.A van Bliterswijk, K. de Groot, P. Layrolle, Biomimetic hydroxyapatite coating on metal implants, J. Am. Ceram. Soc., 85 (2002), 517-522.

[20] P. Li, C. Ohtsuki, T. Kokubo, K. Nakanishi, N. Soga, Apatite formation induced by silica gel in a simulated body fluid, J. Am. Ceram. Soc., 75 (1992), 2094-2097.

[21] H.Y. Kim, T. Himeno, T. Kokubo, T.Nakamura, Process and kinetics of bonelike apatite formation on sintered hydroxyapatite in a simulated body fluid, Biomaterials, 26 (2005), 4366-4373.

[22] T.T. Demirtaş, G. Kaynak, M. Gümüşderelioğlu, Bone-like hydroxyapatite precipitated from 10×SBF-like solution by microwave irradiation, Mat. Sci. and Eng. C, 49 (2015), 713-719.

[23] T. Kokubo, H. Kushitani, S. Sakka, T. Kitsugi, T. Yamamuro, Solutions able to reproduce in vivo surface-structure changes in bioactive glass-ceramic A-W, J. Biomed. Mater. Res., 24 (1990), 721-734.

[24] M. Uchida, H.M. Kim, T. Kokubo, M. Nawa, T. Asano, K. Tanaka, T. Nakamura, Apatite-forming ability of a zirconia/alumina nano-composite induced by chemical treatment, J. Biomed. Mater. Res., 60 (2002), 277-282.

[25] K. Parduna, L. Treccani, E.Volkmann, P. Streckbein, C. Heiss, G.L. Destri, G. Marletta, K. Rezwana, Mixed zirconia calcium phosphate coatings for dental implants: Tailoring coating stability and bioactivity potential, Mater. Sci. Eng. C, 48 (2015), 337-346.

[26] V. Ponnilavan, S. Vasanthavel, M.I.K. Khan, A.K. Dhayalan, S. Kannan, Structural and bio-mineralization features of alumina zirconia composite influenced by the combined Ca^{2+} and PO_4^{3-} additions, Mater. Sci. Eng. C, 98 (2019), 381–391.

[27] Y. Cao, T. Shi, C. Jiao, H. Liang, R. Chen, Z. Tian, A. Zou, Y. Yang, Z. Wei, C. Wang, et al., Fabrication and properties of zirconia/hydroxyapatite composite scaffold based on digital light processing, Ceram. Int., 46 (2020), 2300-2308.

[28] M.G. Faga, A. Vallée, A. Bellosi, M. Mazzocchi, N.N. Thinh, G. Martra, S. Coluccia, Chemical treatment on alumina–zirconia composites inducing apatite formation with maintained mechanical properties, J. Eur. Ceram., 32 (2012), 2113-2120.

[29] F. Baino, J.M. Canela, F. Korkusuz, P. Korkusuz, B. Kankılıç, M.A. Montealegre, M.A.D.S. López, C.V. Brovarone, In Vitro assessment of bioactive glass coatings on alumina/zirconia composite implants for potential use in prosthetic applications, Int. J. Mol. Sci., 20 (2019), 722.

[30] M. Dehestani, D. Zemlyanov, E. Adolfsson, L.A. Stanciu, Improving bioactivity of inert bioceramics by a novel Mg-incorporated solution treatment, Appl. Surf. Sci., 425 (2017), 564-575.

[31] G. Qi, S. Zhang, K.A. Khor, S.W. Lye, X. Zeng, W. Weng, C. Liu, S.S. Venkatraman, L.L. Ma, Osteoblastic cell response on magnesium-incorporated apatite coatings, Appl. Surf. Sci., 225 (2008), 304-307.

[32] L. Ren, K. Yang, Bio-functional design for metal implants, a new concept for development of metallic biomaterials, J. Mater. Sci. Technol., 29 (2013), 1005-1010.

[33] G. Wang, J. Li, W. Zhang, L. Xu, H. Pan, J. Wen, Q. Wu, W. She, T. Jiao, X. Liu, J. Xinquan, Magnesium ion implantation on a micro/nanostructured titanium surface promotes its bioactivity and osteogenic differentiation function, Int. J. Nanomed., 9 (2014), 2387-2398.

[34] J.W. Park, C.H. An, S.H. Jeong, J.Y Suh, Osseointegration of commercial microstructured titanium implants incorporating magnesium: A histomorphometric study in rabbit cancellous bone, Clin. Oral Implant. Res., 23 (2012), 294-300.

[35] M.A. Barbosa, F.J. Monteiro, R. Correia, B. Leon, The effect of magnesium ions on bone bonding to hydroxyapatite coating on titanium alloy implants, Key Eng. Mater., 254 (2003), 447-450.

[36] S. Zhao, Q. Jiang, S. Peel, X. Wang, F. He, Effects of magnesium-substituted nanohydroxyapatite coating on implant osseointegration, Clin. Oral Implant. Res., 24 (2013), 34-41.

[37] J.A. Juhasz, S.M. Best, M. Kawashita, N. Miyata, T. Kokubo, T. Nakamura, W. Bonfield, Bonding strength of the apatite layer formed on glass-ceramic apatite-wollastonite-polyethylene composites, J. Biomed. Mater. Res., 67 (2003), 952-959.

[38] W.R. Lacefield, Hydroxyapatite coatings, pp. 331–347. In: An Introduction to Bioceramics, 2nd ed. Ed. by L.L. Hench, Imperial College Press, London, UK, 2013.

[39] T. Miyazaki, H.M. Kim, T. Kokubo, C. Ohtsuki, K. Kato, T. Nakamura, Enhancement of bonding strength by graded structure at interface between apatite layer and bioactive tantalum metal, J. Mater. Sci. Mater. Med., 13 (2002), 651-655.

[40] A. Noro, M. Kaneko, I. Murata, M. Yoshinari, Influence of surface topography and surface physicochemistry on wettability of zirconia (tetragonal zirconia polycrystal), J. Biomed. Mater. Res. B Appl. Biomater., 101 (2013), 355-363.

[41] C. Ohtsuki, T. Kokubo, T. Yamamuro, Mechanism of apatite formation on CaO-SiO2-P2O5 glasses in a simulated body fluid, J. Non-Cryst. Solids, 143 (1992), 84-92.

[42] A. Bigi, G. Falini, E. Foresti, A. Ripamonti, M. Gazzano, N. Roveri, Magnesium influence on hydroxyapatite crystallization, J. Inorg. Biochem., 49 (1993), 69-78.

[43] J. Chevalier, L. Gremillard, A.V. Virkar, D.R. Clarke, The tetragonal - monoclinic transformation in zirconia: lessons learned and future trends, J. Am. Ceram. Soc., 92 (2009), 1901–1920.

[44] J. Chevalier, B. Cales, J.M. Drouin, Low-temperature aging of Y-TZP ceramics, J. Am. Ceram. Soc., 82 (1999), 2150-2154.

[45] T. Yabutsuka, R. Karashima, S. Takai, T. Yao, Effect of doubled sandblasting process and basic simulated body fluid treatment on fabrication of bioactive stainless steels, Materials, 11, (2018), 1334.

[46] M.H. Salimi, J.C. Heughebaert, G.H. Nancollas, Crystal growth of calcium phosphates in the presence of magnesium ions, Langmuir, 1 (1985), 119-122.

[47] B. Tomazic, M. Tomson, G.H. Nancollas, Growth of calcium phosphates on hydroxyapatite crystals: the effect of magnesium, Arch. Oral Biol., 20 (1975), 803-808.

[48] J.D. Termine, R.A. Peckauskas, A.S. Posner, Calcium phosphate formation in vitro. II. Effects of environment on amorphous-crystalline transformation, Arch. Biochem. Biophys., 140 (1970), 318-325.

[49] F. Barrere, C.A. van Blitterswijk, K. de Groot, P. Layrolle, Nucleation of biomimetic Ca–P coatings on Ti6Al4V from a SBF×5 solution: Influence of magnesium, Biomaterials, 23 (2002), 2211-2220.

Chapter 4

Bioactivity Assessment of Apatite Nuclei-PVDF Composite Thin Films

4.1 Introduction

Simulated body fluid (SBF) has inorganic ion concentration similar to human blood plasma. When either pH or temperature of SBF is raised, fine particles of calcium phosphate are precipitated in the fluid. It has been reported that these particles actively induce hydroxyapatite formation in SBF and body fluid, hence were named Apatite Nuclei (AN) [1].

Bone is composed of about 19 wt. % of proteins, 70 wt. % of minerals and the remaining 11 wt. % of water, cells, and other substances [2]. Pure collagen, which is the protein component of the bone, and hydroxyapatite, which is the major inorganic component of the bone, also shows piezoelectric properties [3, 4]. Piezoelectric materials have demonstrated significant potential for tissue engineering and regeneration. Various piezoelectric materials have been used for different tissue repair applications, especially in bone repair, where charges induced in the materials by mechanical stress can enhance bone formation [5].

Polyvinylidene fluoride (PVDF) is a fluoropolymer known for its piezoelectric properties, biocompatibility and being cheapest among fluoropolymers. Being a non-biodegradable polymer, possessing high elasticity and good processability PVDF can serve as a suitable biomedical material for implants, vascular grafts, and biosensing applications. Ficat et.al.

showed the effect of bone regeneration ability of an implanted piezoelectric PVDF film [6].

However, intrinsically PVDF is a non-bioactive material which means it lacks bone bonding ability. In this chapter, the author aimed to impart bioactivity to PVDF by incorporation of AN and subsequently investigated the fabrication process and effective procedure of enriching bioactivity.

4.2 **Materials and Methods**

4.2.1 *Preparation of SBF*

Reagent-grade NaCl, $NaHCO_3$, KCl, $K_2HPO_4 \cdot 3H_2O$, $MgCl_2 \cdot 6H_2O$, $CaCl_2$ and Na_2SO_4 were dissolved in ultrapure water and buffered at pH 7.40 with tris(hydroxymethyl)aminomethane ($(CH_2OH)_3CNH_2$) and 1 M HCl at 36.5 °C [7].

4.2.2 *Preparation of AN*

A similar methodology for the preparation of AN is utilized as mentioned in the chapter 2. 2.0SBF, an aqueous solution having double concentration compared to SBF was prepared. This solution was adjusted at pH 8.2 at 36.5°C by dissolving tris-buffer and subsequently was held in an incubator at 36.5°C for 1 day for precipitation of AN. AN were collected by suction filtration with a membrane filter with 50 nm for average pore size (Merck Millipore, USA), washed with distilled water, and dried at room temperature.

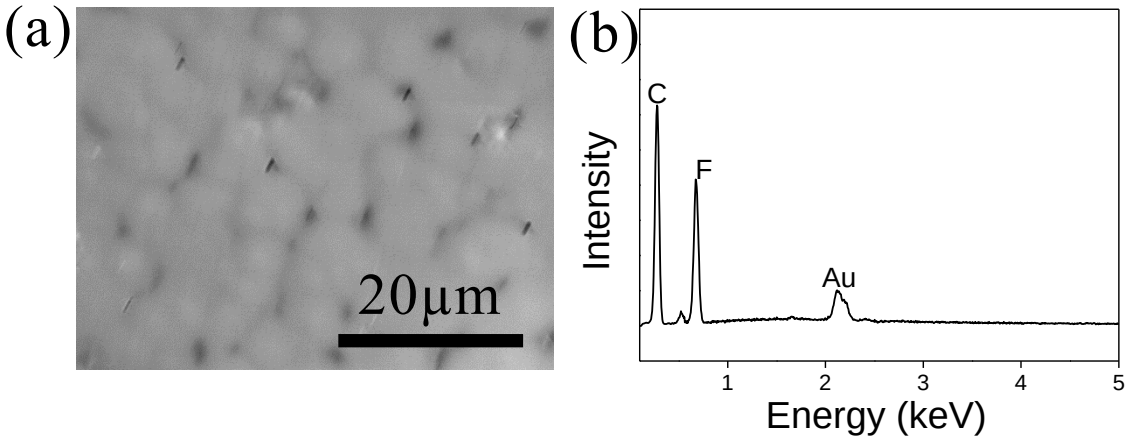

Figure 1 (a) SEM image and (b) EDX profile of the surface of untreated PVDF film.

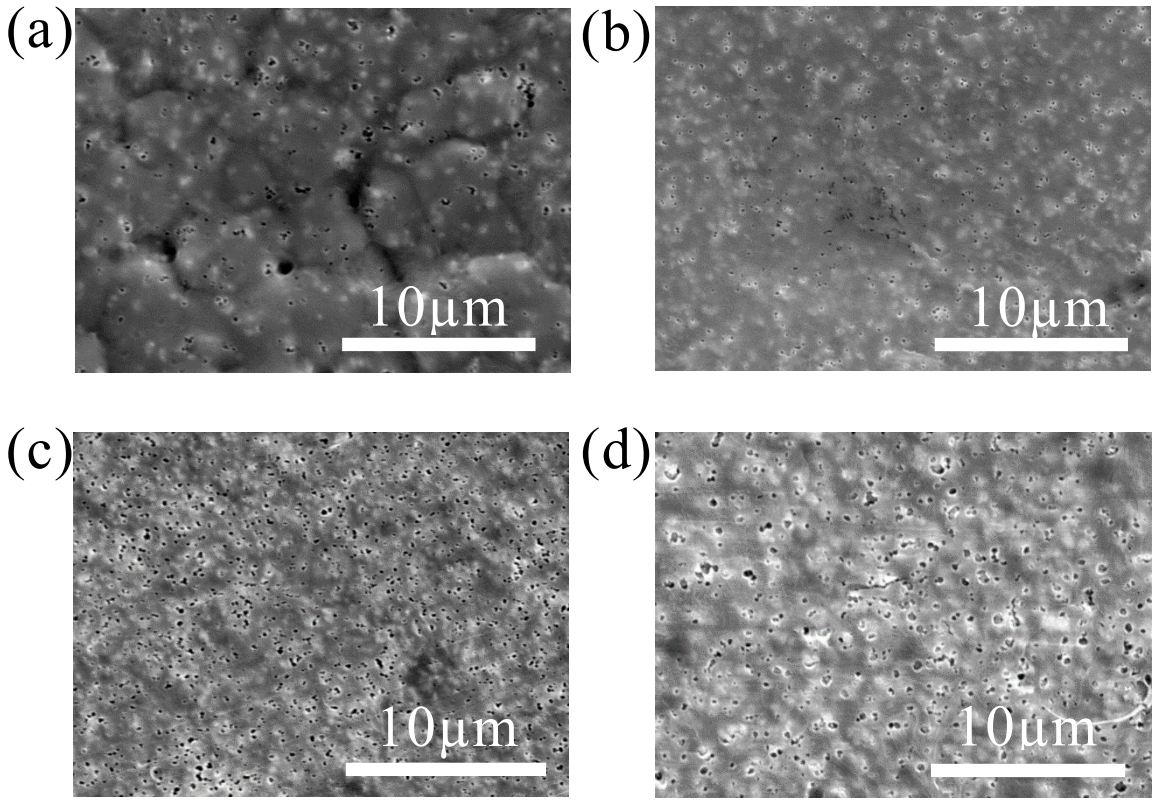

Figure 2 SEM images of the surface of (a) 10 wt.%, (b) 20 wt.%, (c) 30 wt.% and (d) 40 wt.% AN-PVDF films.

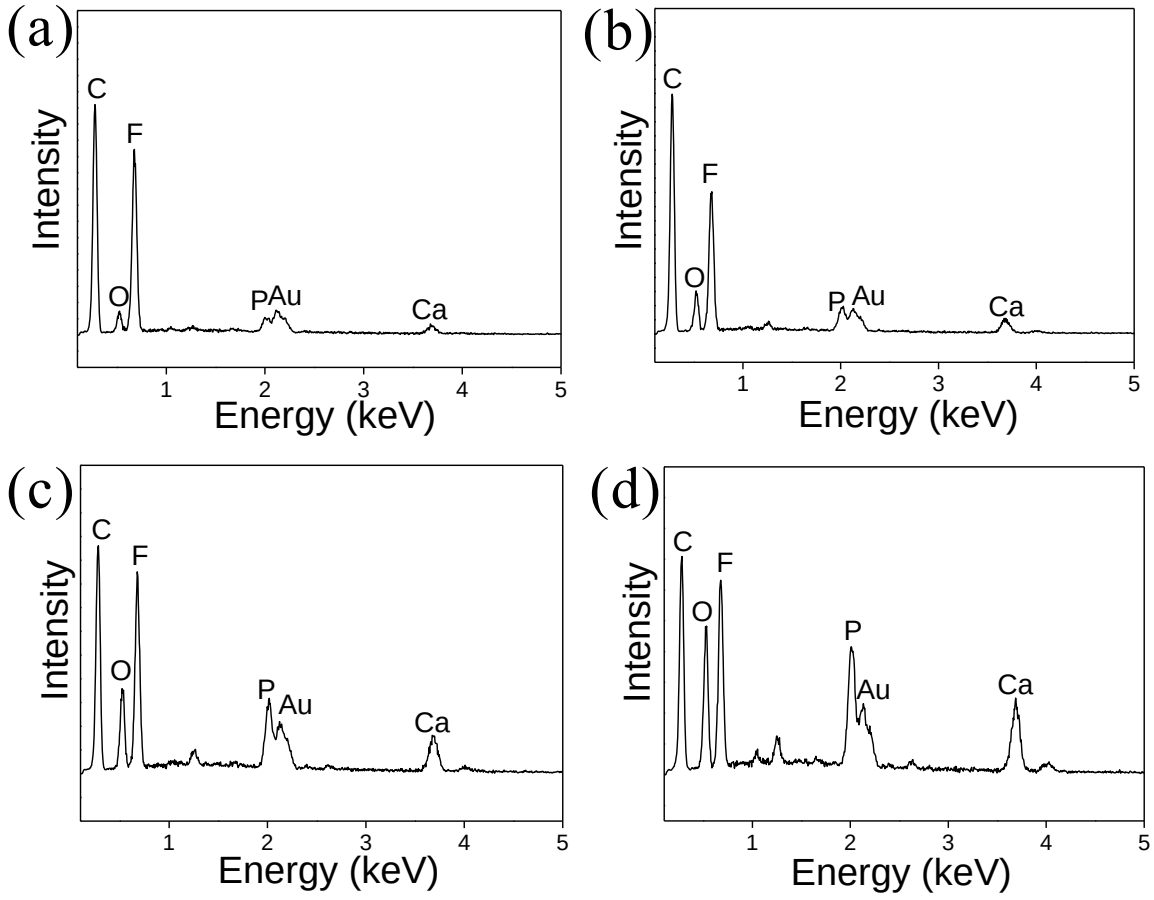

Figure 3 EDX profiles of the surface of (a) 10 wt.%, (b) 20 wt.%, (c) 30 wt.% and (d) 40 wt.% AN-PVDF films.

4.2.3 *Fabrication process of AN-PVDF composite thin films*

Dimethylformamide (DMF) (Wako chemicals, Japan) was used as solvent to dissolve PVDF (Sigma Aldrich, Japan). AN-PVDF composite thin films were made by solution casting technique using doctor blade method. An appropriate amount of AN was dispersed in DMF, to maintain a weight percentage of 0 wt.%, 10 wt.%, 20 wt.%, 30 wt.% and 40 wt.% of AN in PVDF by ultrasonication at room temperature. Then PVDF was dissolved by continuous magnetic stirring at the room temperature. The viscous solution was drawn into thin films using doctor blade and kept at 90 °C for 4 hours to remove the solvent. The obtained films were subjected to SBF test in which films were immersed in SBF, pH 7.40 at 36.5 °C. Analysis of hydroxyapatite formation was done by SEM (SU6600, Hitachi High-Technologies, Japan), EDX (XFlash® 5010, Bruker, Germany), and TF-XRD (Ultima IV, Rigaku corp., Japan) using CuKα radiation after immersion in SBF for 1 day and 3 days respectively. For the hydroxyapatite formed samples, the cross-sectional analysis was done by SEM and EDX.

4.3 **Results and Discussion**

Figure 1 shows the SEM image and the EDX profile of the surface of the untreated PVDF film. The PVDF film showed a semi porous globular morphology. C and F peaks in the EDX were observed from PVDF. The Au peak was caused by sputtering for the SEM observation.

Figure 2 and Figure 3 show the SEM images and the EDX profiles of 10 wt.%, 20 wt.%, 30 wt.% and 40 wt.% AN-PVDF composite thin films, respectively. All the films showed a semi-porous morphology and C and F peaks in the EDX were observed from PVDF. In addition, P, O and Ca peaks

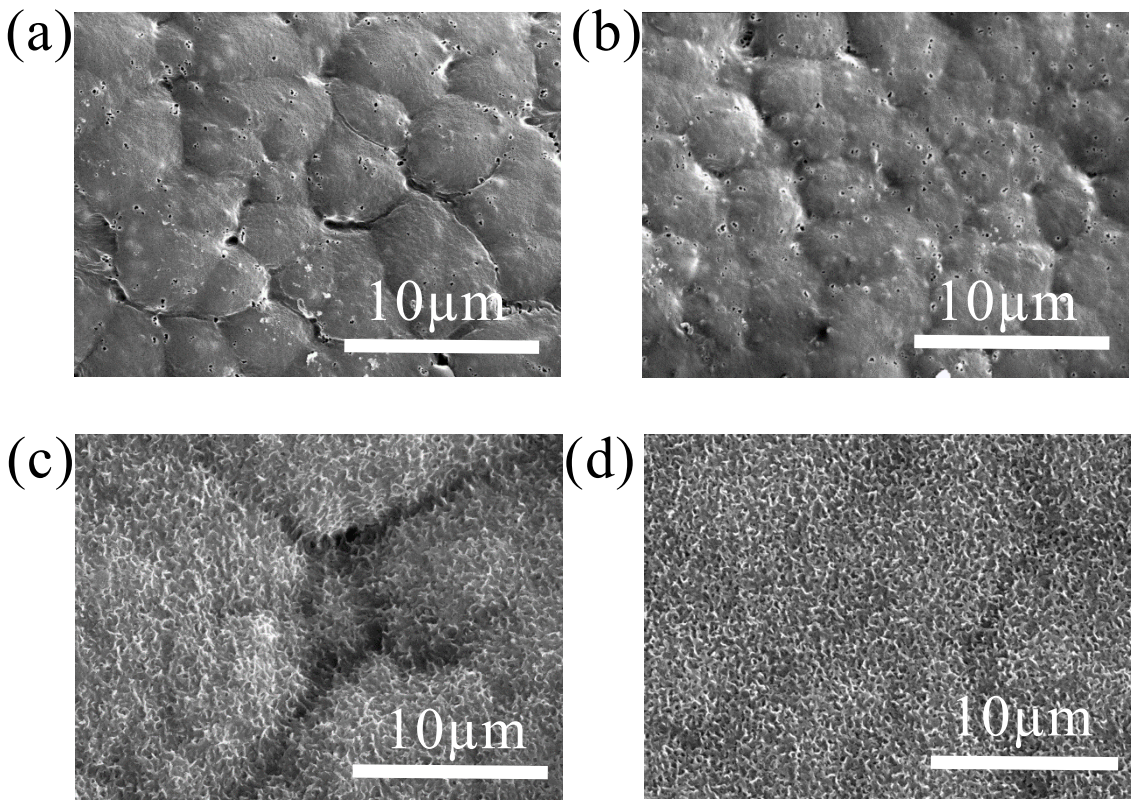

Figure 4 SEM images of the surface of the (a) 10 wt.%, (b) 20 wt.%, (c) 30 wt.% and (d) 40 wt.% AN-PVDF films after the immersion in SBF (pH 7.40 at 36.5 °C) for 3 days.

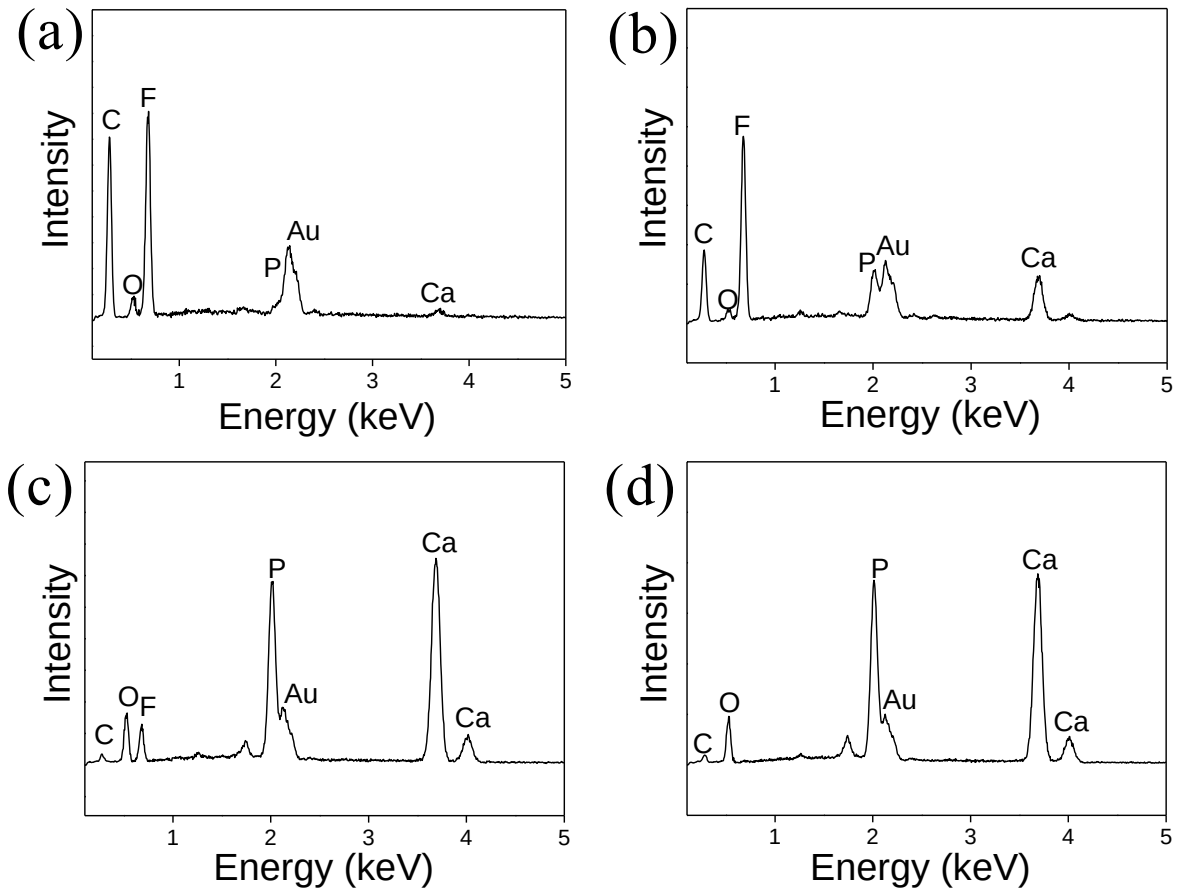

Figure 5 EDX plots of the surface of the (a) 10 wt.%, (b) 20 wt.%, (c) 30 wt.% and (d) 40 wt.% AN-PVDF films after the immersion in SBF for 3 days.

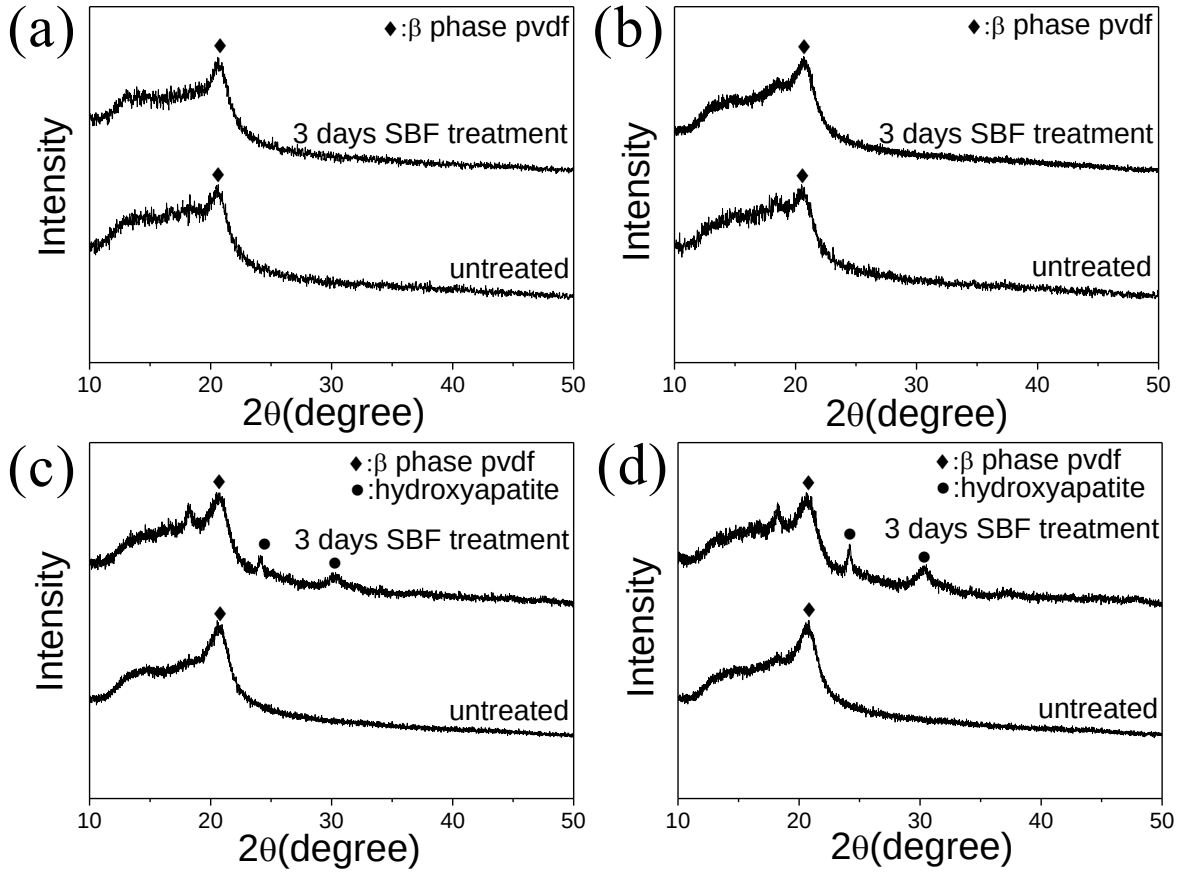

Figure 6 XRD plots of the surface of the (a) 10 wt.%, (b) 20wt.%, (c) 30 wt.% and (d) 40 wt.% AN-PVDF films after the immersion in SBF for 3 days.

were derived from AN, which could be observed to be uniformly distributed in PVDF matrix, and the peaks got intensified with increasing concentration of AN in PVDF.

Figure 4 and Figure 5 show the SEM images and the EDX profiles of 10 wt.%, 20 wt.%, 30 wt.% and 40 wt.% AN-PVDF films after the immersion in SBF (pH 7.40 at 36.5 °C) for 3 days, respectively. In the SEM images as shown in Figure 4, flake-like crystallites, which characterize bone-like apatite, covered the whole surface of 30 wt.% and 40 wt.% AN-PVDF film (Figure 4(c, d)) while 10 wt.% and 20 wt.% AN-PVDF films did not show any change in the surface morphology (Figure 4 (a, b)). Peaks of the EDX shown in Figure 5 revealed that Ca and P, the main constituents of apatite, were observed for all samples. For 30 wt.% and 40 wt.% AN-PVDF films as shown in Figure 5(c, d), high intensity Ca and P peaks were observed while low intensity Ca and P peaks which was due to the AN present in the films were observed for 10 wt.% and 20 wt.% films as shown in Figure 5 (a, b).

Figure 6 shows the XRD plots of 10 wt.%, 20 wt.%, 30 wt.% and 40 wt.% AN-PVDF films before and after 3 days SBF soaking period treatment, respectively. Diffraction peaks of hydroxyapatite were detected for 30 wt.% and 40 wt.% of AN-PVDF films as shown in Figure 6 (c, d). In contrast, such peaks were not observed in the case 10 wt.% and 20 wt.% AN-PVDF films as shown in Figure 6 (a, b). Peak around 20.6° shows that AN-PVDF films were predominantly having β phase, which is a highly piezoelectric phase of PVDF. Nucleating fillers and solution recrystallization have been reported to effect β phase formation in PVDF [8]. Hydroxyapatite formation ability for 1 day SBF soaking period for all the films was also checked. However, no significant

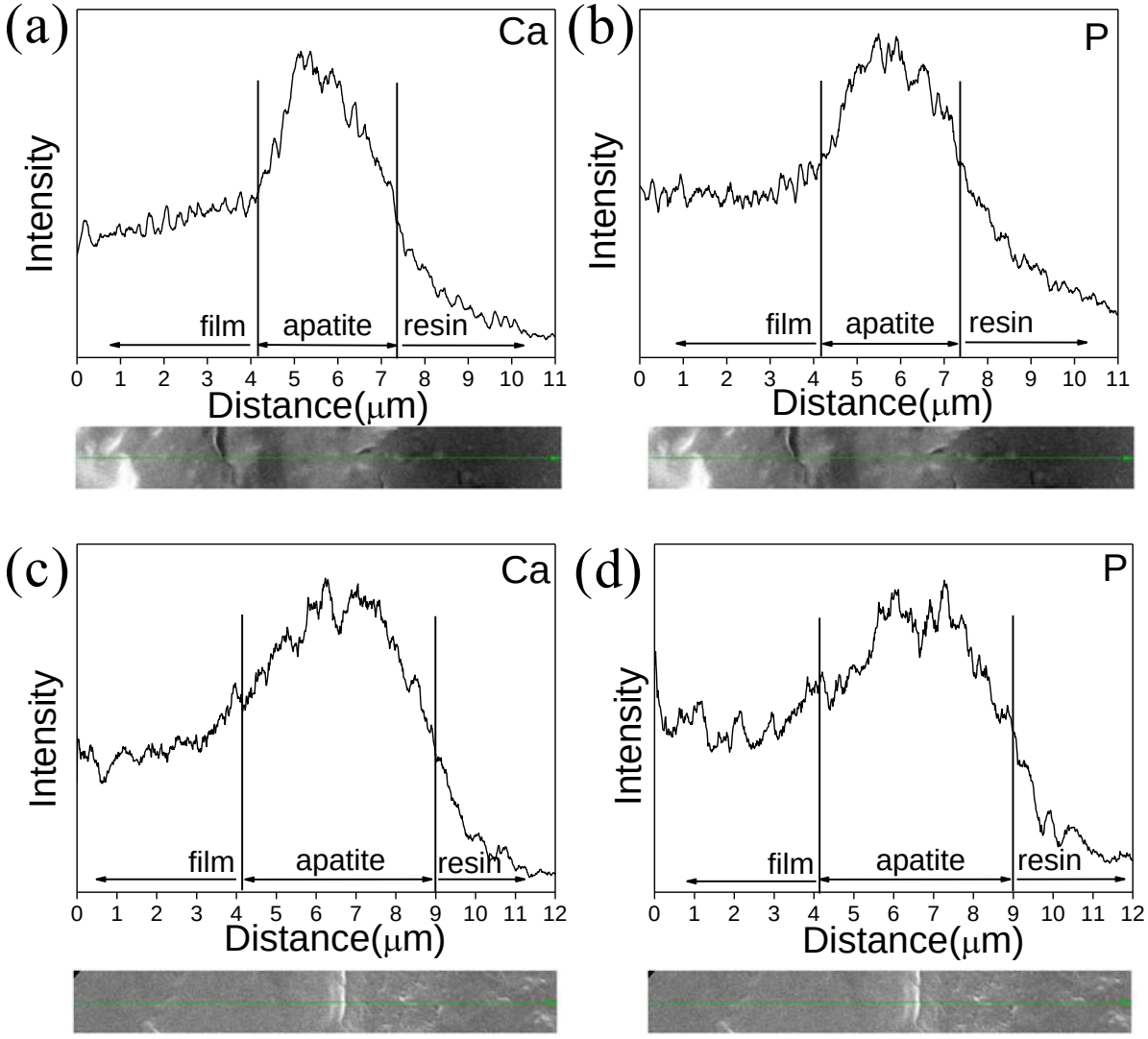

Figure 7 The results of line scanning of the EDX analysis of (a, c) Ca and (b, d) P for (a, b) 30 wt.% and (c, d) 40 wt.% AN-PVDF film after 3 days SBF immersion and, the SEM images of corresponding part of the cross section.

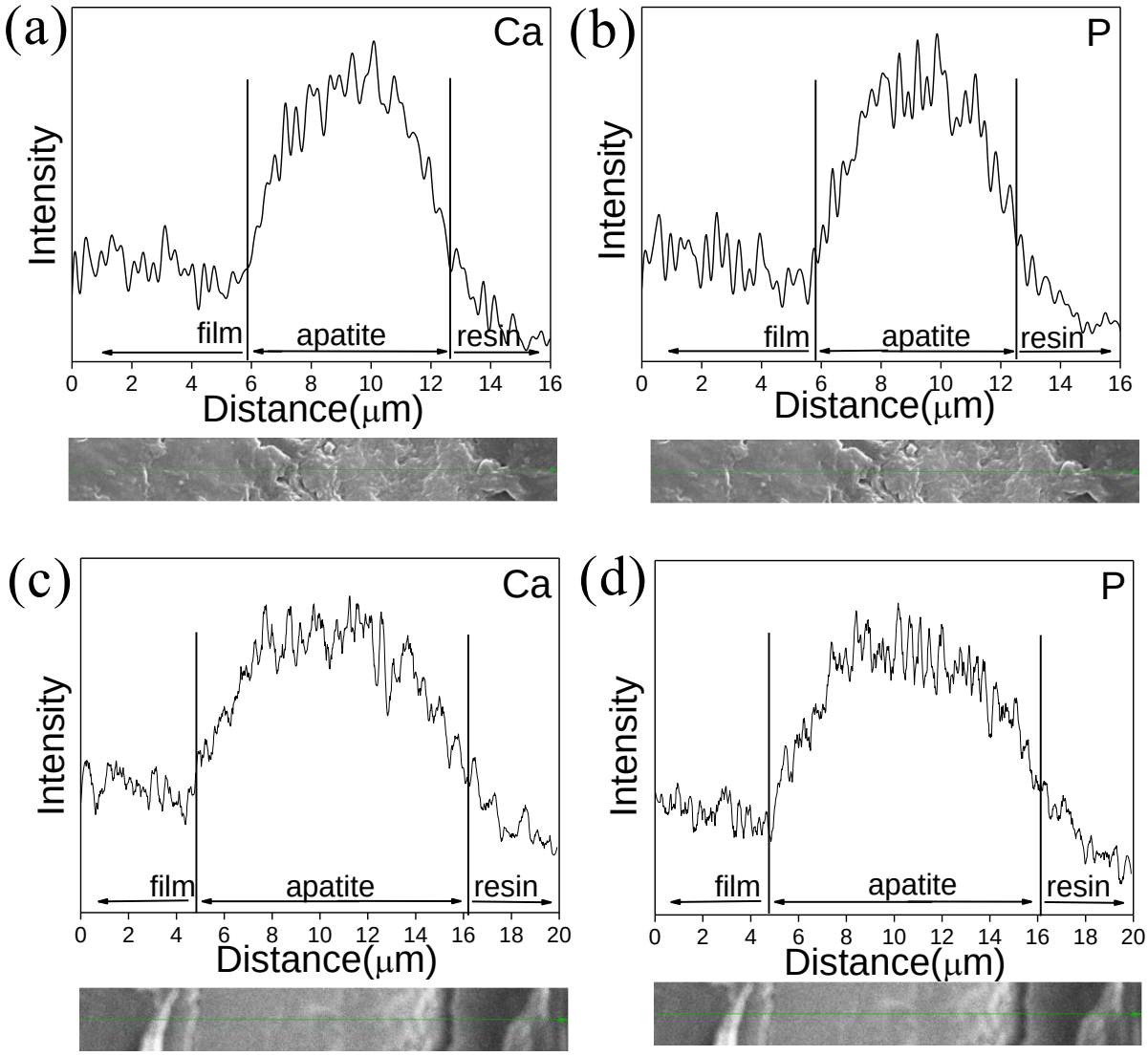

Figure 8 The results of line scanning of the EDX analysis of (a, c) Ca and (b, d) P for (a, b) 30 wt.% and (c, d) 40 wt.% AN-PVDF film after 7 days SBF immersion and, the SEM images of corresponding part of the cross section.

changes in surface morphology were noticed from SEM observation nor diffraction peaks of hydroxyapatite were detected in XRD analysis.

Figure 7 and Figure 8 show the results of the line scanning of the EDX analysis for the cross section of the 30 wt.% and 40 wt.% AN-PVDF film after 3 days and 7 days SBF soaking period treatment, respectively. The peaks of Ca and P were detected on the apatite layer. It can be observed that peaks lack sharp edges for Ca and P which was due to the AN present in the films and the semi porous morphology of the films. As indicated from the figures, the thickness of the films could be approximately found to be 3 μm for 30 wt.% AN-PVDF film and 5 μm for 40 wt.% AN-PVDF film for 3 days SBF immersion. The thickness of the films rose to be 6 μm for 30 wt.% AN-PVDF film and 10 μm for 40 wt.% AN-PVDF film for 7 days SBF immersion. The thickness of the films doubled with doubling soaking time period in the SBF.

4.4 **Conclusion**

Bioactive PVDF thin films was successfully fabricated by blending the AN. Films showed the dominance of β phase, a piezoelectric phase of PVDF. It was found that a minimum amount of AN in PVDF must be 30 wt.%, for the formation of fully covered hydroxyapatite layer in 3 days soaking period in SBF whose thickness was approximately found to be 3 μm which double doubling the soaking time period in the SBF.

4.5 **References**

[1] T. Yao, M. Hibino and T. Yabutsuka, U.S. Patent 8,512,732., Japanese Patent 5, 252, 399 (2013).

[2] M.J. Olszta, X. Cheng, S.S. Jee, R. Kumar, Y.Y. Kim, M.J. Kaufman, E.P. Douglas, L.B. Gower, Bone structure and formation: a new perspective. Mater. Sci. Eng. R. Rep., 58 (2007) 77-116.

[3] E. Fukada, I. Yasuda, Piezoelectric effects in collagen. Jpn. J. Appl. Phys., 3 (1964), 117-121.

[4] B. Sidney, Lang Review of ferroelectric hydroxyapatite and its application to biomedicine. Phase Transitions, 89 (2016) 678-694.

[5] G.W. Hastings, F.A. Mahmud, Electrical effects in bone. J. Biomed. Eng., 10 (1988) 515-521.

[6] J. Ficat, G. Escourron, M.J. Fauran, R. Durroux, P. Ficat, C. Lacabanne, F. Micheron, Osteogenesis induced by bimorph polyvinylidene fluoride films. Ferroelectrics, 51 (1983) 121-128.

[7] T. Kokubo, H. Takadama, How useful is SBF in predicting in vivo bone bioactivity?, Biomaterials, 27 (2006), 2907-2915.

[8] P. Martins, A.C. Lopes, and S. Lanceros-Mendez, Electroactive phases of poly(vinylidenefluoride): Determination, processing and applications. Prog. Polym. Sci., 39 (2014) 683-706.

Chapter 5

A Comparative In Vitro Bioactivity Evaluation of Polyvinylidene Fluoride and Polycaprolactone Incorporated with Amorphous Calcium Phosphate Particles

5.1 Introduction

Polymers, in general, are lightweight, relatively inexpensive, and have excellent mechanical toughness while showing biocompatibility and/or biodegradability. These properties make polymers highly suitable for application as biomaterials independently or in form of multifunctional composites in combination with other organic or inorganic functional materials [1].

Bone is a natural composite in which inorganic components are embedded in collagen fibrils. Bioactive ceramics are attractive candidates as bone implants, as they directly bond with bone by forming apatite layer compared to non-bioactive materials which get encapsulated with non-calcified organic tissue and is isolated from the surrounding bone tissue. This tissue formation is immune defense response against exogenous substance of the human body. However, ceramics are highly brittle which make it difficult to fit in the defect area and have high young modulus which causes stress shielding effects after implantation. One of the most suitable alternates are polymer-bioceramic composites to mimic natural bone properties.

An effective approach is to provide biological interaction between the non-bioactive implant and the host tissue and is to coat or integrate the implants

with suitable bioactive materials. Various bioactive materials such as bioactive glasses and calcium phosphates including hydroxyapatite make the connection between the host bone and the implant which helps in tissue regeneration.

Biomimetic method such as simulated body fluid (SBF) treatment is one of the suitable methods for the synthesis of calcium phosphate based bioactive materials with similar composition to human bones [2-4]. SBF has inorganic ion concentration similar to that of human blood plasma and can reproduce spontaneous hydroxyapatite formation on the surface of bioactive materials. When either the pH, temperature or the concentration of SBF is raised, fine particles of calcium phosphate are precipitated in the fluid in the absence of the bioactive ceramics. In previous studies, based on this mechanism amorphous calcium phosphate particles were fabricated from the SBF by raising its concentration, pH and temperature and it was found that these particles actively induce hydroxyapatite formation in conventional SBF, and hence were named as apatite nuclei (AN) [5,6]. Various bioactive polymers, ceramic and metals have been successfully prepared through biomimetic apatite nuclei treatment [7-10].

Polyvinylidene fluoride (PVDF) and polycaprolactone (PCL) are semicrystalline biocompatible polymers. PVDF is a non-biodegradable fluoropolymer known for its electroactive properties [11]. Piezoelectric materials display significant potential for tissue engineering and regeneration. Piezoelectric materials are widely been utilized for the tissue repair applications, especially in bone repair, where charges induced in the materials by mechanical stress can enhance bone formation [12]. Ficat et.al. showed the effect implanted piezoelectric PVDF film on bone regeneration [13]. Being a

piezoelectric polymer, also showing high elasticity and good processability, PVDF is highly suitable for biomedical applications such as bone implants, vascular grafts, neural regeneration, biosensing applications, etc. [14,15].

Whereas, PCL is a biodegradable aliphatic polyester and has good processability due to its low glass transition temperature (~ -60°C) and melting temperature (~ 60°C). PCL also has a low biosorption rate suitable enough for bone tissue regeneration, which makes it a good candidate for bone tissue engineering [16].

However, both PVDF and PCL are bioinert, which means that they lack direct bone bonding ability. In this chapter, the author reports and discusses a comparative study done to impart bioactivity and the apatite forming ability of PVDF and PCL incorporated with AN in SBF environment.

5.2 **Materials and Methods**

5.2.1 *Preparation of AN*

A similar methodology is utilized as mentioned in the chapter 2 for the preparation of AN. Firstly, 2.0SBF, having twice the concentration of inorganic ions compared to the normal SBF, was prepared. Then, the pH was raised to 8.2 at 36.5°C using tris(hydroxymethyl)aminomethane (THAM; Hayashi Pure Chemical Ind., Ltd., Osaka, Japan) and the solution was kept at the same temperature for 1 day. After 1 day, fine particles precipitated in the solution which were filtered by vacuum filtration using a filter paper having 50 nm for average pore size (Merck Millipore, USA). Finally, these particles were characterized using field emission scanning electron microscopy (SEM; SU6600, Hitachi High-Technologies Corporation, Tokyo, Japan), energy

dispersive X-ray spectrometry (EDS; XFlash® 5010, Bruker, Germany), X-ray diffraction (Ultima IV, Rigaku), and Fourier transform infrared spectroscopy (FT-IR; FT-720, Horiba, Ltd., Kyoto, Japan).

5.2.2 *Fabrication of composite films*

Solvent casting technique was used for the fabrication of films. PVDF (Sigma-Aldrich Japan, Tokyo, Japan) was dissolved in dimethylformamide (DMF) (Fujifilm Wako Pure Chemical Corporation, Osaka, Japan). An appropriate amount of AN was added to the solution to maintain a weight percentage of 0 wt.%, 10 wt.%, 20 wt.% and 30 wt.% of particles in PVDF. Magnetic stirring and subsequent ultrasonication were performed to uniformly disperse the AN in the PVDF solution. The solution was deposited as film onto the aluminum substrate using doctor blade method. Finally, the deposited films were kept at 90°C for 4 hours for drying, which were peeled off from the substrate after drying.

Similar method was used to fabricate PCL films. Acetone (Fujifilm Wako Pure Chemical) was used to dissolve PCL (Fujifilm Wako Pure Chemical) and an appropriate amount of AN were added to the solution to maintain a weight percentage of 0 wt.%, 10 wt.%, 20 wt.% and 30 wt.% of AN in PCL. Similarly, magnetic stirring, ultrasonication and doctor blade deposition of film on aluminum substrate was performed. Instead of drying at 90°C, the deposited films were kept at room temperature for the evaporation of the acetone and peeled off after drying.

The surface of the films was observed by (SEM; SU6600, Hitachi High-Technologies Corporation, Tokyo, Japan), energy dispersive X-ray

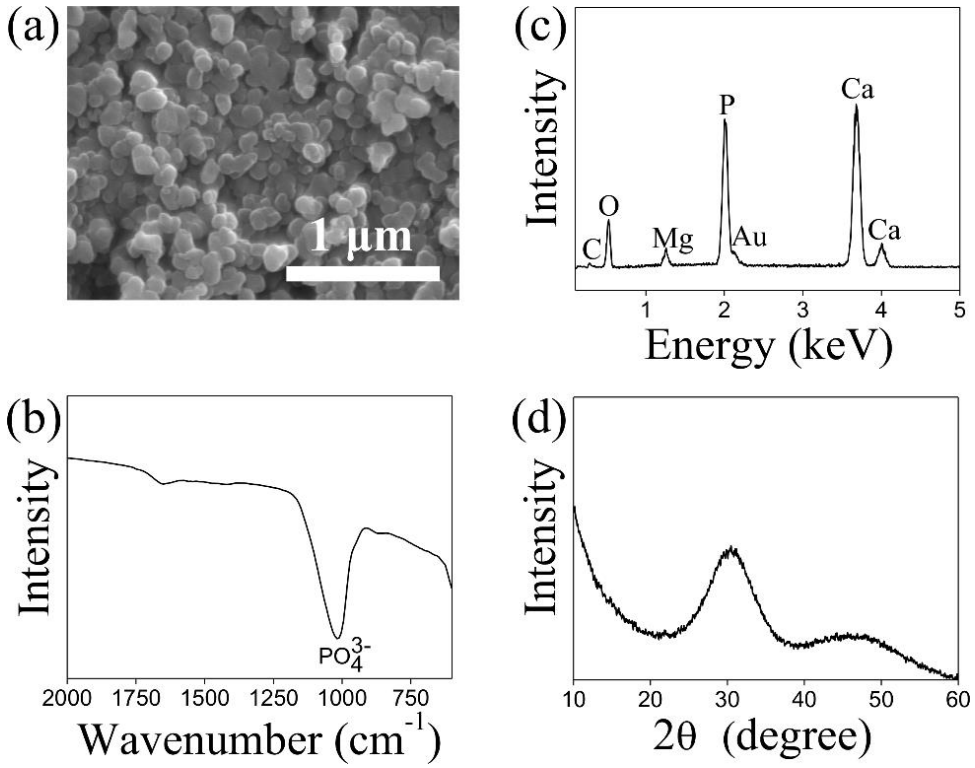

Figure1 (a) SEM image, (b) FTIR plot, (c) EDX profile and (d) XRD plot of AN.

spectrometry (EDS; XFlash® 5010, Bruker, Germany), thin film X-ray diffraction (XRD; Rint 2500, Rigaku Corporation, Tokyo, Japan). In order to compare the difference of hydrophilicity, water contact angle of PVDF and PCL films was measured by contact angle meter (CAX-150, Kyowa Interface Science, Saitama, Japan). The surface roughness was measured by ultra-precision point autofocus probe 3D measuring instrument (NH-3SP, Mitaka Kohki Co., Ltd., Tokyo, Japan) to evaluate difference of the roughness between PVDF films and PCL ones.

5.2.3 *Evaluation of bioactivity*

The prepared films were immersed in SBF solution for 1 day and 3 days to test in vitro bioactivity [17]. The surface of the films was observed by SEM, EDX and TF-XRD to evaluate apatite forming ability.

5.3 **Results and Discussion**

Figure 1 shows the SEM image, EDX profile, FTIR and XRD plot of the AN. Spherical particles having size around 100-200 nm were observed in the SEM image. The FTIR plot showed P=O stretching from the surface around 1050 cm^{-1} and Ca and P peaks were detected in the EDX elemental analysis. While the XRD shows a broad hump around 31° instead of strong peaks as in case of hydroxyapatite. These results indicate that these were fine-sized amorphous calcium phosphate particles.

Figure 2 shows SEM images and EDX profiles comparing properties of the surface of the 0 wt.%, 10 wt.%, 20 wt.% and 30 wt.% AN-PVDF and AN-PCL films. For PVDF, the SEM images revealed globular surface morphology and C and F peaks were detected in the EDX. In the case of PCL, the SEM

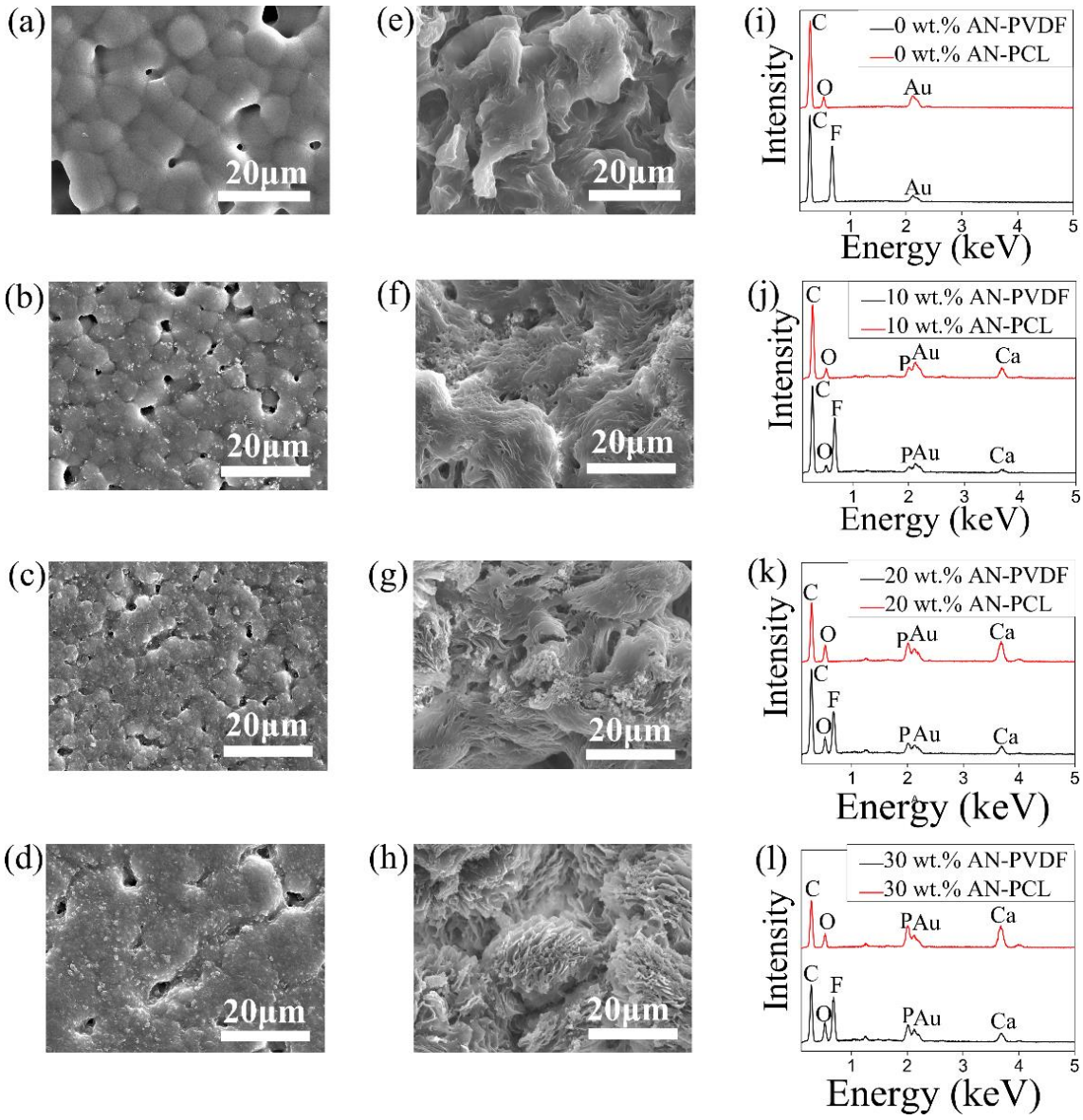

Figure 2 (a-h) SEM images of the surface of (a) 0 wt.%, (b) 10 wt.%, (c) 20 wt.% and (d) 30 wt.% AN-PVDF and (e) 0 wt.% (f) 10 wt.%, (g) 20 wt.% and (h) 30 wt.% AN-PCL films. (i-l) EDX profiles comparing properties of (i) 0 wt.% (j) 10 wt.%, (k) 20 wt.% and (l) 30 wt.% AN-PVDF and AN-PCL films.

image revealed highly rough surface morphology and C and O peaks were obtained in the EDX. As it can be noticed in the SEM images that the particles were homogenously distributed and exposed on the surface of the matrix. In the EDX profiles, Ca and P peaks are obtained from AN which increased as the content of AN increased in PVDF and PCL.

Figure 3 show the water contact angle of 0 wt.%, 10 wt.%, 20 wt.% and 30 wt.% AN-PVDF and AN-PCL films. The error bar represents the standard deviation from three reading obtained for each type of samples. The average water contact angle for pure PVDF film was found to be 94.6° and for pure PCL film was found to be 86.7°. No significant changes in contact angle were observed at intermediate weight percentages of AN in PVDF but a higher weight percentage of 30 wt.% AN in PVDF resulted in slight decrease of the contact angle. While in the case of AN PCL films the decrease in contact angle was also not so significant which gradually decreased with the increase of AN concentration in PCL.

Figure 4 compares the surface roughness of 0 wt. AN-PVDF and 0 wt.% AN-PCL films. As it can be observed from the 3D images, the surface was highly roughened for AN-PCL film compared to AN-PVDF film. The R_a (average roughness) values were found to be ~0.24 and ~1.37 μm for the 0 wt.% AN-PVDF and 0 wt.% AN-PCL films, respectively.

Figure 5 shows the EDX surface elemental scanning to measure atomic percentage of Ca with respect to other elements (C, O, P & F) exposed on the surface of the films. The error bar represents the standard deviation from three reading obtained for each type of samples. It can be observed that the atomic %

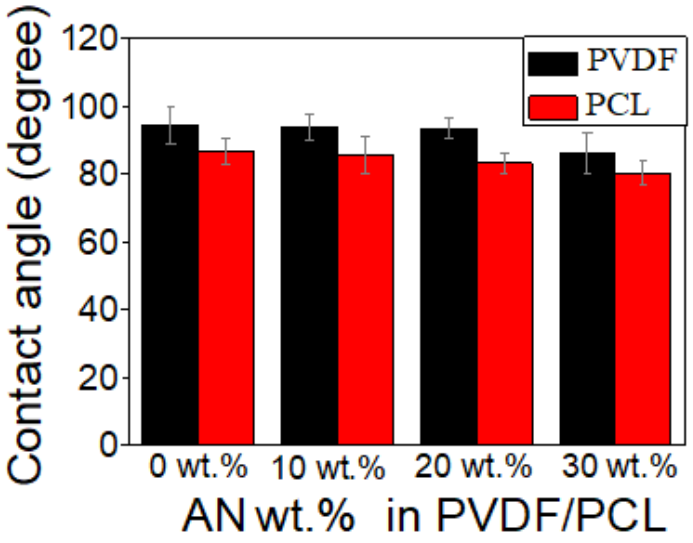

Figure 3 Comparison of water contact angle on 0 wt.%, 10 wt.%, 20 wt.%, and 30 wt.% AN-PVDF and AN-PCL films.

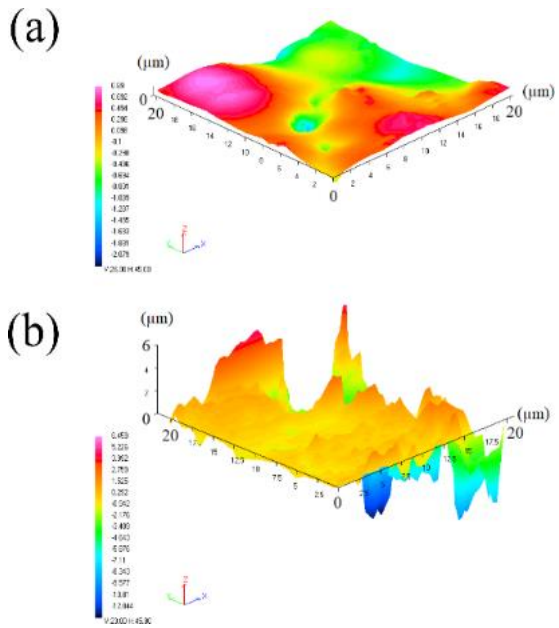

Figure 4 3D images of surface of (a) 0 wt.% AN-PVDF and (b) 0 wt.% AN-PCL films.

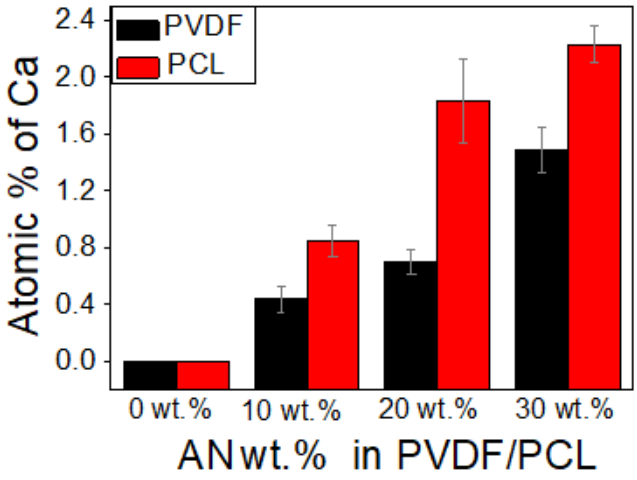

Figure 5 Comparison of atomic % of Ca on the surface of 0 wt.%, 10 wt.%, 20 wt.%, and 30 wt.% AN-PVDF and AN-PCL films w.r.t. C, O, P & F.

of Ca increases with increasing the wt.% of AN in PVDF/PCL. Furthermore, for each wt.% of AN in PVDF/PCL higher atomic% of Ca was observed for PCL films compared to the PVDF films suggesting higher exposure of AN in PCL due to higher surface roughness.

Figure 6 shows SEM images and EDX profiles comparing properties of the surface of the 0 wt.%, 10 wt.%, 20 wt.% and 30 wt.% AN PVDF and AN-PCL films after 1 day SBF immersion. No changes in the surface morphology were observed for AN-PVDF films except for 30 wt.% AN-PVDF film, where partially formed precipitates were observed. The EDX plots also showed similar intensity of the Ca and P peaks compared to films prior to the SBF treatment. Minute pores were formed on the surface of these films presumably due to the dissolution of AN in SBF. In the case of AN-PCL films, hemispherical precipitates were observed on 10 wt.%, 20 wt.% and 30 wt.% films and relative higher intensity of Ca and P peaks were observed for 20 wt.% and 30 wt.% films compared to films prior to SBF treatment. However, it is noticeable from SEM image and high intensity C peak in the EDX that these precipitates partially covered the surface and the surface coverage increased with the increase in AN in content in PCL.

Figure 7 SEM images and EDX profiles comparing properties of the surface of the 0 wt.%, 10 wt.%, 20 wt.% and 30 wt.% AN- PVDF and AN-PCL films after 3 days SBF immersion. Partially formed crystallite on the surface of 30 wt.% AN-PVDF film which were observed for 1 day SBF immersion had fully developed into flakes like crystallite representing bone-like apatite. Low intensity F peaks and high Ca and P peaks observed in the EDX indicates that the surface was fully covered by these crystallites. While, no changes on the surface morphology were observed on 0 wt.% 10 wt.% and 20 wt.% AN-PVDF

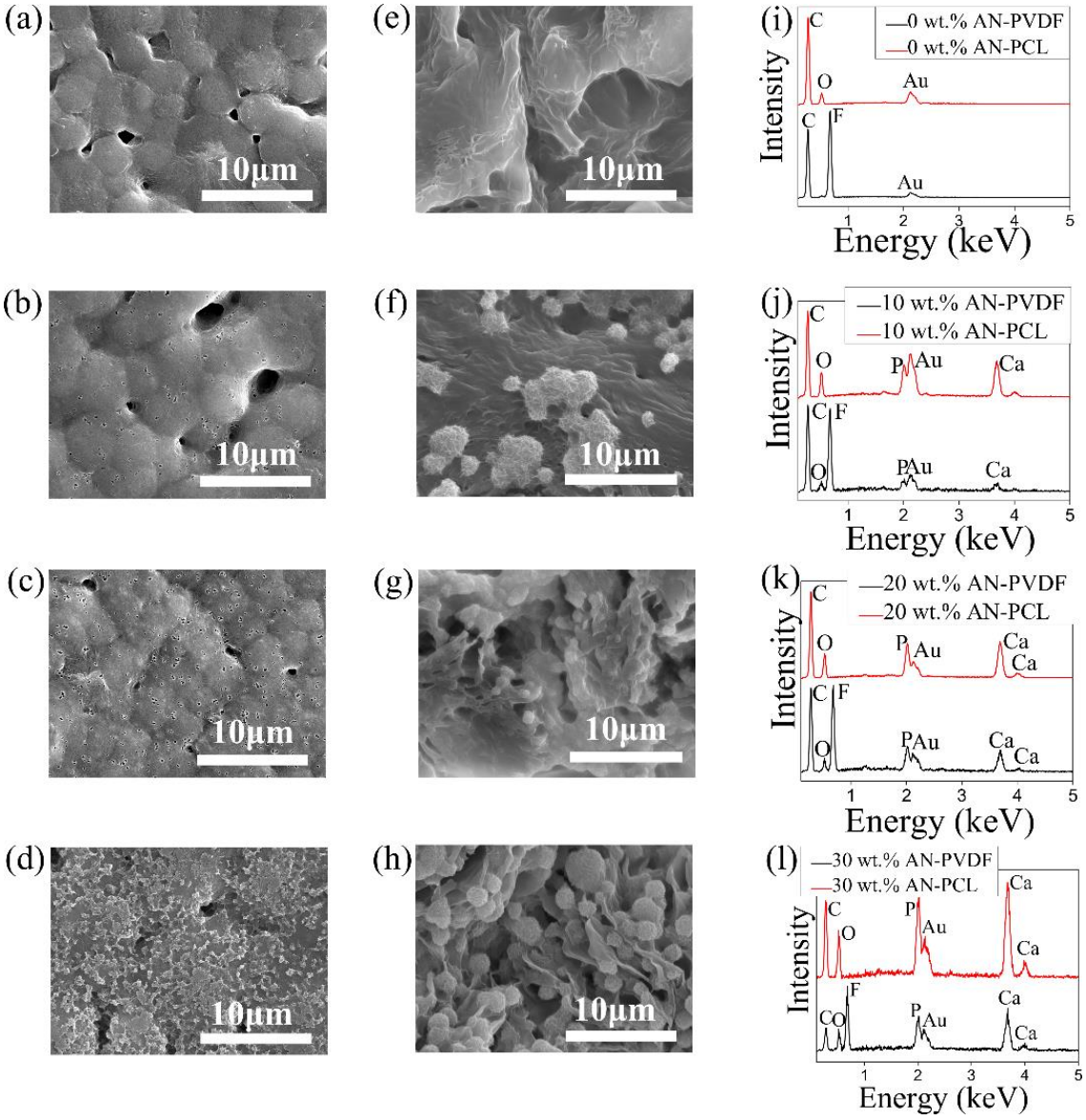

Figure 6 (a-h) SEM images of the surface of (a) 0 wt.%, (b) 10 wt.%, (c) 20 wt.% and (d) 30 wt.% AN-PVDF and (e) 0 wt.% (f) 10 wt.%, (g) 20 wt.% and (h) 30 wt.% AN-PCL films after 1 day SBF immersion. (i-l) EDX profiles comparing properties of (i) 0 wt.% (j) 10 wt.%, (k) 20 wt.% and (l) 30 wt.% AN-PVDF and AN-PCL films after 1 day SBF immersion.

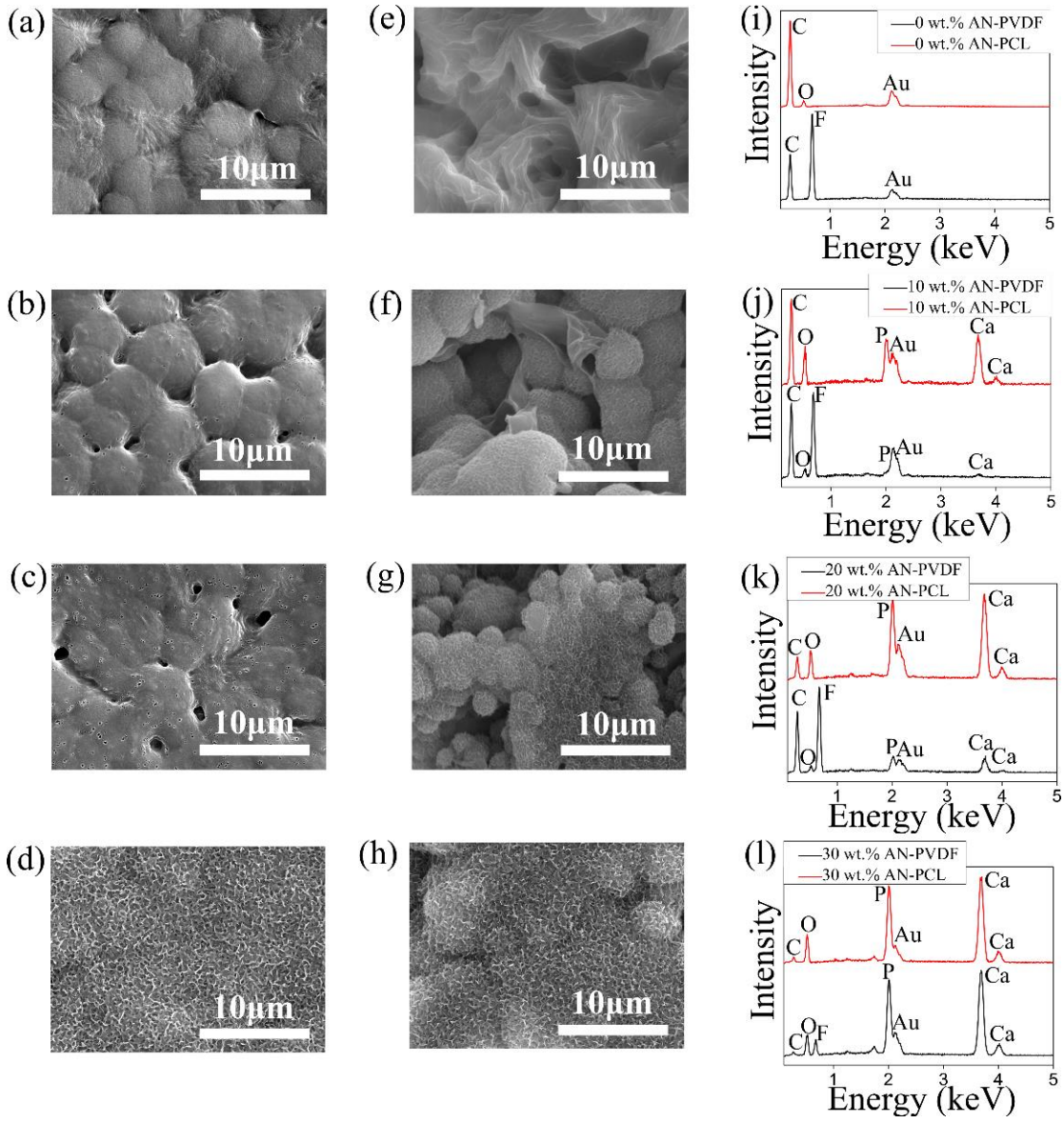

Figure 7 (a-h) SEM images of the surface of (a) 0 wt.%, (b) 10 wt.%, (c) 20 wt.% and (d) 30 wt.% AN-PVDF and (e) 0 wt.% (f) 10 wt.%, (g) 20 wt.% and (h) 30 wt.% AN-PCL films after 3 day SBF immersion. (i-l) EDX profiles comparing properties of (i) 0 wt.% (j) 10 wt.%, (k) 20 wt.% and (l) 30 wt.% AN-PVDF and AN-PCL films after 3 day SBF immersion.

films. Similarly, in the case of AN-PCL films hemispherical precipitates formed after 1 day SBF immersion had fully developed into flakes like crystallites representing bone-like apatite for 10 wt.%, 20 wt.% and 30 wt.% AN-PCL film. In the EDX result for 20 wt.% and 30 wt.% AN-PCL low intensity of C peak and high intensity Ca and P peaks were observed suggesting high surface coverage by the crystallites which increased with increasing the content of AN in PCL.

Figure 8 compares the XRD plots of 0 wt.%, 10 wt.%, 20 wt.% and 30 wt.% AN-PVDF and AN-PCL films after 1 day and 3 days immersion in SBF. Peak around 20.6° suggest that β phase, a highly piezoelectric phase of PVDF was observed for all AN-PVDF films. Nucleating fillers and solvent casting technique have been reported to cause β phase dominance in PVDF [18]. Peaks representing hydroxyapatite, 25.8° and 31.7°, were observed for 30 wt.% AN-PVDF film after 3 days SBF immersion. Similarly, in the case of 10 wt.%, 20 wt.% and 30 wt.% AN-PCL films, peaks representing hydroxyapatite were detected in XRD after 3 days immersion in SBF. The intensity of hydroxyapatite peaks increased with the increase of content of AN in PCL. Though the precipitates were deposited on the surface of these films after 1 day SBF immersion, no peaks of hydroxyapatite were detected after 1 day SBF immersion, indicating that the crystallinity or the surface coverage of the films was not enough to be detected in the XRD. These XRD results compliments the SEM and the EDX result.

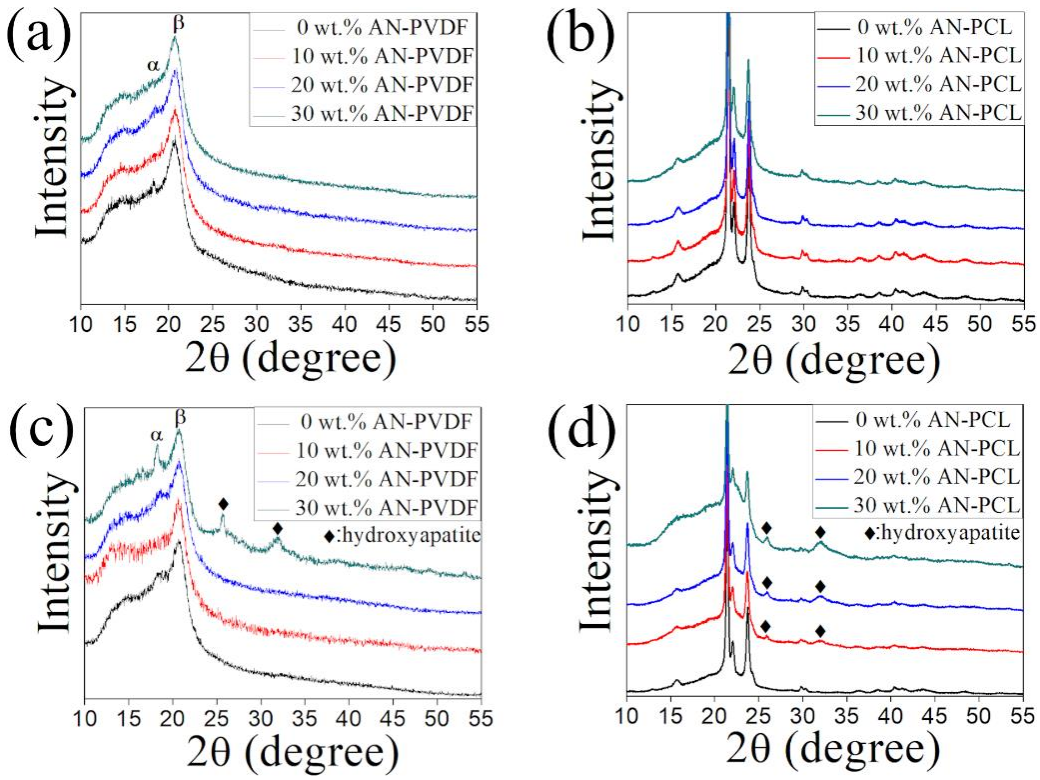

Figure 8 XRD plots of (a, c) AN-PVDF and (b, d) AN-PCL films after (a, b) 1 day and (c, d) 3 days SBF immersion.

The formation of hydroxyapatite from the constituent ions in an aqueous solution is represented by the following chemical equilibrium.

$$10Ca^{2+} + 6PO_4^{3-} + 2OH^- \rightleftharpoons Ca_{10}(PO_4)_6(OH)_2$$

Ionic activity product (IP) of the apatite in the solution is depicted by the following formula where '[ ]' is the concentration of each ion and 'γ' is the activity coefficient.

$$IP \rightleftharpoons (\gamma Ca^{2+})^{10}(\gamma PO_4^{3-})^6(\gamma OH^-)^2 \times [Ca^{2+}]^{10}[PO_4^{3-}]^6[OH^-]^2$$

The conventional SBF at physiological condition, which is pH 7.40 at 36.5 °C, is supersaturated against hydroxyapatite. However, generally because of high energetic obstacles toward the hydroxyapatite formation in SBF, it is induced only on the surface of specific materials as in the case bioactive materials. The increase in concentration of Ca^{2+} ions would increase the ionic product and degree of supersaturation which is IP/K_s (K_s=solubility product) thus favoring hydroxyapatite nucleation [19]. In the light of previous studies, it was found that AN were amorphous calcium phosphate which is easier to dissolve in SBF compared to the crystalline hydroxyapatite. It is considered that this leads to increase in the concentration of calcium and phosphate ions accelerating hydroxyapatite nucleation on the substrate [7-10].

In this study, both PVDF and PCL successfully formed hydroxyapatite layer in SBF. For PCL, however, lower concentration of AN was achieved shorter induction time of hydroxyapatite formation compared to PVDF. The PCL films as observed from the SEM analyses showed deposited hemispherical hydroxyapatite precipitates in 1 day immersion period for all concentrations of AN in PCL while no hydroxyapatite formation was observed

for the films less the 30 wt.% of AN in PVDF. To clarify this difference in hydroxyapatite forming ability, water contact measurements and surface roughness analyses of the films were performed as depicted in Figures 3 and 4. Surface wettability determines the interaction between the SBF and the substrate, thus effecting the apatite formation. Though at a higher weight percentage of 30 wt.% of AN in PVDF resulted in slight decrease of water contact angle, a large difference in the contact angle between PVDF and PCL films was not observed. This result indicates that in this case, wettability factor might only have contributed a little in hydroxyapatite formation. It is considered that the difference in the hydroxyapatite formation is because of the higher surface roughness of the PCL films compared to the PVDF films which resulted in exposing a higher amount of AN to the SBF in the PCL films.

5.4 **Conclusion**

PVDF and PCL successfully showed apatite forming ability in SBF by incorporation of AN. It was found that for all compositions of AN in PCL for apatite precipitated in 1 day immersion in SBF which fully developed into hydroxyapatite layer in 3 days SBF immersion. Whereas, PVDF formed hydroxyapatite layer at higher weight percentage of 30 wt.% AN in PVDF. This difference could be attributed to the higher surface roughness of PCL which exposed more AN to SBF. Such types of bioactive polymeric composites such as of PCL and PVDF can serve as a suitable candidate as bone tissue engineering.

5.5 **References**

[1] J. Jordan, K. I. Jacob, R. Tannenbaum, M.A. Sharaf, I. Jasiuk, Experimental trends in polymer nanocomposites - A review, Mater. Sci. Eng. C, 393 (2005), 1-11.

[2] K. Hata, T. Kokubo, T. Nakamura, T. Yamamuro, Growth of a Bonelike Apatite Layer on a Substrate by a Biomimetic Process, J. Am. Ceram. Soc.,78 (1995), 1049 -1053.

[3] Y. Abe, T. Kokubo, T. Yamamuro, Apatite coating on ceramics, metals and polymers utilizing a biological process, J. Mater. Sci.: Mater. Med., 1 (1990), 233-238.

[4] H.M. Kim, K. Kishimoto, F. Miyaji, T. Kokubo, T. Yao, Y. Suetsugu, J. Tanaka, T. Nakamura, Composition and structure of the apatite formed on PET substrates in SBF modified with various ionic activity products, J. Biomed. Mater. Res., 46 (1999), 228-35.

[5] T. Yao, M. Hibino, S. Yamaguchi and H. Okada, US Patent, 8, 178, 066 (2012), Japanese Patent 5, 261, 712 (2013).

[6] T. Yao, M. Hibino, T. Yabutsuka, US Patent, 8, 512, 732 (2013), Japanese Patent 5, 252, 399 (2013).

[7] T. Yabutsuka, H. Mizutani, S. Takai, T. Yao, Fabrication of bioactive Co-Cr-Mo-W alloy by using doubled sandblasting process and apatite nuclei treatment, Trans. Mat. Res. Soc. Japan, 43 (2018), 143-147.

[8] T. Yabutsuka, R. Karashima, S. Takai, T. Yao, Effect of doubled sandblasting process and basic simulated body fluid treatment on fabrication

of bioactive stainless steels, Materials, 11 (2018), 1334.

[9] T. Yabutsuka, K. Fukushima, T. Hiruta, S. Takai, T. Yao, Fabrication of bioactive fiber-reinforced PEEK and MXD6 by incorporation of precursor of apatite, J. Biomed. Mater. Res. B. Appl. Biomater., 106 (2018), 2254-2265.

[10] T. Yabutsuka, K. Fukushima, T. Hiruta, S. Takai, T. Yao, Effect of pores formation process and oxygen plasma treatment to hydroxyapatite formation on bioactive PEEK prepared by incorporation of precursor of apatite, Mater. Sci. Eng. C, 81 (2017), 349-358.

[11] H. Kawai, The piezoelectricity of poly (vinylidene fluoride), Jpn. J. Appl. Phys., 8 (1969), 975-976.

[12] G.W. Hastings, F.A. Mahmud, Electrical effects in bone, J. Biomed. Eng., 10 (1988), 515-521.

[13] J. Ficat, G. Escourron, M.J. Fauran, R. Durroux, P. Ficat, C. Lacabanne, F. Micheron, Osteogenesis induced by bimorph polyvinylidene fluoride films Ferroelectrics, 51 (1983), 121-128.

[14] C. Ribeiro, V. Sencadas, D. M. Correia, S.L. Méndez, Piezoelectric polymers as biomaterials for tissue engineering applications, Coll. Surf. B, 136 (2015), 46-55.

[15] A. H. Rajabi, M. Jaffe, T. L. Arinzeh, Piezoelectric materials for tissue regeneration: A Review, Acta Biomaterialia, 24 (2015), 12-23.

[16] N. Bölgen, Y.Z. Menceloglu, K. Acatay, I. Vargel, E. Piskin, In Vitro and in vivo degradation of non-woven materials made of Poly(epsilon-Caprolactone) nanofibers prepared by electrospinning under different

conditions, J. Biomater. Sci. Polym., 16 (2005), 1537-1555.

[17] T. Kokubo, H, Takadama, How useful is SBF in predicting in vivo bone bioactivity?, Biomaterials, 27 (2006), 2907-2915.

[18] P. Martins, A.C. Lopes, S. L. Mendez, Electroactive phases of poly(vinylidene fluoride): Determination, processing and applications, Prog. Polym. Sci., 39 (2014), 683-706.

[19] C. Ohtsuki, T. Kokubo, T. Yamamuro, Mechanism of apatite formation on $CaOSiO_2P_2O_5$ glasses in a simulated body fluid, J. Non-Cryst. Solids, 143 (1992), 84-92.

Chapter 6

General Summary

The present thesis describes the studies on development of bioenvironment compatible implant materials by the function of precursors of apatite or apatite nuclei. Simulated body fluid (SBF), is a biomimetic, acellular aqueous solution, that has the concentration of inorganic ions similar to human blood plasma and is maintained at a physiological condition, i.e. pH, 7.4 at 36.5 °C. SBF can mimic bone-bonding ability of a material similar to the in-vivo condition and has been widely used to predict bioactivity of a material. Precursors of apatite can be broadly described as fine calcium phosphate particles precipitated from modified SBF. Conventionally, calcium phosphate particles are precipitated when either concentration, pH or temperature of SBF is altered. These particles were found to be highly active in hydroxyapatite formation in conventional SBF and were named as precursors of apatite or apatite nuclei (AN). Herein, the author designed two kinds of AN preparation methods and utilized three different procedures to deposit AN or integrate AN in form of composites to fabricate bio-environmentally compatible bioactive materials. The content of the respective chapters from the chapter 2 to chapter 5 are summarized as follows.

In chapter 2, author presented the fabrication of bioactive zirconia. In this chapter, a double sandblasting technique was used to roughen the zirconia surface which allowed the amorphous AN to be deposited on surface pores from ‘2.0 SBF’. The inorganic ions concentration of 2.0SBF is twice compared to the conventional SBF. The solution was prepared at 36.5 °C at slightly increased pH of 8.2 from physiological pH of 7.4 to accelerate the AN

precipitation. Then, the zirconia samples were incubated in the solution at 36.5°C for 1 and 3 days, respectively. These apatite nuclei deposited zirconia samples showed high bioactivity, as the hydroxyapatite layer fully covered the surface in 1-day SBF immersion.

In chapter 3, the author illustrated bioactive treatment of tetragonal zirconia polycrystals (3Y-TZP) by following a different approach of AN treatment as presented in chapter 2. In this chapter the AN treatment consisted of two different kinds of calcium-phosphate (Ca-P) aqueous solutions treatments with the similar concentration of calcium and phosphate ions as the conventional SBF. However, only one Ca-P solution additionally contained magnesium (Mg) ions also at a concentration similar to the conventional SBF, while no Mg ions were present in the other Ca-P solution. To distinguish the effect of Mg ions on the hydroxyapatite formed in SBF the rest of the ions were removed. Initially, two different types of above-mentioned Ca-P aqueous solutions were prepared at a slightly higher pH of 8.2 compared to physiological pH of 7.4 and at a temperature of 25°C, less than the physiological temperature of 36.5 °C to deaccelerate the AN precipitation. 3Y-TZP samples were first chemically etched with hydrofluoric acid (HF) and then were soaked in the two types of prepared Ca-P solutions at 70 °C to accelerate the precipitation of AN for 1-day. Both types of Ca-P solutions treated 3Y-TZP samples showed dense hydroxyapatite formation in 1-day SBF immersion. Adhesive strength of the formed hydroxyapatite layer to the HF-etched 3Y-TZP samples surface was found out and compared with polished 3Y-TZP samples after 14 days immersion in the SBF. Polished 3Y-TZP samples treated with both types of Ca-P solutions showed significantly low adhesive strength (<1 MPa) of hydroxyapatite layer to the 3Y-TZP surface

irrespective of the type Ca-P solution treatments when compared to HF-etched 3Y-TZP samples due to mechanical interlocking effect. Furthermore, a significant difference in the adhesive strength of hydroxyapatite layer to HF-etched 3Y-TZP surface was observed for the two different type Ca-P aqueous solution treatments. Mg incorporated Ca-P solution treatment (~8 MPa) showed significantly higher adhesive strength compared to non-Mg incorporated Ca-P solution treatment (~4.5 MPa). The fractured surface analysis showed that both the types of Ca-P solution treatments resulted in mixed modes of failure. However, Mg incorporated Ca-P solution treated HF-etched 3Y-TZP samples predominantly showed cohesive failure while non-Mg incorporated Ca-P solution treated HF-etched 3Y-TZP samples showed adhesive failure. Hydroxyapatite crystallization is greatly affected by the presence of additional ions such as Mg besides Ca^{2+} and PO_4^{3-} which causes the reduction of Ca/P ratio and decrease of crystal size. The higher adhesive strength for Mg incorporated Ca-P solution treated HF-etched 3Y-TZP samples compared to non-Mg incorporated Ca-P solution treated HF-etched 3Y-TZP samples is presumably due to the effect that released Mg ions near the vicinity of the samples surface in the SBF have inhibited the rate of crystallization of hydroxyapatite crystals. This might have initially resulted in the formation smaller crystals, which penetrated better inside the pores of HF-etched 3Y-TZP samples surface. These crystals later developed into hydroxyapatite layer with prolonged immersion in the SBF and adhered strongly to the surface.

In chapter 4, the author discussed about the bioactivity of AN and polyvinylidene fluoride (PVDF) composite films. In this work, AN were prepared utilizing a similar methodology from 2.0SBF as in chapter 2.

Different weight percentages of the AN were mixed into PVDF solution in the DMF. Finally, solvent casting technique was used to fabricate AN-PVDF films. SBF test revealed that films having a weight percentage of AN of 30 wt.% or more showed dense hydroxyapatite formation and full surface coverage in the 3-days SBF immersion. The thickness of the hydroxyapatite layer was ~ 3 μm for 30 wt.% AN-PVDF film after 3 days SBF immersion. Analysis of the thickness of the hydroxyapatite films for 3-days and 7-days showed that thickness doubled with doubling the soaking time in SBF.

In chapter 5, a comparative study of the bioactivity of polycaprolactone (PCL) and PVDF thin films incorporated with AN is presented. For the preparation of the AN-PCL films a similar method was used as the AN-PVDF films, mentioned in chapter 4. Acetone was used as a solvent to dissolve PCL instead of DMF. SBF immersion test showed that PCL films containing 10 wt.% or more of AN in PCL partially formed hydroxyapatite crystal in 1-day immersion, which fully covered the surface in 3-days SBF immersion. This result is significantly different from AN-PVDF films, where films containing AN less than 30 wt.% did not show any hydroxyapatite formation. To understand this difference wettability of PCL and PVDF was measured which determines the interaction of films with the SBF. However, there was no significant difference in water contact angle between the PCL and PVDF. Finally, surface roughness was compared, and it was found the PCL had highly roughened surface compared to PVDF. Our results concluded that significant shortened incubation period and less concentration of AN required for the formation of hydroxyapatite of PCL films can be attributed to higher surface roughness compared to PVDF thereby exposing a larger amount of apatite nuclei to the surface.

In conclusion, based on the results mentioned in the above chapters, precursors of apatite or apatite nuclei fabricated utilizing biomimetic environment friendly method are found to be very effective in inducing apatite-forming ability. Various materials with unique properties and also possessing bioactivity or the ability to bond with the living bone can be fabricated by successfully integrating precursors of apatite in a form of coatings as described in chapter 2 and chapter 3 or composites as described chapter 4 and chapter 5. Furthermore, based on the two different methods utilized for precursors of apatite synthesis as illustrated in chapter 2, chapter 4 and chapter 5 compared to chapter 3, it is very crucial depending on the properties of the bioinert materials to take into consideration the synthesis conditions of precursors of apatite. For example, physical and chemical parameters such as temperature, concentration, and pH should be evaluated for effective precipitation and deposition of the precursors of apatite. In addition, the surface properties of the bioinert material would finally contribute to the formation and growth of the hydroxyapatite layer. In light of these studies, it is expected that precursors of apatite would actively induce hydroxyapatite formation in a brief period of time. Precursors of apatite composites and coated materials would develop a hydroxyapatite layer, and eventually form a stable bond to the living bone tissue through this layer over a prolonged period of time. Thus, various kinds of bio-environment adjusted materials can be developed by the function of precursors of apatite. These materials can serve as excellent candidates for biomedical applications in various medical fields.

List of Publications

Chapter 2

Hasnat Zamin, Takeshi Yabutsuka, Shigeomi Takai, Hiroshi Sakaguchi, Takeshi Yao, Fabrication of Bioactive Zirconia by Doubled Sandblasting Process and Incorporation of Apatite Nuclei, Key Eng. Mater., **829** (2019), 151-156.

Chapter 3

Hasnat Zamin, Takeshi Yabutsuka, Shigeomi Takai, Hiroshi Sakaguchi, Fabrication of Bioactive Zirconia by Deposition of Low Crystalline Hydroxyapatite Particles using Solution Treatment, Bioceramics, **31** (2019), 36-42.

Hasnat Zamin, Takeshi Yabutsuka, Shigeomi Takai, Hiroshi Sakaguchi, Role of Magnesium and the Effect of Surface Roughness on the Hydroxyapatite-Forming Ability of Zirconia Induced by Biomimetic Aqueous Solution Treatment, Materials, **13** (2020), 3045.

Chapter 4

Hasnat Zamin, Takeshi Yabutsuka, Shigeomi Takai, Bioactivity Assessment of Apatite Nuclei-PVDF Composite Thin Films, Key Eng. Mater., **782** (2018), 78-83.

Chapter 5

Hasnat Zamin, Tomoko Hiruta, Takeshi Yabutsuka, Shigeomi Takai, Fabrication of Bioactive Polycaprolactone by Incorporation of Apatite Nuclei, Key Eng. Mater., **782** (2018), 91-97.

Hasnat Zamin, Takeshi Yabutsuka, Shigeomi Takai, Hiroshi Sakaguchi, A Comparative Bioactivity Evaluation of PVDF and PCL Incorporated with Amorphous Calcium Phosphate Particles. (submitted in Phosphorus Research Bulletin)

Acknowledgment

My sincere appreciation goes to my supervisor Prof. Sakaguchi who gave me the opportunity to pursue Ph.D. research and to work under his supervision at the Graduate School of Energy Science, Kyoto University.

I would also like to express my deepest gratitude to Assoc. Prof. Takai for guiding at each step of the Doctoral program which helped me to smoothly progress through the Ph.D. course.

I especially want to thanks Asst. Prof Yabutsuka for his help and effort in training me in the field of Bioceramics. Without his help, I would not have gained the necessary skills and knowledge, starting from the fundamentals, designing the experiments, analyzing the data, and finally up to preparing the manuscripts.

I would also like to thanks Prof. Sagawa for reviewing the thesis.

Big thanks also to all the current and past members of the laboratory for their help and most importantly, creating an enjoyable working atmosphere. Thanks to Ms. Yamamura for organizing events and all the paperwork about university activities and life in Japan.

Thanks to JICA (Japan International Cooperation Agency) for providing financial support.

Finally, I would like to appreciate my family and friends for care and support during this crucial time.

Hasnat Zamin